ANALYSIS OF DATA CENTER COOLING STRATEGIES AND THE IMPACT OF THE DYNAMIC THERMAL MANAGEMENT ON THE DATA CENTER ENERGY EFFICIENCY

by

VEERENDRA PRAKASH MULAY

Presented to the Faculty of the Graduate School of

The University of Texas at Arlington in Partial Fulfillment

of the Requirements

for the Degree of

DOCTOR OF PHILOSOPHY

THE UNIVERSITY OF TEXAS AT ARLINGTON

December 2009

ACKNOWLEDGEMENTS

I would like to thank Prof. Dereje Agonafer for the guidance he has provided me through the years. It would not have been possible to accomplish the milestones I have accomplished without his mentoring and support.

I would also like to thank Prof. Chan, Prof. Haji-Sheikh and Prof. Nomura for serving on the committee. Also, special thanks to Dr. Roger Schmidt of IBM Corp. for spending the time in discussing the industrial aspects of the topic. Mr. Gary Irwin of Commscope has been very helpful throughout my association with him and his team. I want to express my gratitude towards Dr. Ali Heydari and the Technical Operations team at Facebook Inc. for their support during my internship.

Ms. Sally Thomson has been helpful throughout the period of my association with UTA. Thank you Sally for making these years less stressful through your prompt help and timely assistance in all the matters. My colleagues and friends from EMNSPC deserve the credit for tolerating me and supporting me during the time of my need.

Finally, I wouldn't be in this position if it weren't for my parents Aarti and Prakash Mulay who worked tirelessly so that I could go to college. They gave up their comfort and their dreams so that I could fulfill mine. This one is for you, Aai and Baba.

I dedicate this work to my wife Meera, who put up with my long hours in lab even on the weekends and still supported me through the thick and the thin. I now look forward to spend more time with my daughter Rucha who has been my lucky charm!

November 23, 2009

ABSTRACT

ANALYSIS OF THE DATA CENTER COOLING STRATEGIES AND THE IMPACT OF THE DYNAMIC THERMAL MANAGEMENT ON THE DATA CENTER ENERGY EFFICIENCY

Veerendra Prakash Mulay, PhD

The University of Texas at Arlington, 2009

Supervising Professor: Dereje Agonafer

The power trend for Server systems continues to grow thereby making thermal management of Data centers a very challenging task. Although various configurations exist, the raised floor plenum with Computer Room Air Conditioners (CRACs) providing cold air is a popular operating strategy. The air cooling of data center however, may not address the situation where more energy is expended in cooling infrastructure than the thermal load of data center. Revised power trend projections by ASHRAE TC 9.9 predict the projected thermal load as high as 5000W/ft^2 of compute servers' equipment footprint by year 2010. These trend charts also indicate that heat load per product footprint has doubled for storage servers during 2000-2004. For the same period, heat load per product footprint for compute servers has tripled. Amongst the systems that are currently available and being shipped, many racks exceed 20kW. Such high heat loads have raised concerns over limits of air cooling of data centers similar to air cooling of microprocessors.

The concept of "Dynamic Thermal Management" depends on sensing local data and actuating the cooling resources dynamically thereby improving thermodynamic efficiencies. This

will result in significant potential energy savings. This research is aimed at developing the guidelines for a dynamic thermal management that will monitor the Rack Inlet Temperature (RIT) and provide feedback to control the cooling resources.

Commercially available CFD tools are used to build and simulate the data center models. The effect of various data center parameters on the temperature distribution and the flow field is studied. The parametric and optimization techniques are used to determine the optimal layouts for various cooling strategies. In the second phase, analytical models were identified which essentially captured the complexities of temperature distribution within data center and the inter-dependence of individual components on one another. Finally, experimental tests were carried out to collect the temperature data, use analytical models to decide the new set points for cooling resources and validate the guidelines of dynamic thermal management by realizing the energy savings.

TABLE OF CONTENTS

LIST OF ILLUSTRATIONS

LIST OF TABLES

CHAPTER 1

INTRODUCTION

1.1 Data Centers

Data center is a facility that contains concentrated equipment to perform one or more of the following functions: Store, process, manage and exchange digital data and information. The compute servers that process the data, storage servers that store the data and network equipment, which is used for communications, are collectively called as “IT Equipment”. In addition to this IT Equipment, data center also houses power conversion equipment and environmental control equipment to maintain operating conditions.

With rapid advance of technology, economies around the world are experiencing paradigm shift in information management. Paper based information exchange is being replaced by digital information. As this shift happens, data centers have become ubiquitous cementing their essentiality in virtually every sector of economy which includes academic, business, communications and government systems.

Typical data centers are housed within buildings that have no windows and minimal fresh air. This is due to fact that data centers are primarily designed for IT equipment and not for the people. It is essential that the operating conditions within facility are within the manufacturer’s limits. In its thermal guidelines for data processing environments, ASHRAE TC 9.9 [1] has introduced four classes of data processing environments and provides the data for following criteria:

- Steady state temperature
- Relative humidity
- Maximum dew point temperature
- Temperature rise.

These four classes and their requirements are given in Table 1.1.

Table 1.1 Class Requirements for Data Processing Environments

Class	Air Conditioning	Environmental Control
1	Yes	Tight
2	Yes	Loose
3	Yes	No
4	No	No

This discussion is focused on Class 1 environment which requires air conditioning of the facility along with tighter controls of criteria stated above.

1.2 Data Center Power Trends

In recent years data center facilities have witnessed rapidly increasing power trends that continue to rise at an alarming rate. The combination of increased power dissipation and increased packaging density has led to substantial increases in chip and module heat flux. As a result, heat load per square feet of server footprint in a data center has increased. Recent heat loads published by ASHRAE [2] as shown in Fig.1.1 indicate that for the period 2000-2004, heat load for storage servers has doubled while for the same period, heat load for compute servers has tripled.

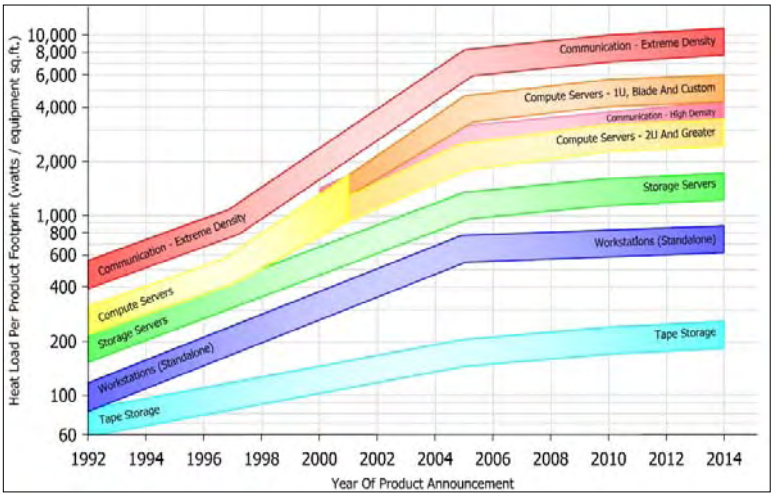

Figure 1.1 Heat Load Trends [2]

According to these trends, compute server rack heat fluxes in 2006 around 4,000 W/ft^2. This corresponds to 27KW for a typical 19 inch rack. There are 19 inch racks commercially available in markets that dissipate more than 30KW which corresponds to 4,800 W/ft^2 rack heat flux. Figure 1.2 shows the measured values for average and hot spot high-density computing data center heat fluxes based on measurements carried out by Schmidt and co-workers [3-6]. In one of the 2005 measurements, a server cluster test facility showed extremely high hot spot heat fluxes of 720 W/ft^2 (7750 W/m^2) over areas of 440 ft^2 (40.1 m^2), or an 11x10 grid of tiles.

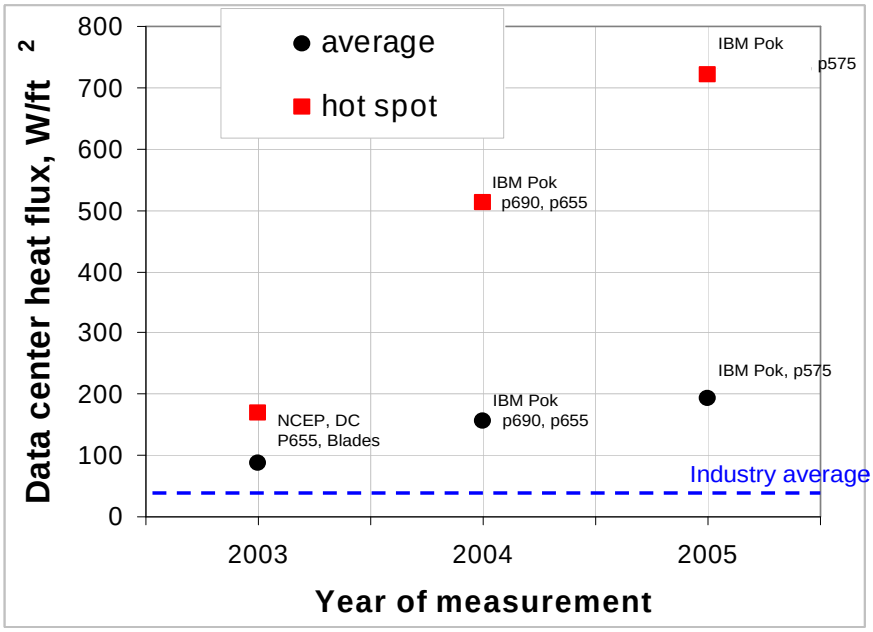

Figure 1.2 Data Center Hot Spot Heat Flux [5]

Such hot spots within data centers cause rise in temperature leading to reliability issues of electronic components. Hence it becomes eminent to use proper cooling solutions to keep the temperature within limits specified by manufacturer. Air cooling is vastly employed to achieve this controlled environment.

1.3 Data Center Cooling

Shown in Fig. 1.3 and 1.4 are two commonly used configurations of air supply namely underfloor and overhead. Both these configurations use hot aisle – cold aisle layout in an attempt to isolate chilled air supply from hot air. The front face of rack, which generally is air inlet for the equipment, is placed facing perforated tiles. The backside of rack from where hot air exhausts, faces backside of another rack forming a hot aisle. A typical arrangement of underfloor air supply configuration is shown in Fig. 1.3.

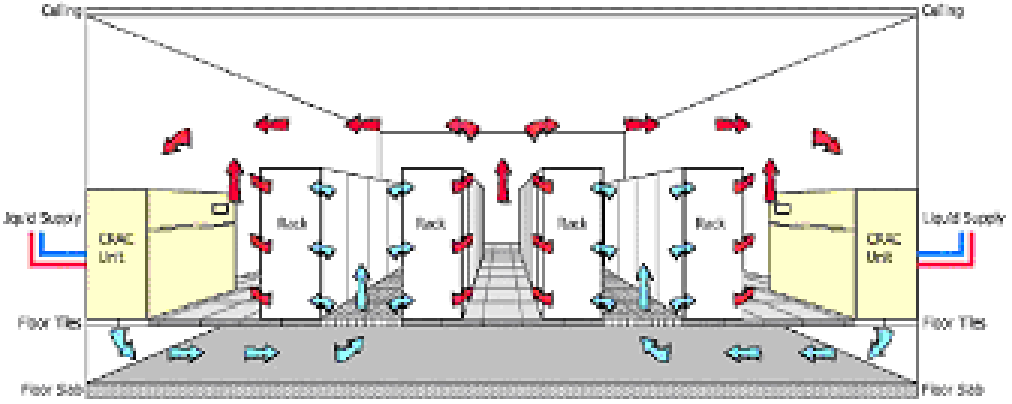

Figure 1.3 Underfloor air supply configuration [2]

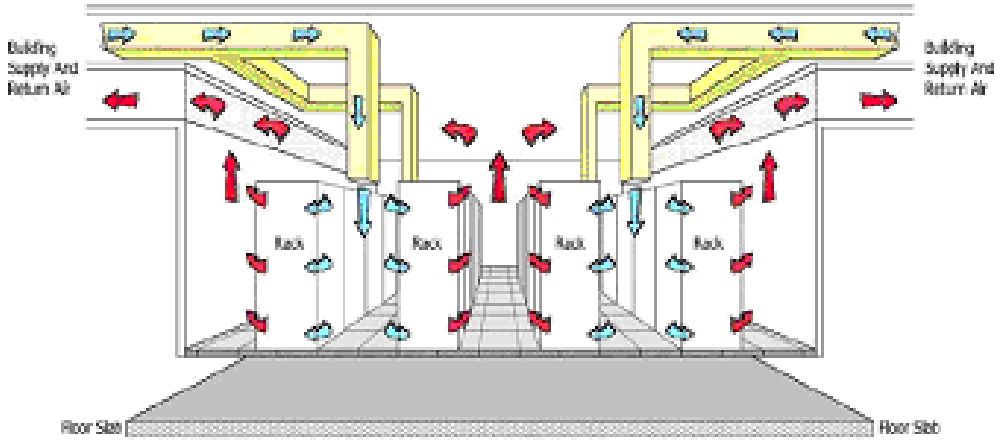

Figure 1.4 Overhead air supply configuration [2]

The Computer Room Air Conditioning unit (CRAC) delivers the chilled air into the space below raised floor. This chilled air enters the room through perforated tiles, passes through the racks and gets heated up. This hot air then returns to CRAC intake. In overhead supply configuration (Fig. 1.4), chilled air enters the room via overhead diffusers. After passing through racks, the heated air then exits room via vents on the wall. This hot air eventually passes through heat exchanger and is then supplied back as chilled air through diffusers.

1.4 Energy Consumption in Data Center

Generally, the data centers are connected to utility grid from where electricity is received at building envelope. This is then split into two broad streams:

1. Uninterruptible loads such as IT equipment that requires continuous operation
2. other loads, which can sustain temporary interruption

Electricity for uninterruptible loads is channeled through Uninterruptible Power Supplies (UPS). The UPS acts as battery in the event of power outage and supplies electricity to IT equipment till backup generator is operational. It also absorbs any fluctuations in incoming supply and provides more uniform power. All incoming AC power is converted to DC and the batteries are charged. This DC power is then converted again to AC before it leaves UPS.
Electricity leaving UPS is then received by Power Distribution Units (PDU) and is supplied to server racks. These servers have Power Supply Unit (PSU) that converts AC power into low voltage DC power which is then consumed internal components such as Central Processing Unit (CPU), memory, disk drive, chipset and fans.

Thus, data centers have three principal components that require significant energy namely IT Equipment, Cooling System and PDUs. A study from Lawrence Berkeley National Laboratory (LBNL) [7] has reported that for year 2005, server driven power usage in U.S. and Worldwide was 5000 MW and 14000 MW respectively which was 1.2% and 0.8% of the total energy consumption of the U.S. and the world respectively. This consumption translated into

energy cost of $2.7B for U.S. and $7.2B for the world. With costs running so high and server density on increase, there is growing interest in understanding and improving the energy efficiency of data centers.

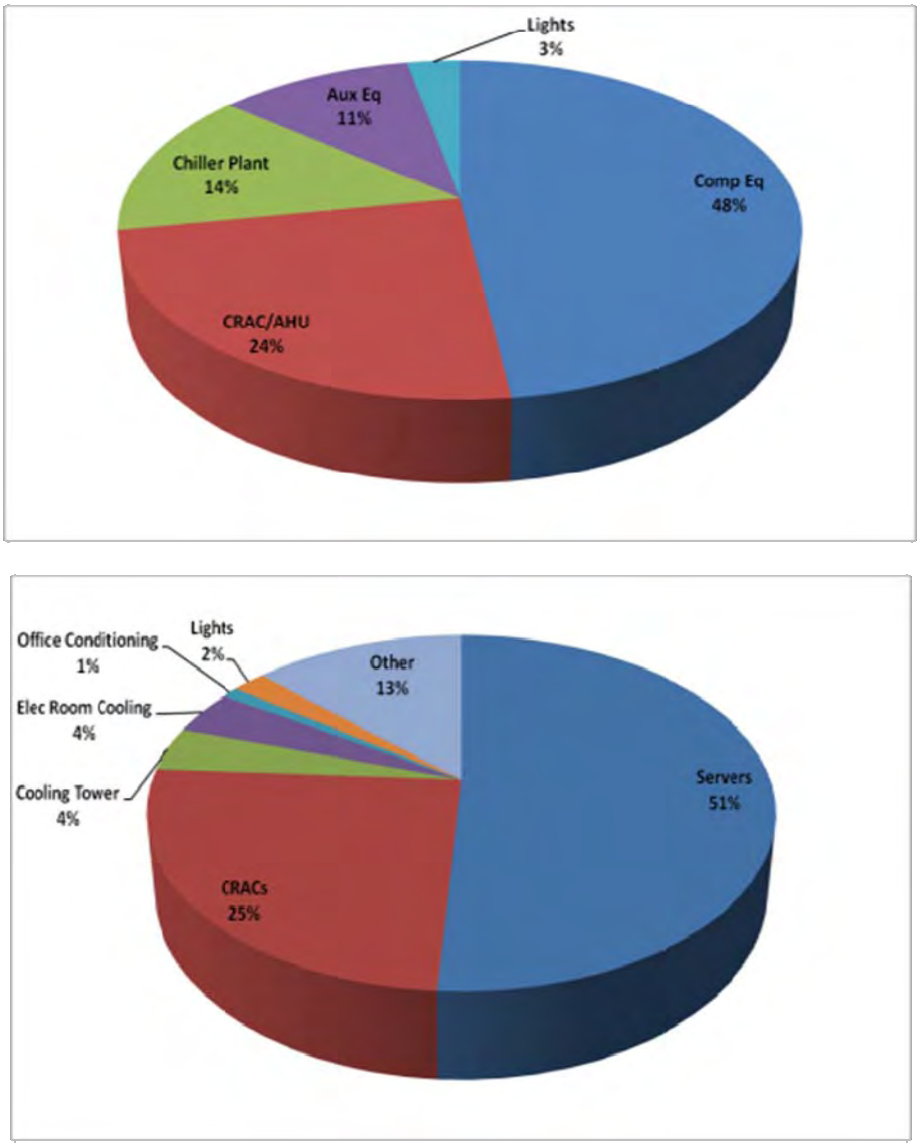

Figure 1.5 Break-down of Power Consumption of Data Centers- (a) [8] and (b) [9]

A break-down of power consumption of data center has been studied. Two such break-downs from two different case studies [8, 9] are presented in Fig. 1.5. Although slight variations are inevitable, these case studies confirm general estimate that Server load constitutes half the power of total consumption where as cooling infrastructure claims almost one third of the total power.

Until recently, data center operators' prime concern was data center operating reliability and not the energy efficiency. Hence most of the data centers were over provisioned based on worst case scenario. However, with power densities reaching to levels that lead to limitations, energy efficiency is now seen as a way to solve these problems. The benefits of reducing energy inputs at various levels are:

- reduction in cost
- lesser demand on utility grid hence improved reliability
- avoided investment in power plants
- reduced dependence on fossil fuels
- Less greenhouse emissions.

1.5 Energy Consumption in Data Center Cooling

Since cooling infrastructure consumes about one third of total data center power, it also provides potential for cooling solutions that will be energy efficient. A case study [10] of a typical data center gives further break down of energy consumption by various components of data center cooling. The study shows that chiller compressors are the largest contributor of cooling energy consumption at 41.2% followed by CRAC units that utilize 27.6% of the total cooling power. Server fans consume about 14% of the energy required for the cooling. Cooling tower and the pumps for building chilled water followed at 13% and 4% respectively.

The cooling resources can be divided into two broad categories namely the facility side and the IT side. In the study stated above, the server fans are the lone resource from the IT

side. All other resources fall under the category of the facility side. If reduction in energy consumption on the facility side is desired, then one has to look into the chiller operation as it is the biggest consumer on facility side. The next opportunity of savings would be the CRAC units.

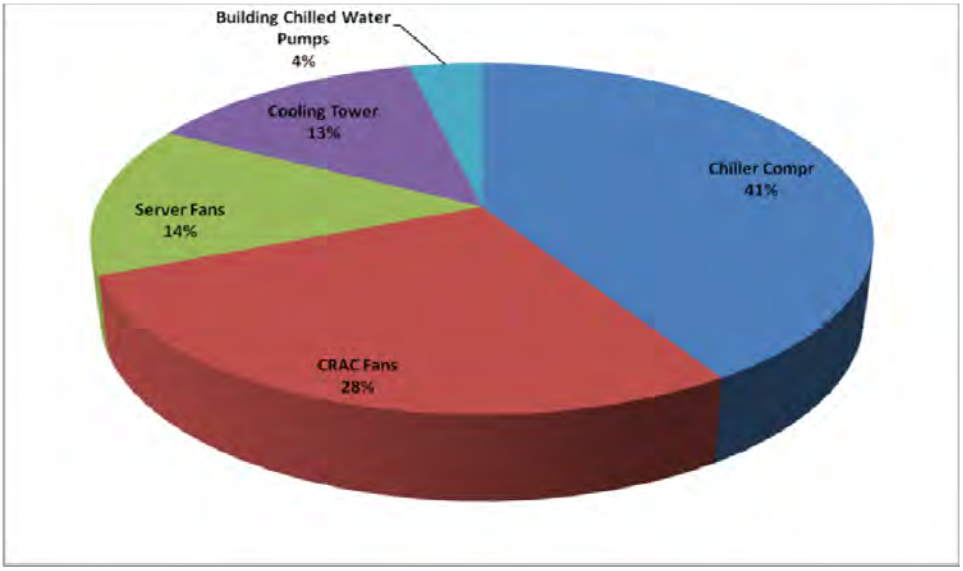

Figure 1.6 Break-down of Cooling Energy Consumption [10]

1.6 The Dynamic Thermal Management

The concept of “the Dynamic Thermal Management” depends on sensing the local data and actuating the cooling resources dynamically thereby improving the thermodynamic efficiencies. The local data includes the temperature, relative humidity and the pressure. This will result in significant potential energy savings.

Most of the data centers employing raised floor (underfloor) configuration, have the CRAC/CRAH units that are set to operate based on the temperature of the returning air. This arrangement causes the temperature of the supply air to fluctuate. This leads to air being supplied by different CRAC/CRAH units into the underfloor plenum at different temperatures. Although there is mixing of these different air streams in the underfloor plenum, it does not

result in uniform temperature. So there exist air streams with different temperatures. This leads to entry of supply air into cold aisle with non uniform temperature. In other words, the air coming out one tile may be at different temperature than the air coming out of another tile in the same cold aisle.

This nonuniform temperature distribution is compounded by the recirculation of hot air into the cold aisle. This causes large variation in the temperature of air entering into the servers at different heights in a rack. This in turn causes server fans to spin at different speeds, many times at higher speeds resulting in more energy consumption.

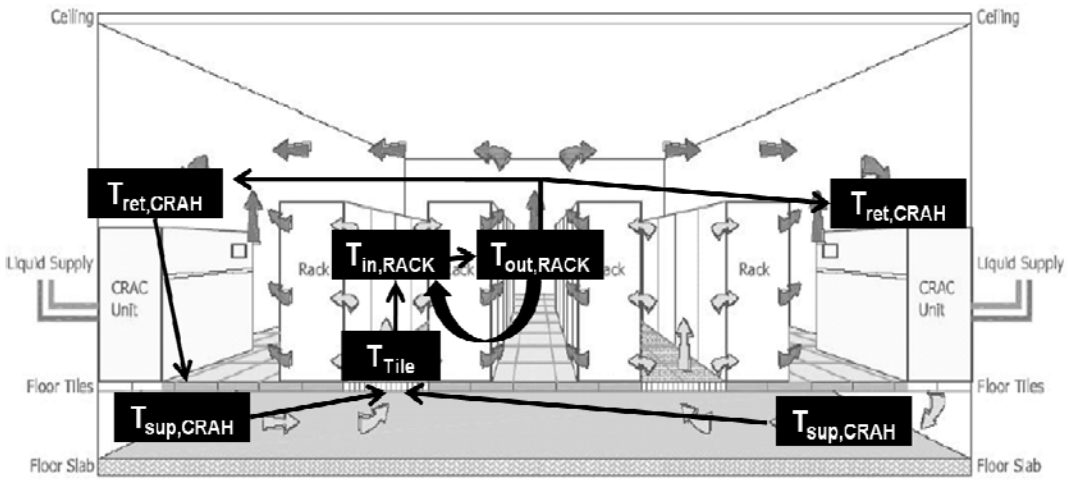

Figure 1.7 The Temperature Dependencies

It therefore becomes necessary to sense this thermal data and adjust the control settings of the cooling resources accordingly to maintain near uniform rack inlet temperatures and run the server fans at relatively lower speeds. It ensures the energy efficient operation of the entire plant and presents the opportunity for significant savings.

1.7 The Scope of the Work

1.7.1. The Objectives

The objectives of this dissertation are as follows:

- Guidelines for configurations of data centers for optimal cooling
  - CFD / mathematical optimization methods to obtain optimal configuration not only for air cooling but also for hybrid solutions employing air + liquid cooling.
- Development of a Sensor network / Data Acquisition System
  - Selection of sensors
  - Determination of sensing nodes
  - A platform to integrate sensors, collect data and control the air flow.
- Guidelines for the control policies for the cooling resources as well as the IT equipment for an energy efficient operation.

1.7.2. The Approach

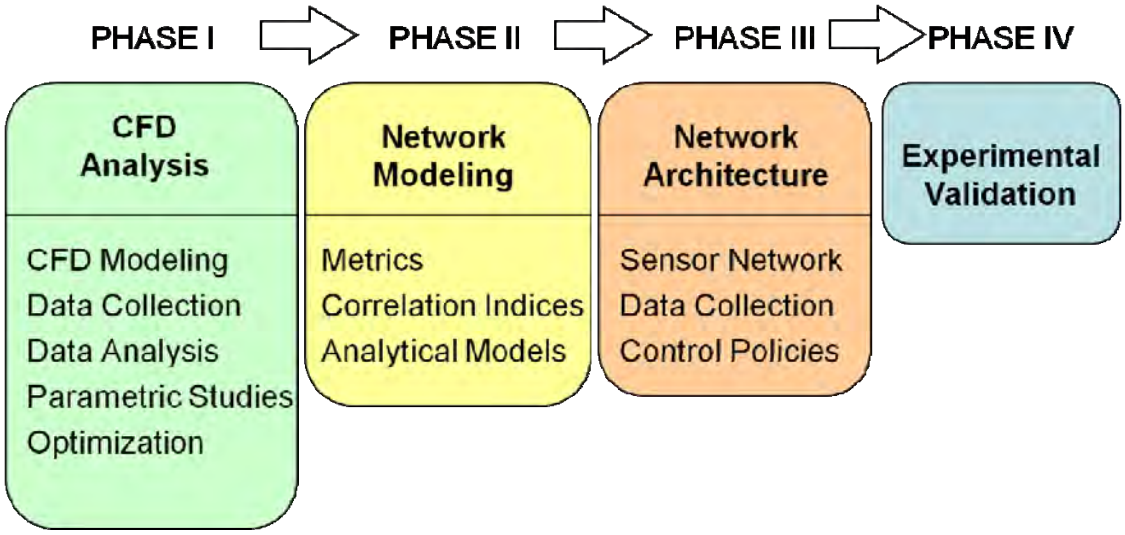

Figure 1.8 The Approach

This work is carried out in 4 phases as shown in fig. 1.8. During the initial phase of this work, different cooling strategies used in data center are studied. There are countless research articles discussing various aspects of the data center cooling. Some of these articles and their findings are summarized in chapter 2. Some of these cooling strategies are then studied in detail with the help of the computational fluid dynamics simulations. Chapter 3 contains the analysis of liquid cooling in data centers using the rear door heat exchangers for both the underfloor and the overhead supply configuration. It is followed by the investigation of the efficient cabinet designs with and without chimney used in data centers with raised floor configuration. The study on airside economizers and the case of hot exhaust containment is also presented in the chapter 3.

In phase II, the network model for the plant is identified. The metrics that will be used to study the effectiveness of the data center, the empirical relations and correlations between different components of the plant are listed in the Chapter 4.

The network architecture was decided in phase III. The sensor selection, the numbers and the location of sensors to be installed, the data collection and the decision on control policies is carried out in this phase. Two different targets for improving the energy efficiency are outlined. The first target falls in the category of facility side cooling resources which is the CRAH unit. The process of determining the optimum airflow and the set points of the CRAH units is described. The second target is the server fan, which represents the IT side of the cooling resources. Achieving the optimum Fan speed control by changing the fan speed control algorithm is also described in the chapter 5.

During the last phase (Phase IV), the experimental tests are carried out to validate the control policies and verify the potential energy savings. The test results are included in the chapter 5. The conclusions drawn from this work are then presented in the form of guidelines in the chapter 6.

CHAPTER 2

LITERATURE REVIEW

The rapid increase in the heat load per server footprint has resulted in an equal increase in the research on how best to tackle this problem. Numerous research articles, papers, studies and guidelines have been presented [1-112]. There are excellent articles reviewing these topics in detail [11, 12]. Some of those topics from these articles are summarized in this chapter. The topics are as follows:

1. The cooling system configuration
2. The structural parameters
3. The placement of CRAC units
4. The energy management
5. Data center metrics
6. Modeling of data centers
7. Experimental investigations of data center systems

2.1 The Cooling System Configuration

Nakao et al. [13] modeled four variations of the data center cooling configurations in their study. These included the underfloor supply with ceiling exhaust, underfloor supply with horizontal exhaust, overhead supply with underfloor exhaust and the overhead supply with horizontal exhaust. Noh et al. [14] modeled three variations of the data center designs for 5-6 kw rack loads for telecommunication applications. These configurations were underfloor supply with ceiling exhaust, overhead supply with underfloor exhaust and overhead supply with wall exhaust. Both these studies concurred that the underfloor supply with ceiling return is the best

alternative. The underfloor supply with wall exhaust is also a good option when the exhaust location is near the top.

Shrivastava et al. [15] studied different data center configurations. CFD models were constructed to assess the effectiveness of those configurations. They characterized the data center performance based on average region RIT and mean region RIT. They reported that for given constraints, underfloor supply ceiling return configuration was found to be most effective. They also reported that amongst the supply air flow fraction, the ceiling height and the location of the return vent, the supply airflow fraction is the most influential factor on rack inlet temperatures for various configurations. They also agreed with Nakao et al. [13] that the overhead supply with underfloor return represents the worst performing cooling configuration.

The suitability of airflow configurations for high density data center clusters was discussed by Schmidt and Iyengar [16]. They considered two airflow configurations namely underfloor and overhead, which are prominently used. CFD models for both configurations are constructed and the data is compared with respect to air supply fraction, rack location and along the height of rack. They found high temperature gradients in the inlet temperatures. They observed that these temperature gradients are in some cases more pronounced in underfloor configuration than the overhead supply design.

Similar studies were presented by Sorell et al. [17], Herrlin and Belady [18], and Mulay et al. [19] to compare the underfloor supply configuration with overhead supply configuration. Sorell et al. [17] were in agreement with Herrlin and Belady [18] that the underfloor supply can result in hot spots at the top of server racks due to severe recirculation patterns. The overhead supply design eliminates this drawback as the supplied air from top provides good mixing. Mulay et al. [19-21] presented the study of the two supply configurations in liquid cooling environment. Their observations that the underfloor supply configuration is preferred for high power clusters over the overhead supply even in the liquid cooling environment, agree with Schmidt and Iyengar.

A cooling technique requiring the control mechanism inside the racks was presented by Furihata et al. [22] and Hayama et al. [23,24]. The control mechanism would monitor the temperature of exhaust air and then would adjust the airflow to yield the uniform temperature of the air exiting from servers. This technique resulted in reduction of airflow while providing adequate cooling to the servers.

In general, there is a strong consensus about the cold aisle-hot aisle layout. Beaty and Davidson [25,26], Beaty and Schmidt [27] recommend that the racks should be laid out in cold aisle-hot aisle arrangement with racks drawing the air from cold aisle and release the hot air into hot aisle. Also, directing the hot air towards ceiling would be much better than simply having the high ceilings as observed by Beaty and Davidson [25]. Mulay et al. [28] presented the cabinet designs that agree with Beaty and Davidson [25].

2.2 The Structural parameters

The structural parameters that can affect the airflow distribution are the plenum depth, the % opening of the perforated tiles and the ceiling height. The plenum depth (the height to which the floor is raised) and the open area of a perforated tile are the crucial factors in determining the underfloor pressure distribution. The ceiling height may very well depend on the cooling configuration and may affect the scheme if not properly optimized.

2.2.1. The Plenum Depth

With increased plenum depth, the velocities are reduced which leads to more uniform subfloor pressure and subsequently uniform airflow distribution. A study conducted by Kang et al. [29] demonstrates the accuracy of pressurized plenum model with reference to CFD analysis. The CFD analysis of recirculating flow under plenum also indicates the limitations of validity of above mentioned pressurized plenum model. Authors have used flow network modeling technique to predict flow rates of perforated tiles.

Karki et al. [30] presented the simulations of raised floor configuration with 25% open perforated tiles. They showed that relatively low plenum depth of up to 1 ft may lead to reverse flow near the CRAC units in some cases. However when plenum depth is increased, the reverse flow is eliminated. Also, the flow variations across the tiles are reduced. Patankar and Karki [31], Beaty and Davidson [26] present the cases that suggest a plenum depth with obstruction free height of 2 ft. The plenum depth of 2 ft recommended by VanGilder and Schmidt [32] also falls in line with the suggestions by others as mentioned above.

Bhopte et al. [33] proposed multi-variable approach to achieve optimal layout that will yield minimum rack inlet temperature. Authors discussed effect of plenum depth, floor tile placement and ceiling height on rack inlet temperature. These variables are used in multi-variable optimization approach to study their interaction and the combined effect on the airflow distribution. The results are presented in the form of guidelines for optimal data center layout. These guidelines confirm that the airflow distribution becomes more uniform with increased plenum depth.

2.2.2. The Ceiling Height

The ceiling height among other factors is dependent on the type of cooling configuration employed in the data center. A study performed by Schmidt [34] indicated the development of the hot spots over the racks where perforated tiles failed to deliver or exceed the required flow rate. For the underfloor supply configuration, these hot spots became more intense with the increased ceiling height. The increased ceiling heights lead to increased rack inlet temperatures.

In his parametric study, Shrivastava et al. [35] found out that the increased ceiling height have immense impact in the hot spot when reductions up to 12°C were reported. The impact of ceiling height was however minimal in the areas of low flux regions. In another study

[36], the authors reported no impact on rack inlet temperatures when the ceiling height of a data center with underfloor supply and the room CRAC return was increased beyond 12 ft.

Sorell et al. [37] presented the three cases of cooling configurations with three different ceiling heights. The three configurations were underfloor supply with and without ceiling return and the overhead supply. The authors reported that with CRACs at 110%, increasing the ceiling height from 12 ft to 16 ft improved the performance of all the three data centers. They also drawn the attention to the fact that increased ceiling height may lead to increased building costs.

2.2.3. The Perforated Tiles

Schmidt [38] presented empirical and flow modeling data and a methodology to thermally characterize a data center. IT equipment power usage, airflow exiting perforated tiles, leakage flow escaping from cable cutouts, CRAC airflow and air inlet temperatures were recorded for a 74 ft x 84 ft data center. Another study by Radmehr et al. [39] is focused on distributed leakage flow in raised floor data centers. The authors have outlined the procedure to measure airflow that escapes through the seams between panels, cable cut-outs and other gaps. The data is used to show the relationship between leakage area and the leakage flow. Authors reported leakage flow to be about 5-15 % of the available cooling air.

Schmidt and Iyengar [40] measured IT equipment power usage, airflow exiting perforated tiles, leakage flow escaping from cable cutouts, and CRAC airflow and air inlet temperatures of three different data centers to study the patterns that will be helpful guidelines on data center layout. VanGilder and Schmidt [32] through the simulations of numerous raised floor data center models quantified the impact of different parameters on the airflow distribution. They studied the factors such as underfloor blockages, tile layout, leakage flow and the total airflow rate.

Bhopte et al. [41] presented a CFD model to demonstrate impact of underfloor blockages on tile flow rates and rack inlet temperatures. They presented a parametric study identifying locations under floor where blockages if installed, will have minimal effect on data center performance. Based on their case studies, authors have presented guidelines on rearranging the blockages and still achieving improved performance.

2.3 The Placement of the CRAC Units

The location of CRAC unit is an important factor in deciding the sub floor pressure distribution and will affect the airflow distribution in cold aisles. It has the potential of being the largest contributor to the energy inefficiency of the data center. Schmidt et al. [42] observed that the tuning vanes and baffles appeared to reduce the CRAC flow rate by 15%.

Koplin [43] in his study indicated that the CRAC units should deliver the air in a way that will increase the sub floor pressure. When CRAC units are installed in parallel, they should not be so aligned that the plumes after delivery are colliding with one another causing loss of static pressure. The study by Schmidt and Iyengar [44] agrees with this observation.

The work of Beaty and Davidson [26] and Schmidt and Iyengar [44] indicated the low inlet temperatures for those racks which have clear path for hot air from racks to the CRACs. They also recommended placing the CRAC facing hot aisles rather than facing the cold aisles.

2.4 The Energy Management of the Data Centers

The increased energy consumption has equally opened up more opportunities for energy savings and efficient operations of the data centers. In their design guidelines, the PG & E [45] discuss among other things on airside and waterside economizers, centralized air handling and liquid cooling. They have established the guidelines and some of these guidelines are discussed below.

2.4.1. The Airside Economizer

An airside economizer uses outside air for cooling the data center when outside temperature is less than or equal to supply temperature. The cooler outer air is brought in and the hot air is exhausted into the ambient. In their proof of concept test, Intel IT has been running 900 production servers at very high rate of utilization [46]. This high density data center used 100% air exchange at 90°F and without humidity restrictions. The filtration was kept at the minimal level. It was estimated that with economizer in use 91% of the time, 67% energy can be saved which is estimated at USD 2.87 million in a 10MW data center. The proof of concept test by Intel also showed no significant rise in server failure rates when air side economizer is used.

A study by Shehabi et al. [47] compares the energy implications of conventional data centers with newer technologies employing waterside and air side economizers in five different climate zones in the state of California. They report that airside economizer performs consistently better in all climate zones. In fact according to another study by Syska Hennessy Group [48], outside air can be used for almost entire year in San Francisco.

2.4.2. The Waterside Economizer

The waterside economizer uses the evaporative cooling capacity of a cooling tower and indirectly produces chilled water for data center cooling. Shehabi et al. [47] in their study compared the five locations in California to judge the impact of waterside economizer. They observed that Sacramento has more potential benefits from waterside economization as compared to Los Angeles or San Francisco. The latent heat of the moisture content in San Francisco was overloading a chiller causing another chiller to start to operate.

2.4.3. The Centralized Air Handling

The centralized air handling units offer following advantages over the conventional CRAC units:

1. They can be placed at some other locations than the data center rooms thus freeing the space for IT equipment.
2. The sizing of centralized air handling unit can be designed to handle redundancy and reliability of operation.
3. The larger fans and equipment yield better efficiency.
4. The centralized systems have better part load efficiencies than the conventional CRAH units.

These centralized air handlers are ideal for the use of variable frequency drives which enhances the part load efficiency.

2.4.4. Liquid Cooling

Liquid cooling systems are also studied. Schmidt et al. [48] reported the design of water cooled rear door heat exchanger aimed to reduce exhaust air temperature in high density racks. The impedance of rear door heat exchanger was reported to be matching with that of IBM standard rear door thereby eliminating the need of extra fans. Mulay et al. [19-21] in their studies studied the liquid cooling in data center for high powered clusters. They used different airflow supply fractions to study the impact of rear door heat exchanger. They also studied the deployment of rear door heat exchangers in both the overhead and the underfloor supply configuration for high power density clusters. The rear door heat exchanger was found to be dissipating up to 55% of the heat.

The HP Modular Cooling Solution as described in its Technology Brief [49], has three air to liquid heat exchangers and three hot swap blowers which are mounted on the side of standard rack. The studies indicating substantial savings by the use of the liquid cooling in addition to the air cooling have been presented by Patel et al. [50], Schmidt et al. [48] and Leonard and Philips [51].

2.4.5. The Dynamic Cooling

Patel et al.[52] introduced the concept of “Smart Cooling” by associating the local cooling to the work load allocation. With this holistic approach of cooling ensemble, the data centers would operate at the highest efficiency levels. Bash et al. [53] presented a distributed network of temperature sensors to provide real time feedback to central controller. Rack inlet temperature at each rack is sensed. The temperature data is then used by controller to control the CRACs. This “Dynamic Smart Cooling” is shown to reduce power consumption.

Patel et al. [54] also discussed CRAC sizing and load balancing, rack layout and the load distribution. In the study, authors present the impact of the non-uniform nature of the heat load on the energy efficiency. The dynamic virtual data center and the algorithms to control the thermal management were presented by White and Abels [55].

CHAPTER 3

THE COOLING STRATEGIES

3.1 Liquid Cooling in Data Center

Most of the data centers use hot aisle – cold aisle layout in an attempt to isolate chilled air supply from hot air. The front face of rack, which generally is air inlet for the equipment, is placed facing perforated tiles. The backside of rack from where hot air exhausts, faces backside of another rack forming a hot aisle. In a large data center with such an arrangement, zones with very high heat load may exist due to use of high performance equipments. Airflow requirements for such high performance racks lies within 1500 to 3500 cfm (0.7 to1.4 m^3/s). These requirements become difficult to meet when packaging density is very high. The inability of underfloor configuration to have flexibility of entry points for chilled air compounds the problem. This results in fractional supply of chilled air to racks causing severe recirculation. The hot air exiting in hot aisle is then drawn to the cold aisle and it makes up for shortage of supply. This leads to complex flow patterns and unusually high inlet temperatures.

3.1.1. Rear Door Heat Exchanger

The high temperature gradients at inlet indicate ineffectiveness of air cooling for high powered clusters. A hybrid cooling solution that consists of air cooling assisted by a liquid to air heat exchanger can be effective in such cases. A method to reduce the effect of the hot air recirculation in a data center is to use water cooled heat exchanger attached to the rear door of the rack. The heat exchanger removes a large portion of the heat from the rack as well as significantly lowering the air temperature exhausting the rear of the rack. The heat exchanger can be comprised of a conventional fin and tube design or a plate fin and flat tube "radiator"

type design. The heat exchanger is of a planar geometry and aligns with the rear of the frame and receives hot exhaust air at its inlet for one coolant stream (hot). For the cold coolant stream the heat exchanger received chilled water. Flexible hose lines couple the heat exchanger to inlet and exit water plumbing headers. The objective of this study is to understand the effects on flow patterns, recirculation and mixing of hot and cold air and eventually on the temperature gradients at inlet if hybrid solution as shown in Fig. 3.1 is employed in high heat flux situations.

Figure 3.1 IBM's Rear Door Heat Exchanger [113]

3.2 Data Center with Underfloor Supply Configuration

3.2.1. Computational Modeling

Because of the typical flow rates and the sizes involved, the flow is turbulent and the effect of turbulent mixing is modeled using the two equations k- ε model for above the floor. The k- ε model is the most appropriate for large, open spaces because of the way it calculates the turbulent viscosity and conductivity. This model computes viscosity on a grid cell per grid cell

basis rather than computing viscosity as it is effected by the walls used more appropriately in smaller space type problems. The field variables in the fluid flow are described by the following governing equations of the fluid flow [*].

Continuity:

$$\frac{\partial \rho}{\partial t} + \vec{\nabla} \cdot (\rho \vec{u}) = 0$$

Conservation of Momentum:

$$\rho \frac{\partial \vec{u}}{\partial t} + \rho \vec{u} \cdot \vec{\nabla} \vec{u} = -\vec{\nabla} P + \vec{\nabla} \cdot \tau + (\rho - \rho_\infty) g$$

Conservation of Energy:

$$\rho \frac{\partial e}{\partial t} + \rho u \cdot \vec{\nabla} e = \nabla \cdot (\lambda \nabla T) - P(\nabla \cdot u)$$

These governing equations are solved for the field variables which are the pressure, temperature, density and the velocity. For a three dimensional incompressible flow, the above governing equations take the following form.

Continuity:

$$\frac{\partial u_x}{\partial x} + \frac{\partial u_y}{\partial y} + \frac{\partial u_z}{\partial z} = 0$$

Conservation of Momentum:

$$\rho \left(\frac{\partial u_x}{\partial t} + \frac{\partial u_x}{\partial x} u_x + \frac{\partial u_x}{\partial y} u_y + \frac{\partial u_x}{\partial z} u_z \right) = \left(\frac{\partial \sigma_x}{\partial x} + \frac{\partial \tau_{xy}}{\partial y} + \frac{\partial \tau_{xz}}{\partial z} \right) + f_x$$

$$\rho \left(\frac{\partial u_y}{\partial t} + \frac{\partial u_y}{\partial x} u_y + \frac{\partial u_y}{\partial y} u_y + \frac{\partial u_y}{\partial z} u_y \right) = \left(\frac{\partial \sigma_y}{\partial y} + \frac{\partial \tau_{yx}}{\partial x} + \frac{\partial \tau_{yz}}{\partial z} \right) + f_y$$

$$\rho \left(\frac{\partial u_z}{\partial t} + \frac{\partial u_z}{\partial x} u_z + \frac{\partial u_z}{\partial y} u_z + \frac{\partial u_z}{\partial z} u_z \right) = \left(\frac{\partial \sigma_z}{\partial z} + \frac{\partial \tau_{zy}}{\partial y} + \frac{\partial \tau_{zx}}{\partial x} \right) + f_z$$

Where,

$$\sigma_i = -p + 2\mu \frac{\partial u_i}{\partial i}$$

$$\tau_{ij} = \mu \left(\frac{\partial u_i}{\partial j} + \frac{\partial u_j}{\partial i} \right)$$

Conservation of Energy:

$$\rho\frac{DE}{DT} = -div(\rho\vec{u}) + \begin{bmatrix} \frac{\partial(u\tau_{xx})}{\partial x} + \frac{\partial(u\tau_{zy})}{\partial y} + \frac{\partial(u\tau_{xz})}{\partial z} + \frac{\partial(v\tau_{xy})}{\partial x} + \frac{\partial(v\tau_{yy})}{\partial y} \\ + \frac{\partial(v\tau_{yz})}{\partial z} + \frac{\partial(w\tau_{xz})}{\partial x} + \frac{\partial(w\tau_{yz})}{\partial y} + \frac{\partial(w\tau_{zz})}{\partial z} \end{bmatrix} + div(kgradT) + S_E$$

Icepak [114], a commercially available CFD tool is used to construct the k- ε model representing data center. The two-equation turbulence model (also known as the standard k- ε model) is more complex than the zero-equation model. The standard k- ε model [115] is a semi-empirical model based on model transport equations for the turbulent kinetic energy (k) and its dissipation rate (ε). The model transport equation for k is derived from the exact equation, while the model transport equation for ε is obtained using physical reasoning and bears little resemblance to its mathematically exact counterpart. In the derivation of the standard k-e model, it is assumed that the flow is fully turbulent, and the effects of molecular viscosity are negligible. The standard k- ε model is therefore valid only for fully turbulent flows. The transport equations [116] are as follows:

$$\frac{\partial}{\partial t}(\rho k) + \frac{\partial}{\partial x_i}(\rho k u_i) = \frac{\partial}{\partial x_i}\left[\left(\mu + \frac{\mu_t}{\sigma_k}\right)\frac{\partial k}{\partial x_i}\right] + G_k + G_b - \rho\varepsilon$$

$$\frac{\partial}{\partial t}(\rho\varepsilon) + \frac{\partial}{\partial x_i}(\rho\varepsilon u_i) = \frac{\partial}{\partial x_i}\left[\left(\mu + \frac{\mu_t}{\sigma_\varepsilon}\right)\frac{\partial\varepsilon}{\partial x_i}\right] + C_{1\varepsilon}\frac{\varepsilon}{k}(G_k + C_{3\varepsilon}G_b) - C_{2\varepsilon}\rho\frac{\varepsilon^2}{k}$$

In these equations, G_k represents the generation of turbulent kinetic energy due to the mean velocity gradients, calculated as described later in this section. G_b is the generation of turbulent kinetic energy due to buoyancy, calculated as described later in this section.$C_{1\varepsilon}$, $C_{2\varepsilon}$, and $C_{3\varepsilon}$ are constants. σ_k and σ_ε are the turbulent Prandtl numbers for k and ε, respectively.

The half symmetry model of data center “cell” has 40 racks arranged in cold aisle – hot aisle layout as shown in Fig. 3.3.From Fig. 3.3, the footprint dimensions of the half-symmetry “cell” are 20ft (6.09 m) by 44 ft (13.42 m), and the room was 10 ft (3.048 m) tall. The computer racks were assumed to be one

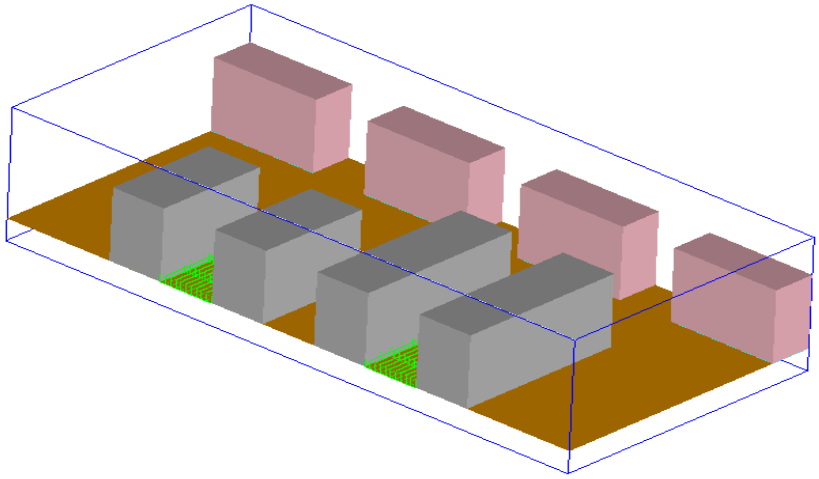

Figure 3.2 Underfloor Supply: A CFD Model of the Representative Data Center.

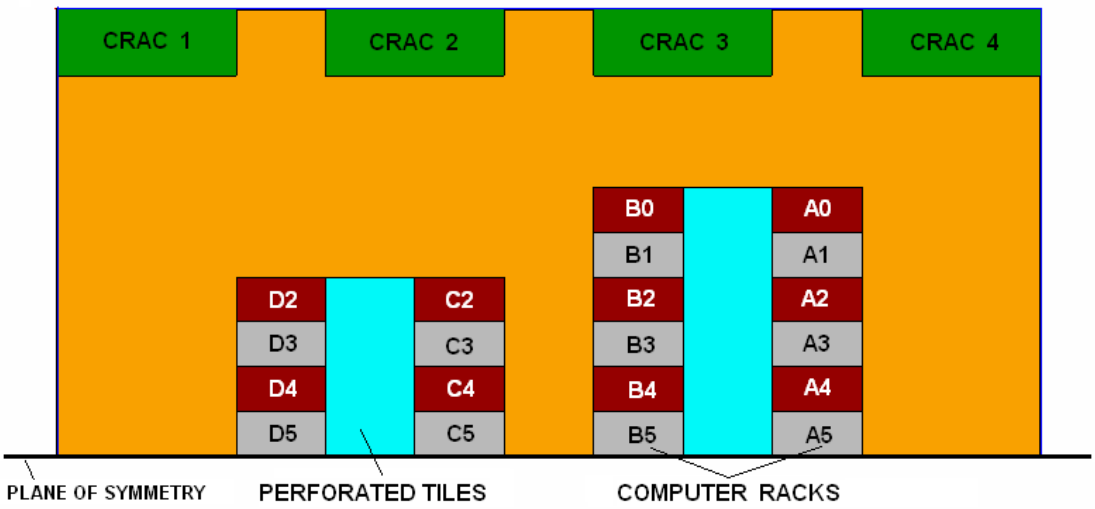

Figure 3.3 Underfloor Supply: Layout of the Representative Data Center.

tile wide (0.61 m or 2 ft.), two tiles deep (1.22 m or 4 ft.), and 1.8 m (6 ft) tall. The air-moving device inside the racks is assumed to force air straight through the rack, with a constant velocity across the front and back of the racks. Each rack is assumed to be a high-performance 32 kW (109,194 Btu/h) rack, with a rack airflow rate of 2905 cfm (1.371 m^3/s). This corresponded to an air temperature rise through the rack of 20°C (36°F). The temperature of the chilled air entering the room through the perforated tiles was fixed at 13°C (56°F). The CRAC unit had a 3 ft × 8 ft (0.91 m x 2.44 m) footprint and was 1.8 m (6 ft) high. Figure 5 shows the racks to be arranged in four rows, A, B, C, and D, respectively, with A0, B0, C2,and D2 being closest to the CRAC units and A5,B5, C5 and D5 located farthest away from the CRAC units. The rear door heat exchanger was modeled using heat exchanger macro in Icepak software [8]. The temperature of chilled water entering into the heat exchanger was set at 18°C. The conductance of heat exchanger which is product of effectiveness and smaller of the two heat capacities was set to 650 W/K which is representative value for such generic heat exchangers. Since the rack inlet temperature varies along the height of rack, heat exchanger was made of six different strips to capture the performance according to varying inlet conditions.

Three various openings are considered for perforated tiles. In CFD analysis of data center, the volumetric flow through perforated tiles is often assumed to be uniform for model simplification. In real situations however, the flow is not uniform and there exists a “maldistribution” at perforated tiles. Schmidt and Iyengar observed in their recent study that temperature difference across CRAC in hot spot regions were as high as 24°C [5]. The brick walling of very high heat load racks and local deficiency of CRAC capacity in such regions are the factors responsible for such temperature difference. The effect of using rear door heat exchanger in such regions is simulated in this study. Three different cases of chilled air supply are considered with CRAC units supplying 60%, 80% and 100% of rack airflow requirement. For each air supply fraction, heat exchangers were employed at all the racks. Three tile openings namely 25%, 50% and 75% were chosen for the parametric study.

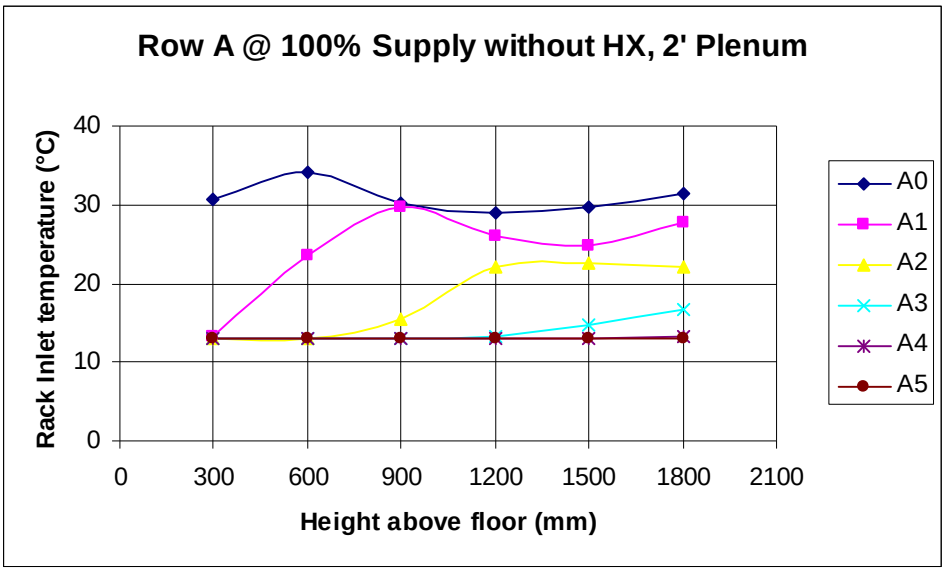

Figure 3.4 Underfloor Supply: Rack Inlet Temperature Variation at racks in Row A for 100% chilled air supply for 25% Tile Opening.

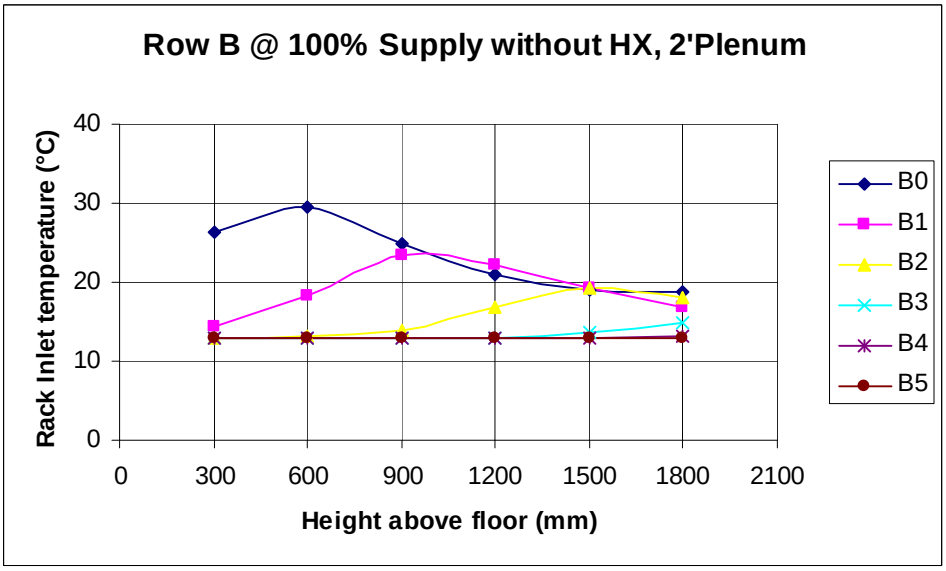

Figure 3.5 Underfloor Supply: Rack Inlet Temperature Variation at racks in Row B for 100% chilled air supply for 25% Tile Opening.

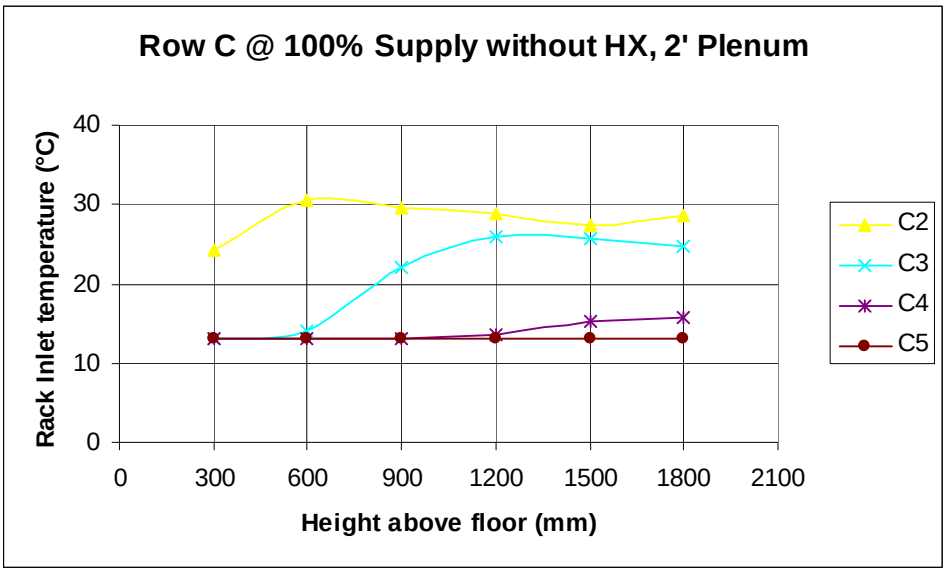

Figure 3.6 Underfloor Supply: Rack Inlet Temperature Variation at racks in Row C for 100% chilled air supply for 25% Tile Opening.

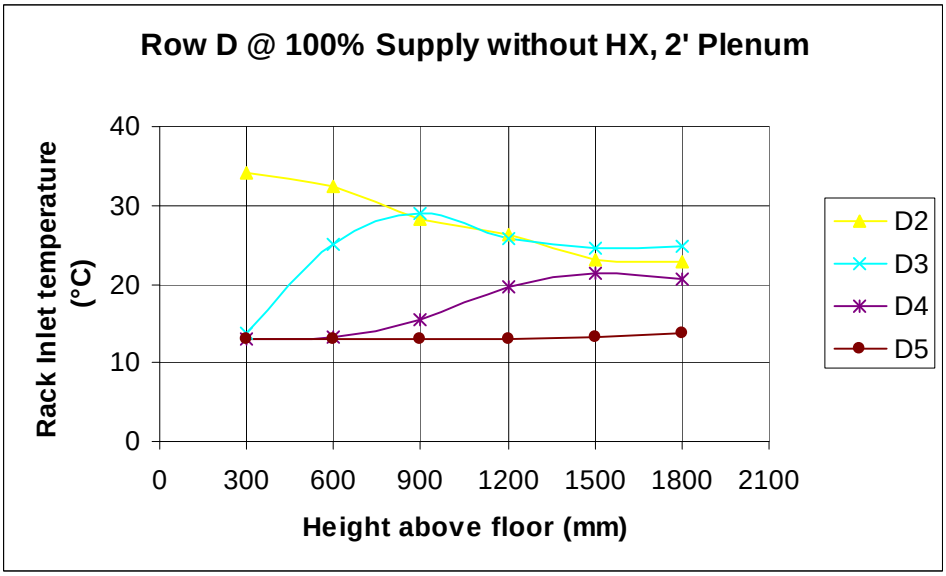

Figure 3.7 Underfloor Supply: Rack Inlet Temperature Variation at racks in Row D for 100% chilled air supply for 25% Tile Opening.

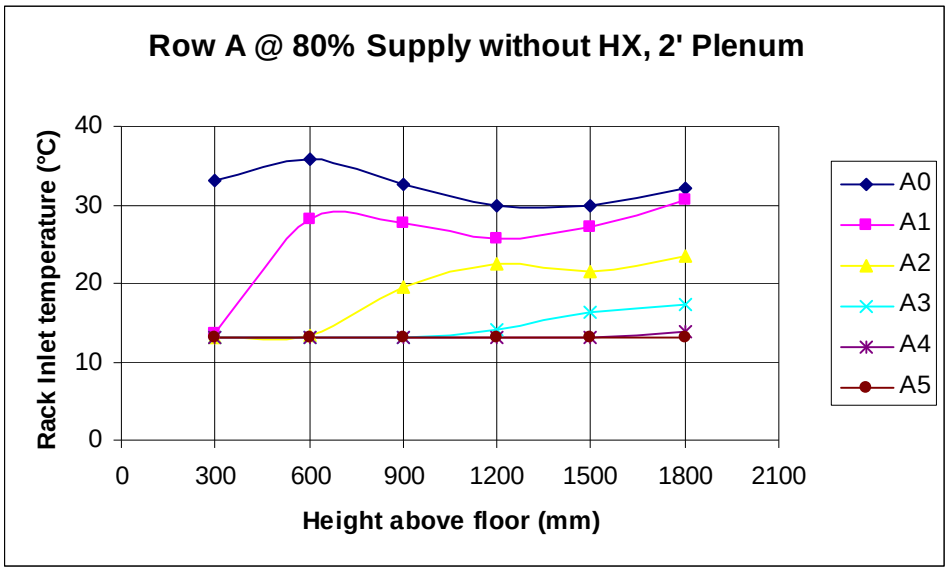

Figure 3.8 Underfloor Supply: Rack Inlet Temperature Variation at racks in Row A for 80% chilled air supply for 25% Tile Opening.

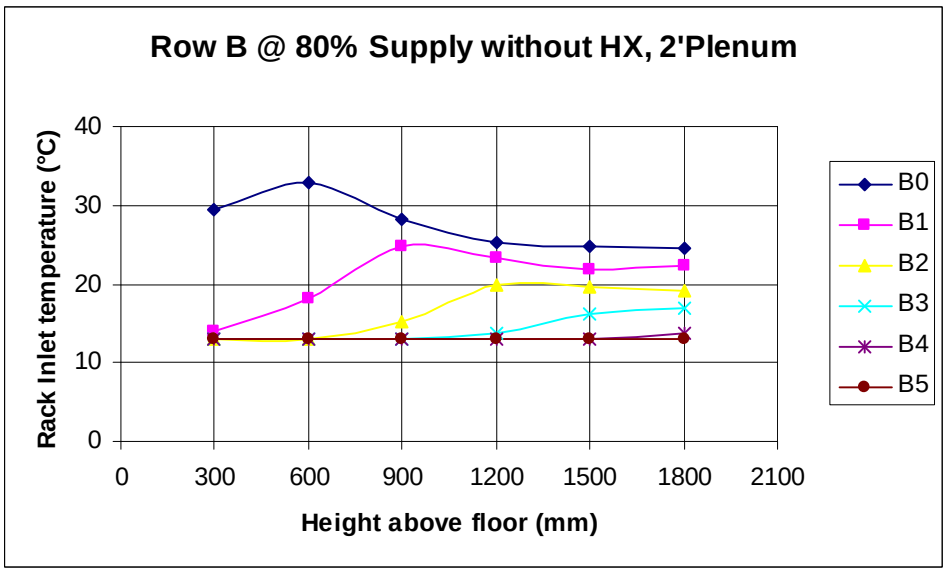

Figure 3.9 Underfloor Supply: Rack Inlet Temperature Variation at racks in Row B for 80% chilled air supply for 25% Tile Opening.

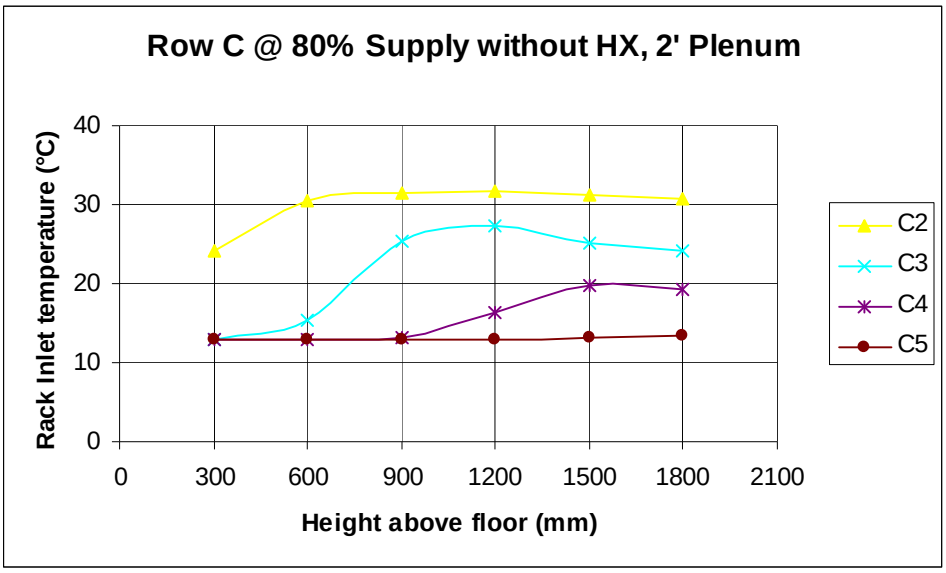

Figure 3.10 Underfloor Supply: Rack Inlet Temperature Variation at racks in Row C for 80% chilled air supply for 25% Tile Opening.

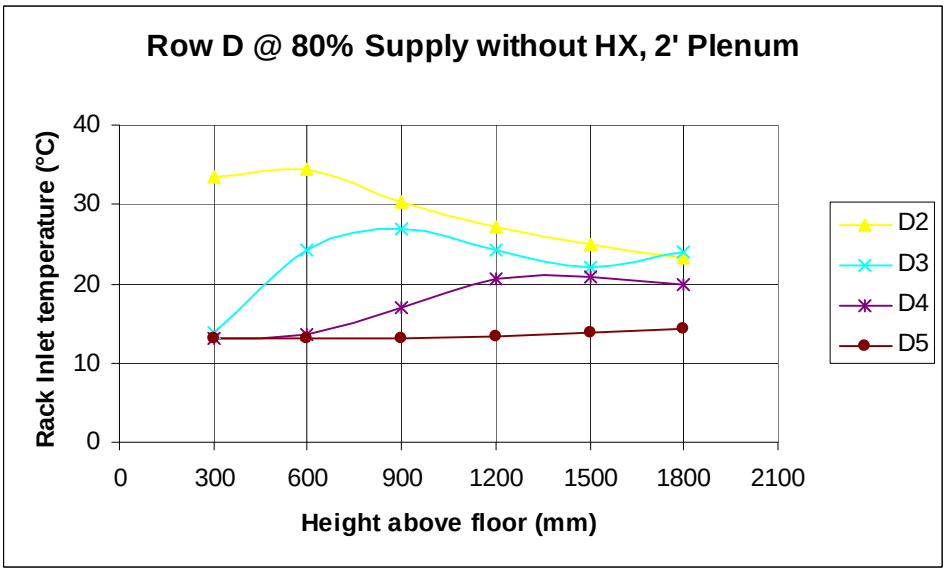

Figure 3.11 Underfloor Supply: Rack Inlet Temperature Variation at racks in Row D for 80% chilled air supply for 25% Tile Opening.

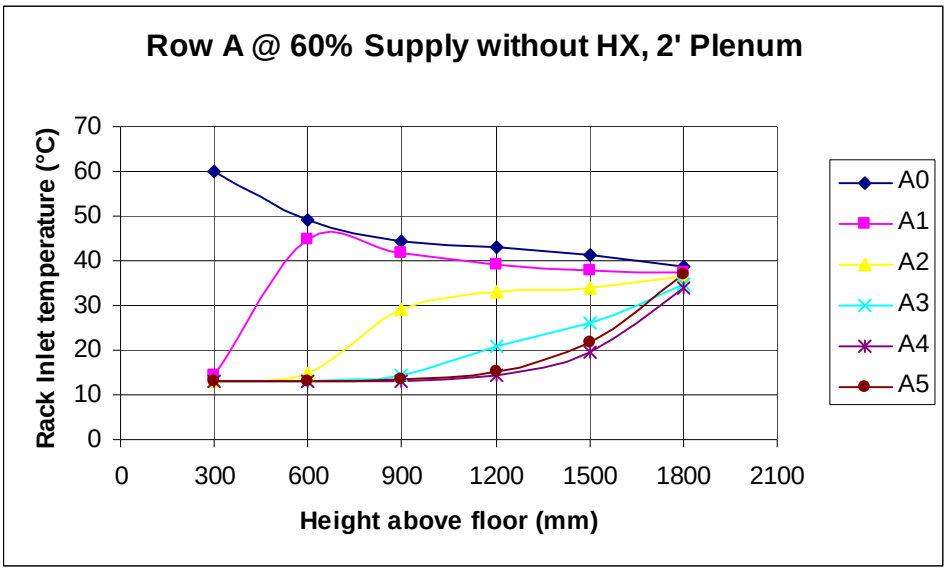

Figure 3.12 Underfloor Supply: Rack Inlet Temperature Variation at racks in Row A for 60% chilled air supply for 25% Tile Opening.

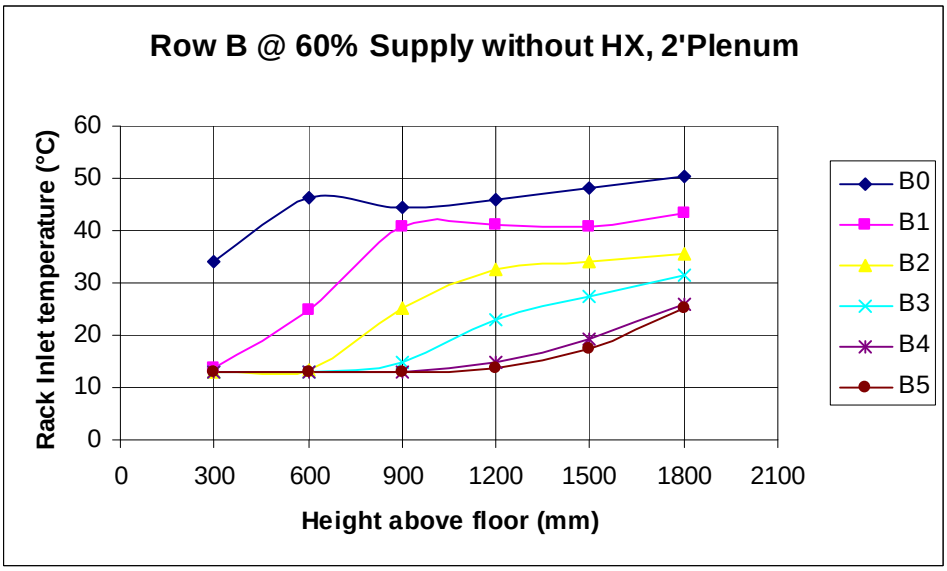

Figure 3.13 Underfloor Supply: Rack Inlet Temperature Variation at racks in Row B for 60% chilled air supply for 25% Tile Opening.

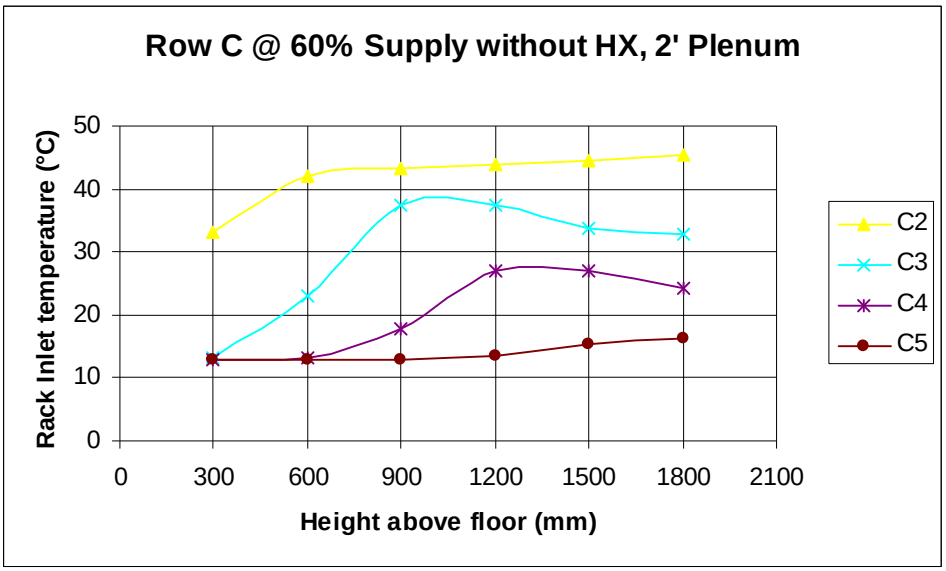

Figure 3.14 Underfloor Supply: Rack Inlet Temperature Variation at racks in Row C for 60% chilled air supply for 25% Tile Opening.

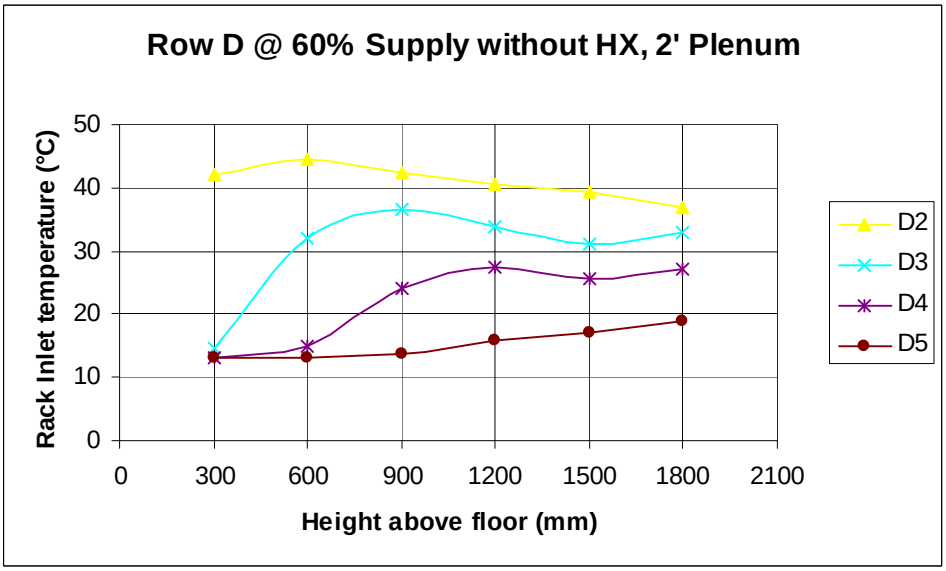

Figure 3.15 Underfloor Supply: Rack Inlet Temperature Variation at racks in Row D for 60% chilled air supply for 25% Tile Opening.

In CFD model, symmetry boundary condition was applied to the wall touching the racks. The elements count was within 300,000 to 700,000. On a PC with Pentium D, 2.8GHz processor and 4 GB RAM, convergence for temperature and continuity was satisfactorily achieved in about 2000 iterations within 8-10 hours. For each rack, inlet temperature was monitored at 300mm, 600mm, 900mm, 1200mm, 1500mm and 1800mm above floor level.

Figures 3.4 through 3.15 show the temperature variation for the cases of 60%, 80% and 100% air supply with 25% tile opening and without any heat exchanger. Racks A0, B0, C2, and D2 are referred to as outside racks, and racks A5, B5, C5, and D5 are referred to as inside racks. Figures 3.4-3.7 show the trends for all the racks for 100% air supply. Figures 3.8-3.11 and 3.12-3.15 indicate the same information for the cases of 80% air supply and 60% air supply respectively. The key observations are summarized below.

3.2.2. Recirculation and Ambient Mixing of Air

For all the cases, large temperature gradients exist at outside racks. Severe recirculation pattern is observed at outside racks as hot air exiting into hot aisle is drawn into cold aisle from the side as well as from top of the racks. For inner racks, although hot and cold air mixing is present, it is less than the outside racks as the air is only drawn from top. The case of 60% air supply represents the worst case scenario for a data center as highest inlet temperatures are monitored for this case. Similar trends are observed for 80% air supply.

3.2.3. The Effect of the Modeling Level

As stated earlier, data center simple CFD models assume uniform air flow by eliminating under floor plenum and replacing perforated tiles with fixed flow devices. This assumption of uniform flow however, does not exist in reality due to complex flow patterns and under floor fluid dynamics [*]. The volumetric flow through each tile may be different and there is “maldistribution” of cold air across cold aisle. Figure 3.16 shows temperature solution of simple

model for 60% air supply. Figure 3.17 depicts the same information for the detailed model where underfloor plenum of 2 ft depth is modeled with 25% open perforated tiles. It can be seen that the global temperature results obtained by simple model or the uniform flow assumption are almost 10% lower.

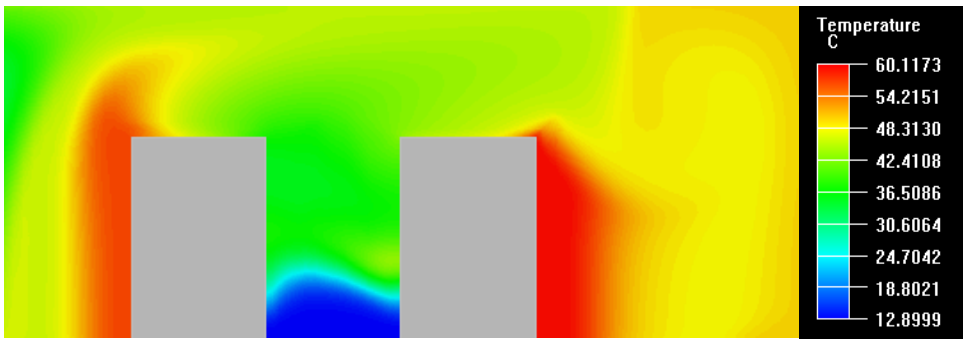

Figure 3.16 Underfloor Supply: Thermal Profile of Simple Model with 60% Supply.

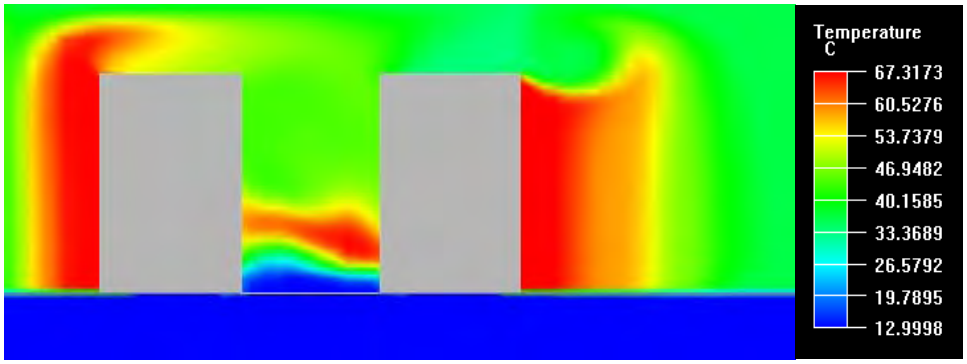

Figure 3.17 Underfloor Supply: Thermal Profile of Detailed Model with 60% Supply.

3.2.4. The Effect of the Liquid Cooling

The temperature variation at outside and inside racks is presented in figs. 3.18 through 3.25 for the 25% open tiles. Severe recirculation exists at outside racks which results in ambient mixing causing high inlet temperatures. These outside racks therefore become prime target for employment of hybrid cooling solution, that is air cooling assisted by liquid cooling. From graphs it is clear that significant temperature reduction occurs at number of monitor points. Reduction

at outer racks is mostly prominent than the reduction at inner racks. For 60% air supply case, the maximum reduction in rack inlet temperature was found to be 18.7°C.

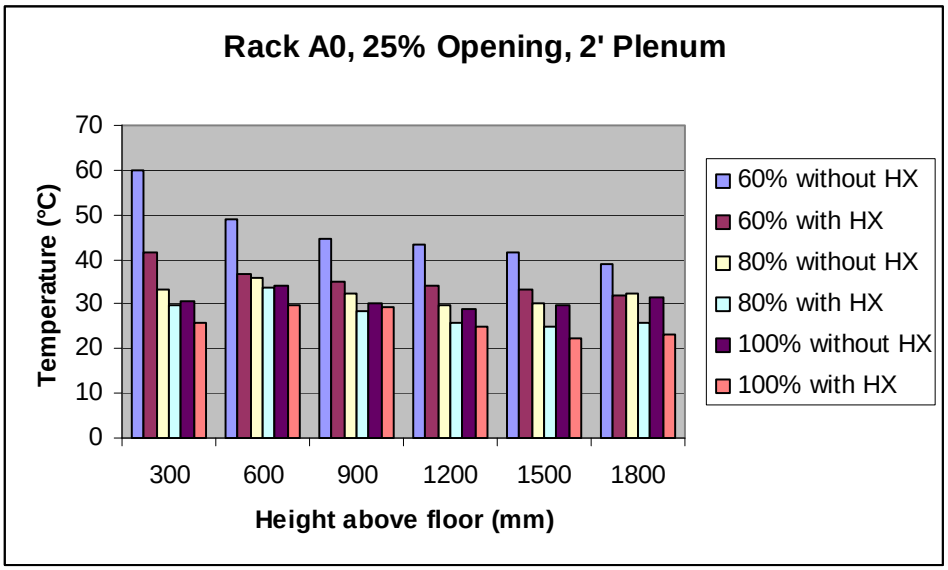

Figure 3.18 Underfloor Supply: Comparisons of Rack Inlet Temperatures at Rack A0.

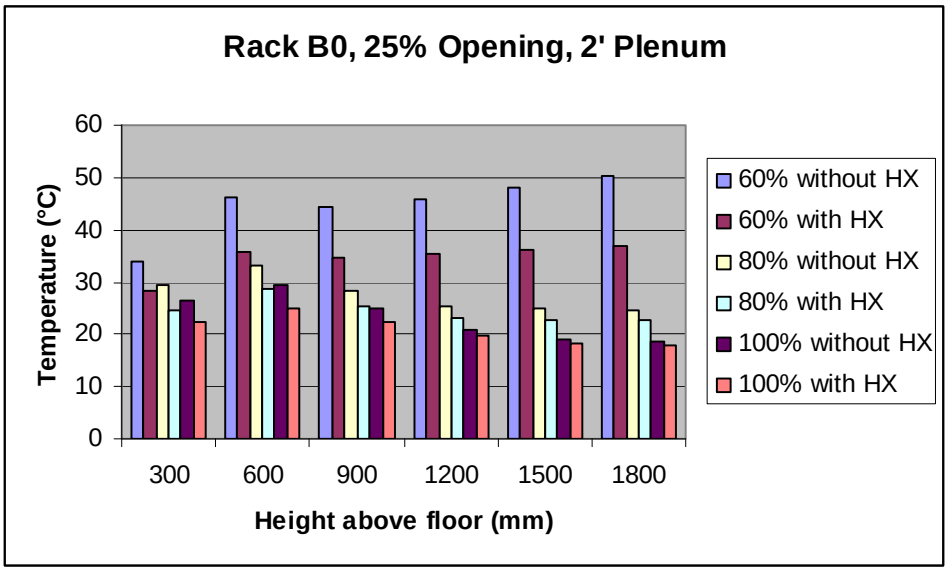

Figure 3.19 Underfloor Supply: Comparisons of Rack Inlet Temperatures at Rack B0.

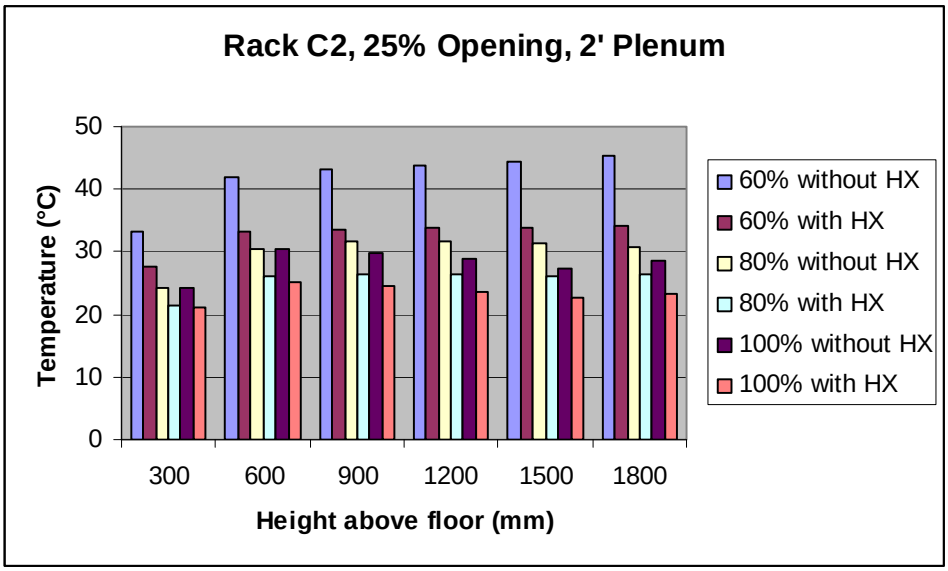

Figure 3.20 Underfloor Supply: Comparisons of Rack Inlet Temperatures at Rack C2.

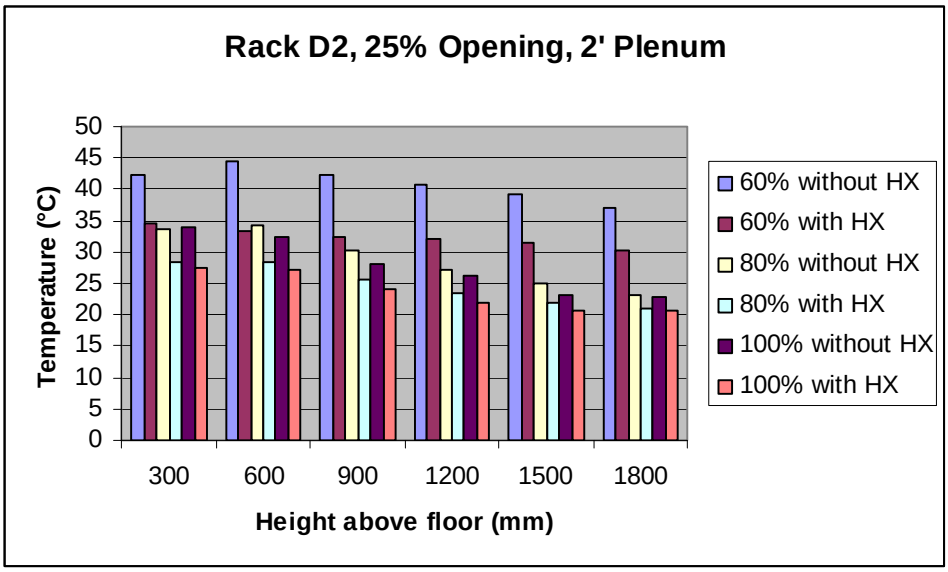

Figure 3.21 Underfloor Supply: Comparisons of Rack Inlet Temperatures at Rack D2.

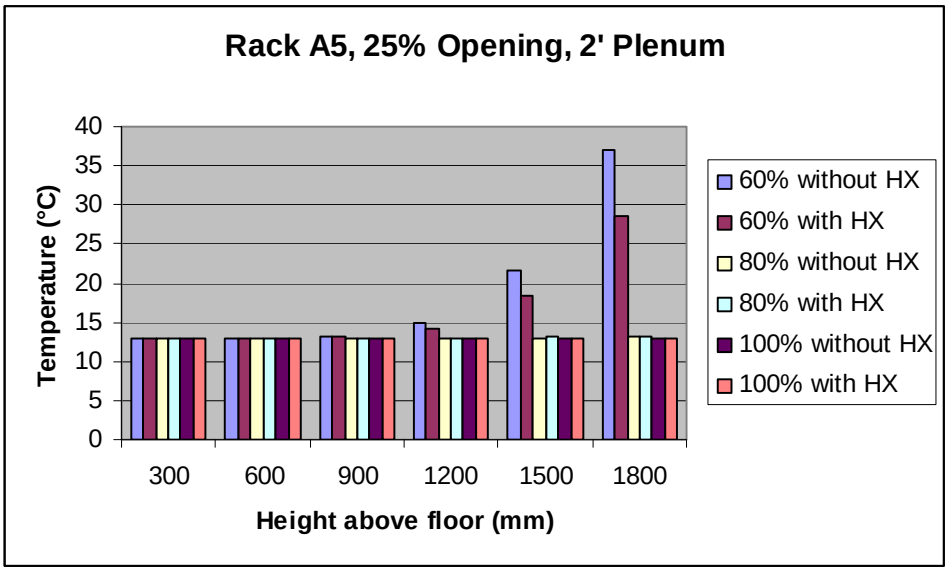

Figure 3.22 Underfloor Supply: Comparisons of Rack Inlet Temperatures at Rack A5.

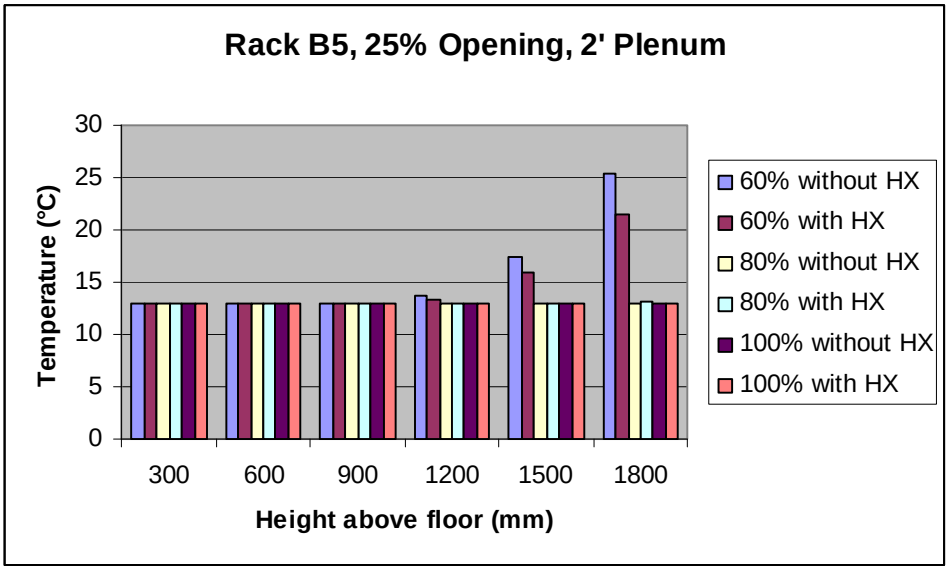

Figure 3.23 Underfloor Supply: Comparisons of Rack Inlet Temperatures at Rack B5.

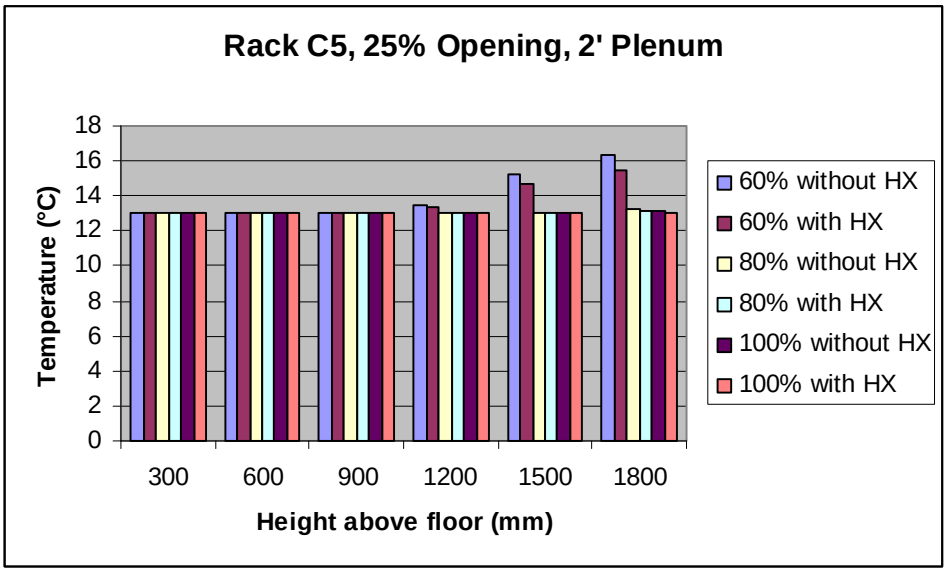

Figure 3.24 Underfloor Supply: Comparisons of Rack Inlet Temperatures at Rack C5.

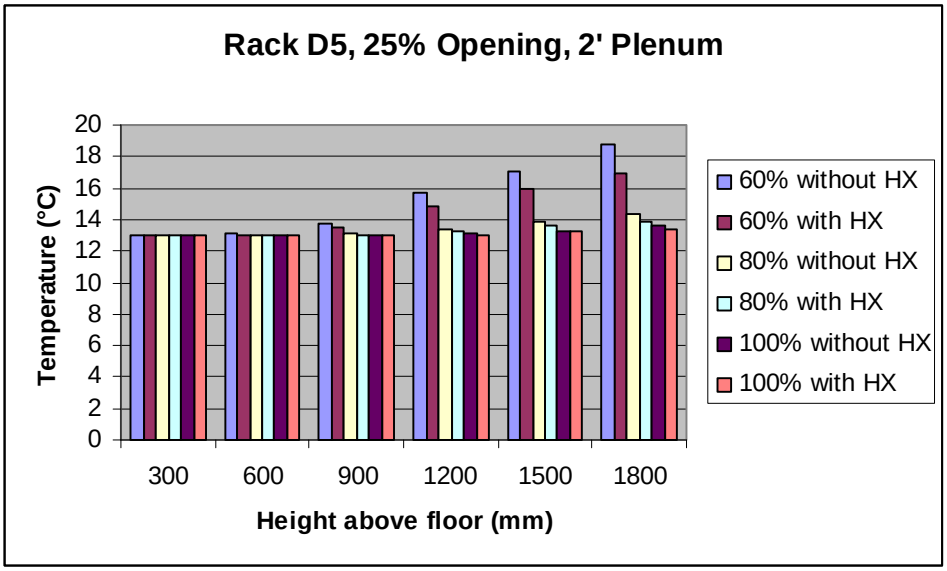

Figure 3.25 Underfloor Supply: Comparisons of Rack Inlet Temperatures at Rack D5.

3.2.5. The Impact of the Rear Door Heat Exchanger

The impact of rear door heat exchanger solution is summarized in fig. 3.26 for different air supply fractions. For 60% air supply case, the heat exchanger removes 55% of the total 32KW heat while reducing the rack inlet temperature by 18.7°C. For the cases of 80% and 100% supply, the heat removal is 43% and 38% respectively and the maximum reduction in rack inlet temperature 8.3°C and 7.3°C respectively.

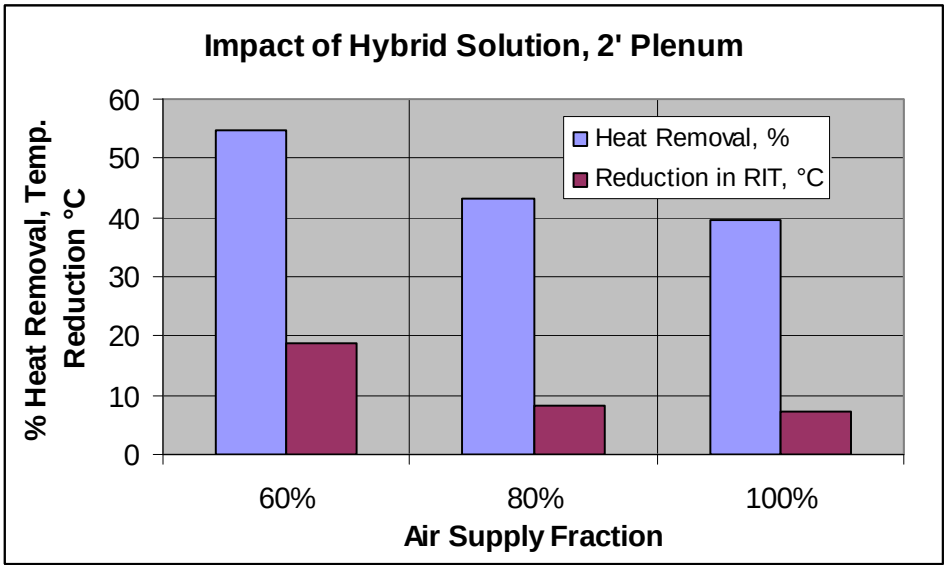

Figure 3.26 Underfloor Supply: The Impact of the Rear Door Heat Exchanger for the Plenum of 2 ft.

Fig. 3.27 indicates the heat removal percentages and reduction in rack inlet temperatures for 60%, 80% and 100% air supply cases for the data center model with 3 ft plenum. For 60% case, the values are almost identical as those recorded in case of 2 ft plenum (53.3% heat removal, 18.7°C reduction). However, there is reduction in the heat removal and the temperature reduction values for higher supply fractions. The 3 ft plenum yields lower % of heat removal at higher supply fractions as compared to 2 ft plenum.

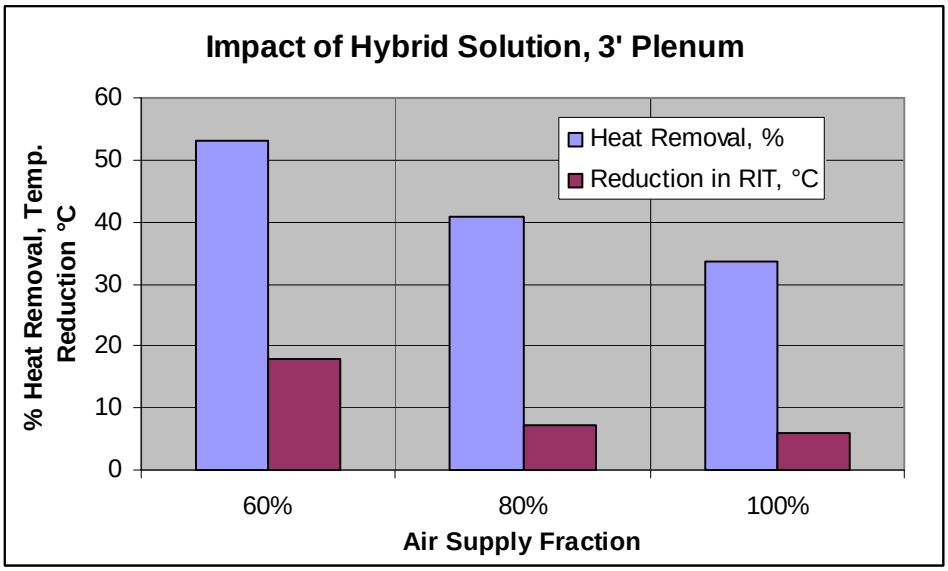

Figure 3.27 Underfloor Supply: The Impact of the Rear Door Heat Exchanger for the Plenum of 3 ft.

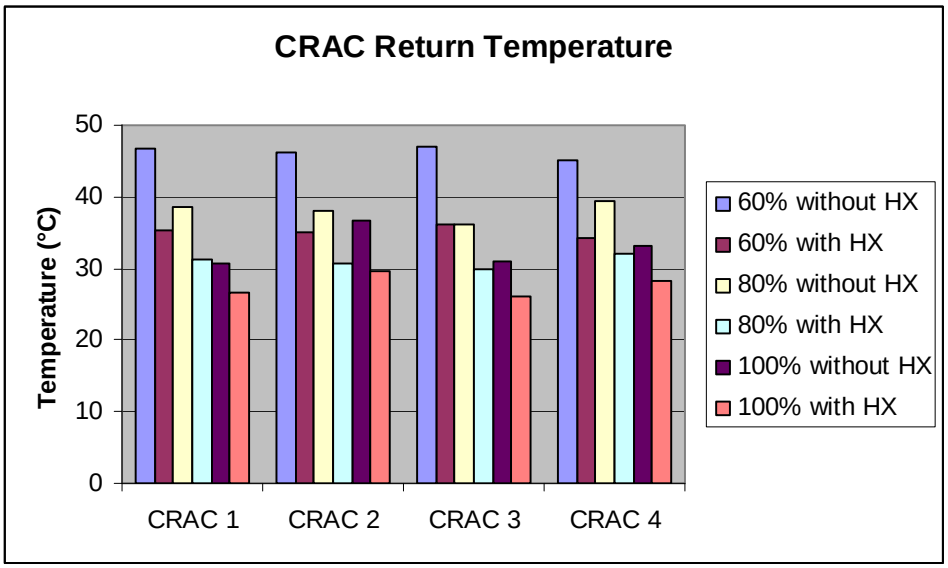

Figure 3.28 Underfloor Supply: Variations in CRAC Return Temperatures for the Plenum of 2 ft.

3.2.6. The Effect on the CRAC Return Temperatures

Another metric to determine the effectiveness of this solution is temperature of air returning to CRAC units. It can be seen from fig. 3.28 that hybrid solution help reducing overall maximum temperature and hence the temperature of air returning to CRAC intake. These low return temperatures in turn reduce the load on CRAC and yield better supply temperatures.

3.3 Data Center with Overhead Supply Configuration

3.3.1. Computational Modeling

A representative data center with overhead configuration as shown in Fig. 3.29 is modeled using commercially available CFD code [8]. The half symmetry model of data center "cell" has 40 racks arranged in cold aisle – hot aisle layout as shown in Fig. 3.30.

From Fig. 3.30, the footprint dimensions of the half-symmetry "cell" are 20ft (6.09 m) by 44 ft (13.42 m), and the room was 10 ft (3.048 m) tall. The computer racks were assumed to be one tile wide (0.61 m or 2 ft.), two tiles deep (1.22 m or 4 ft.), and 1.8 m (6 ft) tall. The air-moving device inside the racks is assumed to force air straight through the rack, with a constant velocity across the front and back of the racks. Each rack is assumed to be a high-performance 32 kW (109,194 Btu/h) rack, with a rack airflow rate of 2905 cfm (1.371 m^3/s). This corresponded to an air temperature rise through the rack of 20°C (36°F). The temperature of the chilled air entering the room through the overhead diffusers was fixed at 13°C (56°F). Figure 5 shows the racks to be arranged in four rows, A, B, C, and D, respectively. The rear door heat exchanger was modeled using heat exchanger macro in Icepak software [8]. The temperature of chilled water entering into the heat exchanger was set at 18°C. The conductance of heat exchanger which is product of effectiveness and smaller of the two heat capacities was set to 650 W/K which is representative value for such generic heat exchangers. Since the rack inlet temperature varies along the height of rack, heat exchanger was made of six different strips to capture the performance according to varying inlet conditions.

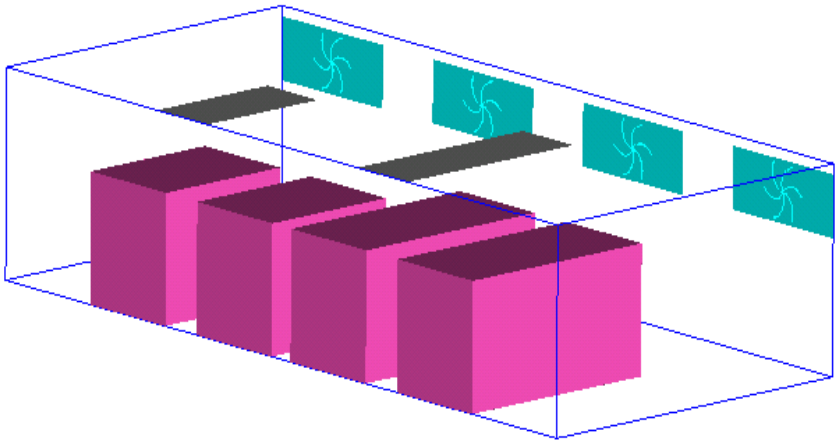

Figure 3.29 Overhead Supply: A CFD Model of the Representative Data Center.

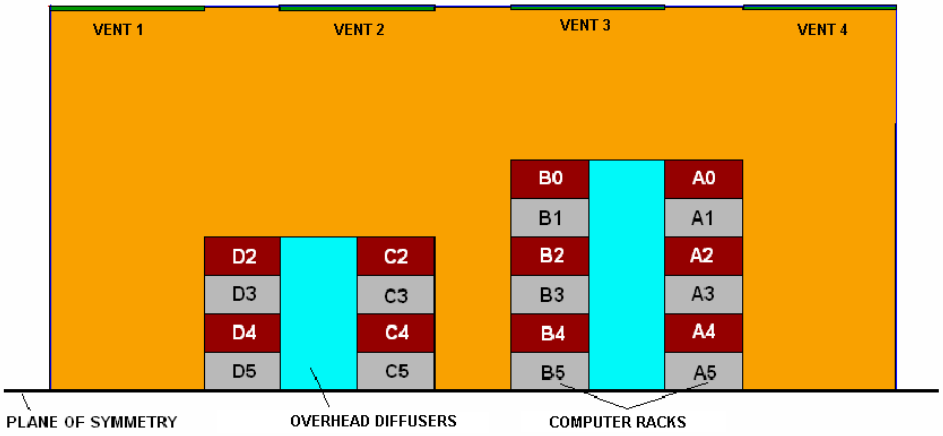

Figure 3.30 Overhead Supply: Layout of the Representative Data Center.

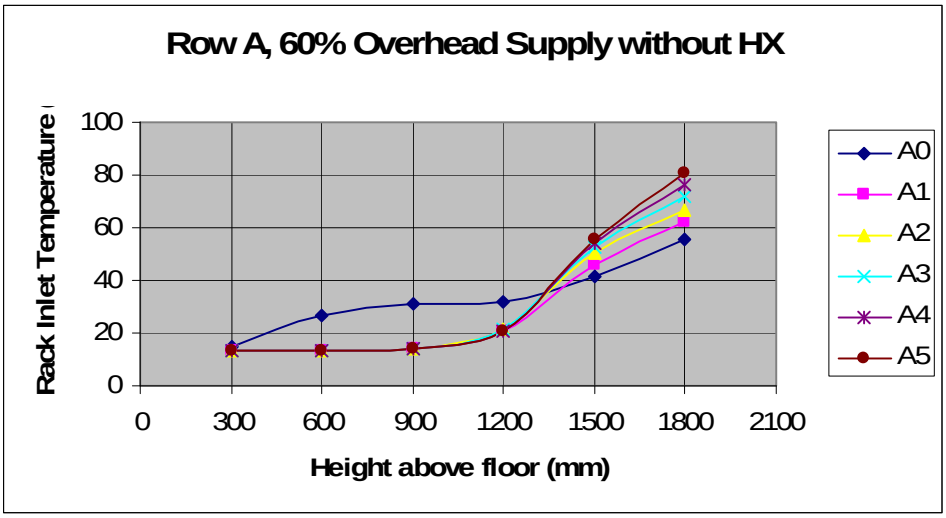

Figure 3.31 Overhead Supply: Rack Inlet Temperature Variation at racks in Row A without Heat Exchanger for 60% chilled air supply.

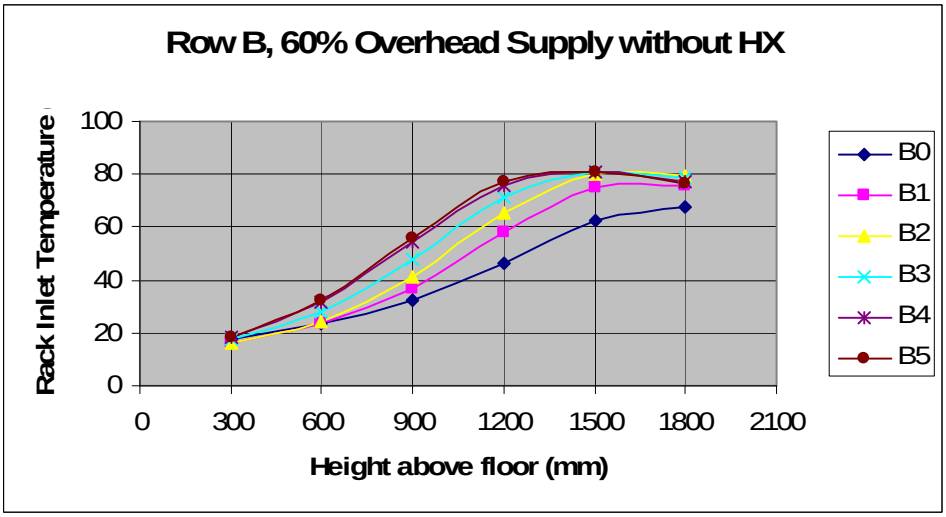

Figure 3.32 Overhead Supply: Rack Inlet Temperature Variation at racks in Row B without Heat Exchanger for 60% chilled air supply.

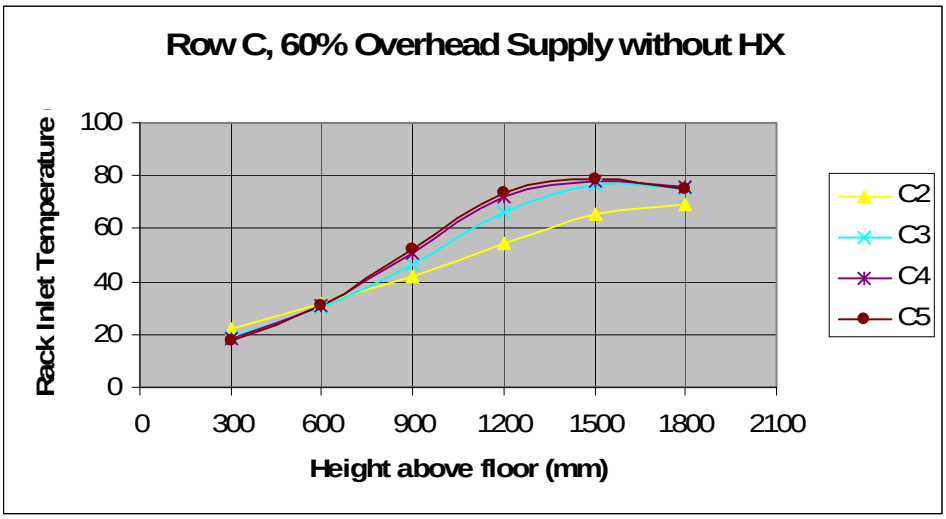

Figure 3.33 Overhead Supply: Rack Inlet Temperature Variation at racks in Row C without Heat Exchanger for 60% chilled air supply.

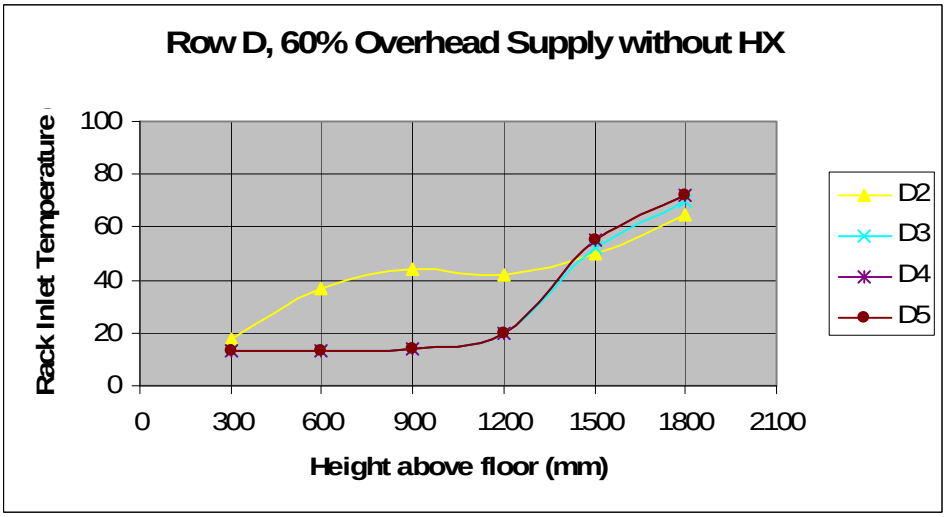

Figure 3.34 Overhead Supply: Rack Inlet Temperature Variation at racks in Row D without Heat Exchanger for 60% chilled air supply.

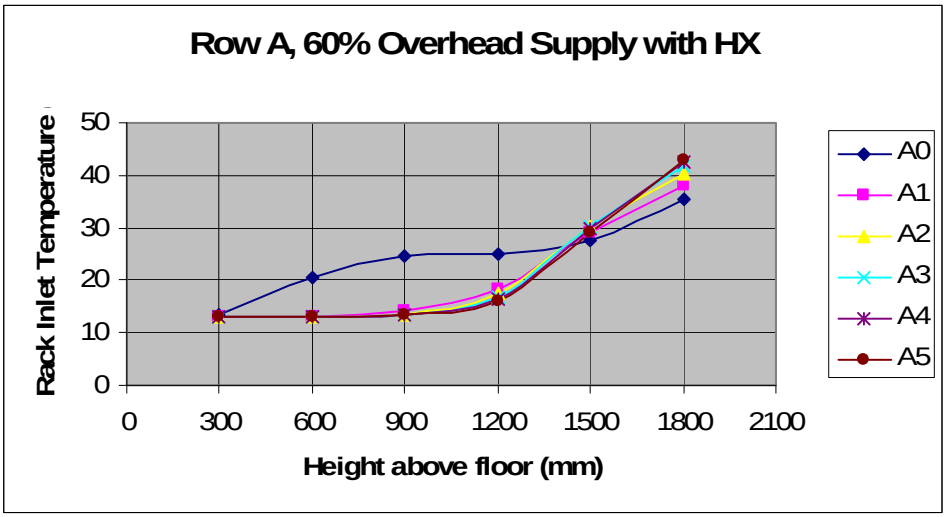

Figure 3.35 Overhead Supply: Rack Inlet Temperature Variation at racks in Row A with Heat Exchanger for 60% chilled air supply.

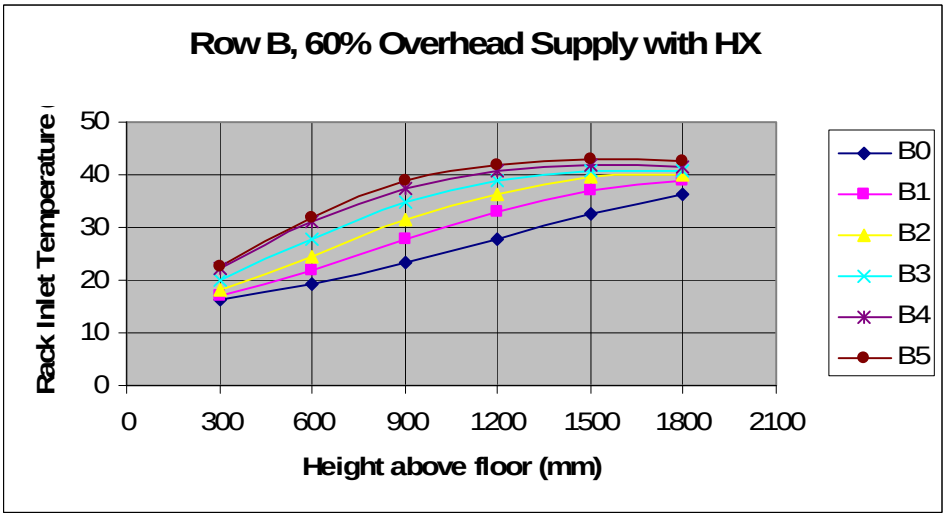

Figure 3.36 Overhead Supply: Rack Inlet Temperature Variation at racks in Row B with Heat Exchanger for 60% chilled air supply.

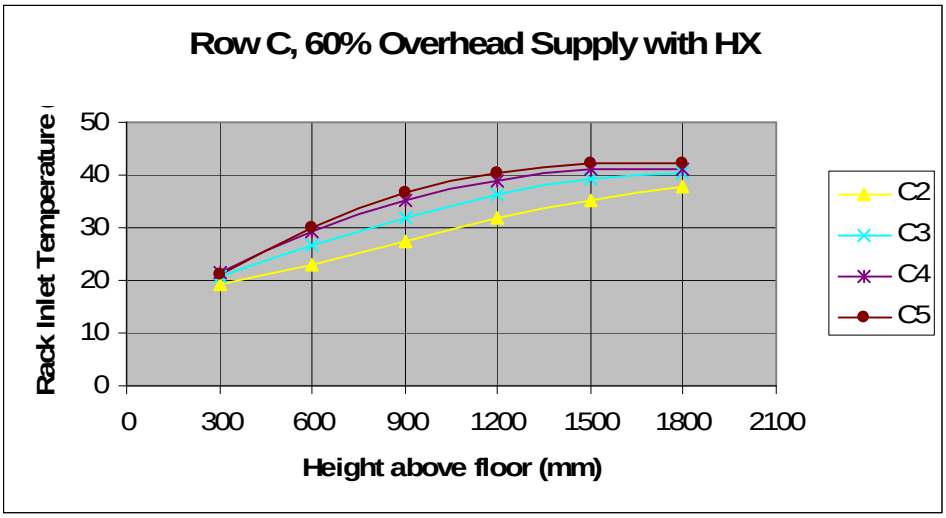

Figure 3.37 Overhead Supply: Rack Inlet Temperature Variation at racks in Row C with Heat Exchanger for 60% chilled air supply.

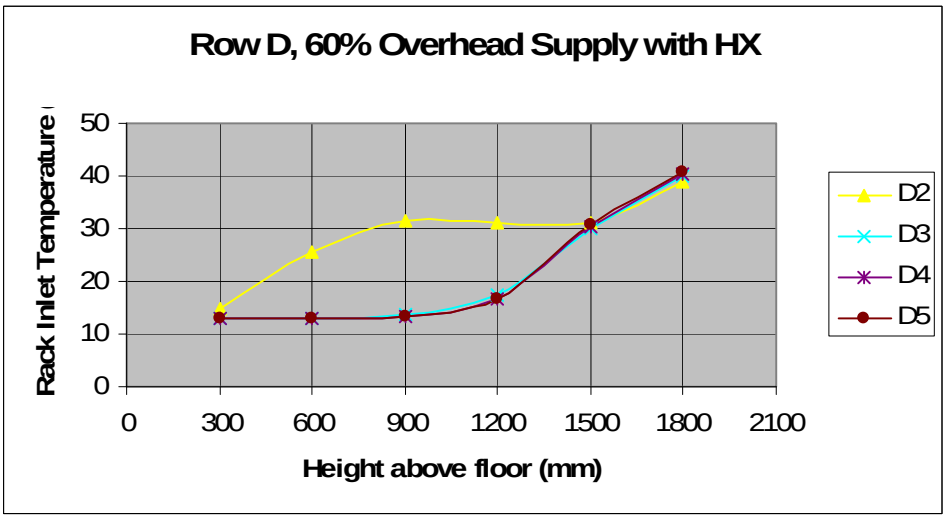

Figure 3.38 Overhead Supply: Rack Inlet Temperature Variation at racks in Row D with Heat Exchanger for 60% chilled air supply.

In CFD model, symmetry boundary condition was applied to the wall touching the racks. The elements count was within 300,000 to 700,000. On a PC with Pentium D, 2.8GHz processor and 4 GB RAM,, convergence for temperature and continuity was satisfactorily achieved in about 2000 iterations within 8-10 hours. For each rack, inlet temperature was monitored at 300mm, 600mm, 900mm, 1200mm, 1500mm and 1800mm above floor level.

Figures 3.31 through 3.38 show temperature variation for the 60%, air supply for the configurations with and without heat exchanger. Racks A0, B0, C2, and D2 are referred to as outside racks, and racks A5, B5, C5, and D5 are referred to as inside racks. Figure 6 shows the trends for all the racks for 60% air supply without any heat exchanger. Figure 7 indicate the same information for the racks for 60% air supply with heat exchangers employed at the rear side of the racks. The key observations are summarized below.

3.3.2. Recirculation and Ambient Mixing of Air

In the case of overhead supply configuration, behavior similar to that in the case of underfloor supply configuration is observed. For all the cases, large temperature gradients exist at outside racks. Severe recirculation pattern is observed at outside racks as hot air exiting into hot aisle is drawn into cold aisle from the side as well as from top of the racks. For inner racks, although hot and cold air mixing is present, it is less than the outside racks as the air is only drawn from top. The case of 60% air supply represents the worst case scenario for a data center as highest inlet temperatures are monitored for this case. Similar trends are observed for 80% and 100% air supply.

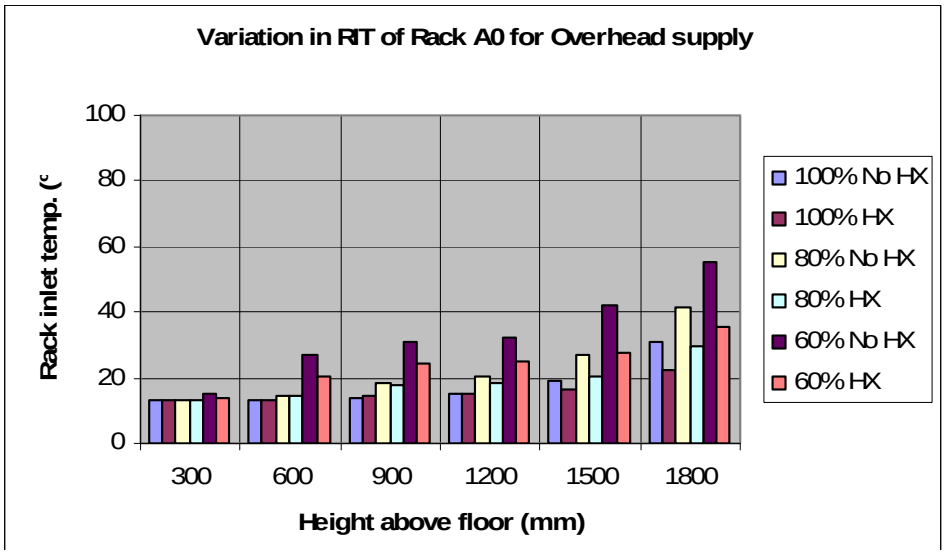

Figure 3.39 Overhead Supply: Comparisons of Rack Inlet Temperatures at Rack A0.

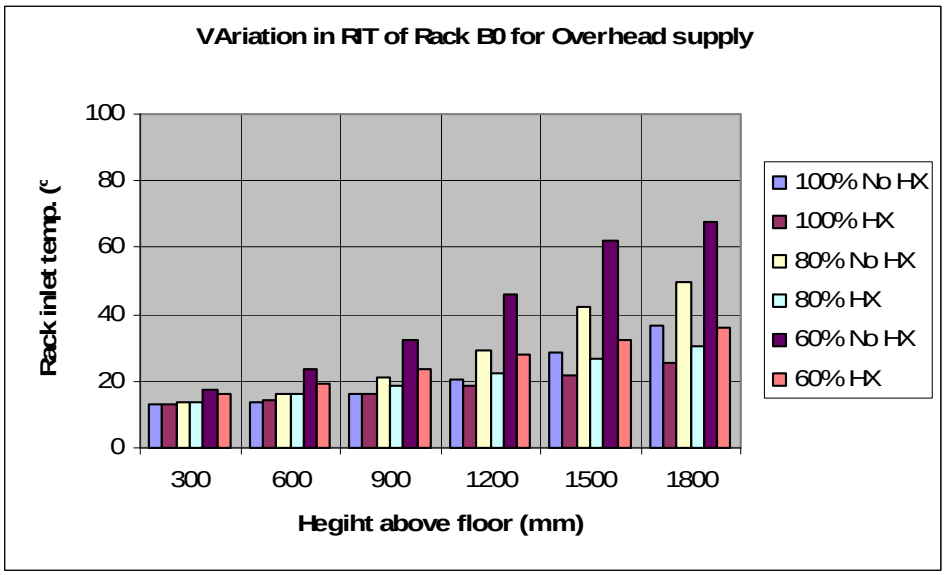

Figure 3.40 Overhead Supply: Comparisons of Rack Inlet Temperatures at Rack B0.

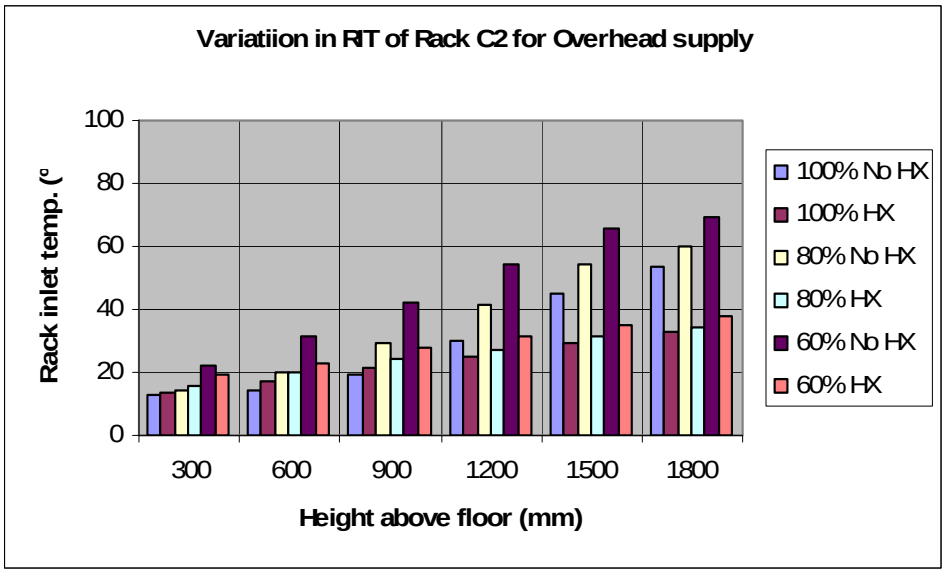

Figure 3.41 Overhead Supply: Comparisons of Rack Inlet Temperatures at Rack C2.

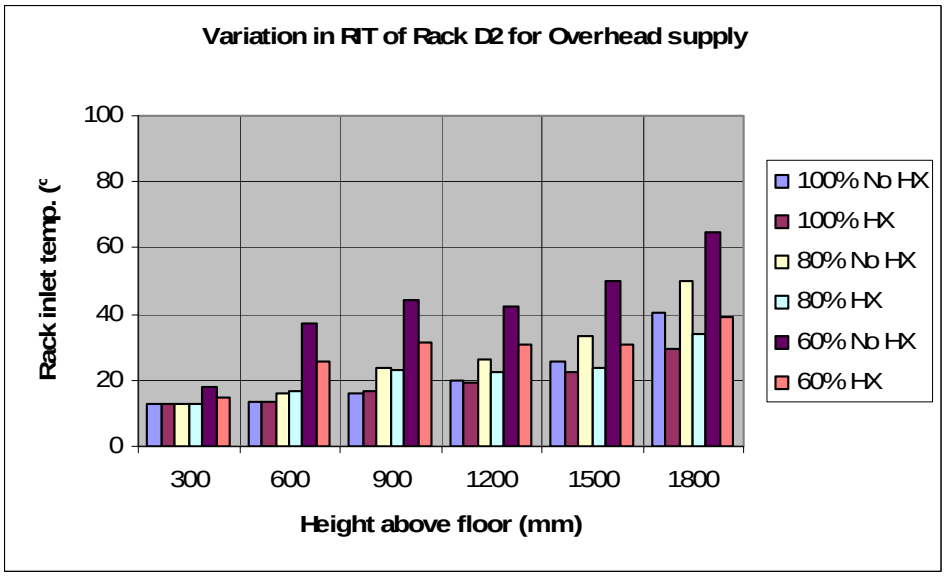

Figure 3.42 Overhead Supply: Comparisons of Rack Inlet Temperatures at Rack D2.

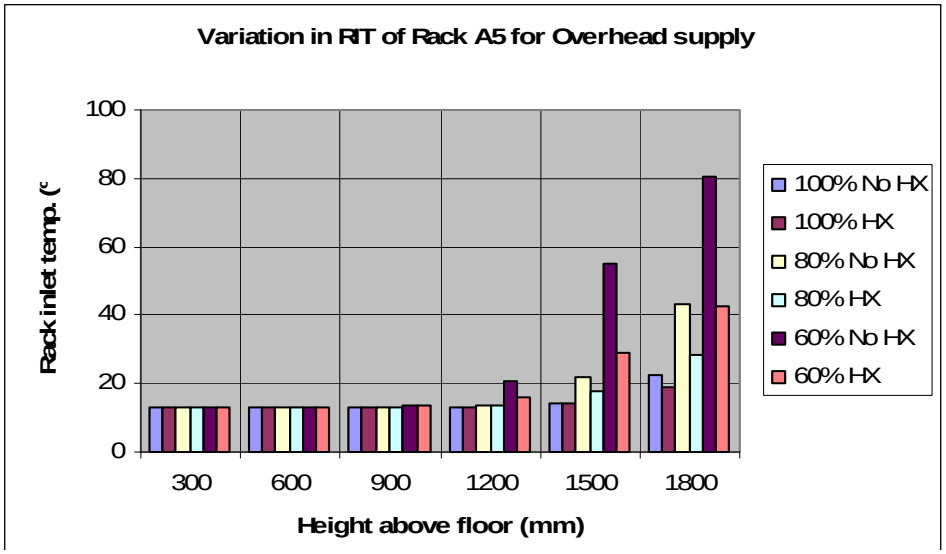

Figure 3.43 Overhead Supply: Comparisons of Rack Inlet Temperatures at Rack A5.

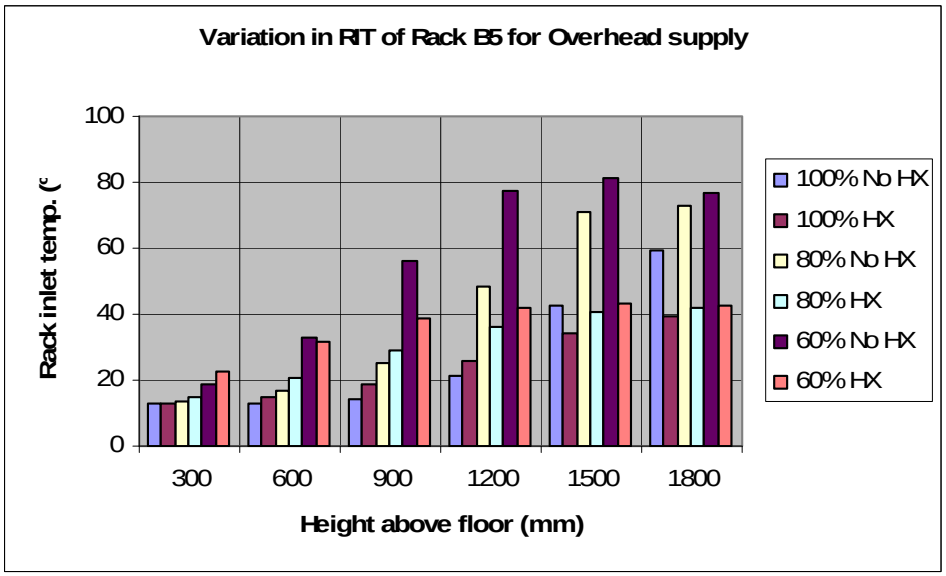

Figure 3.44 Overhead Supply: Comparisons of Rack Inlet Temperatures at Rack B5.

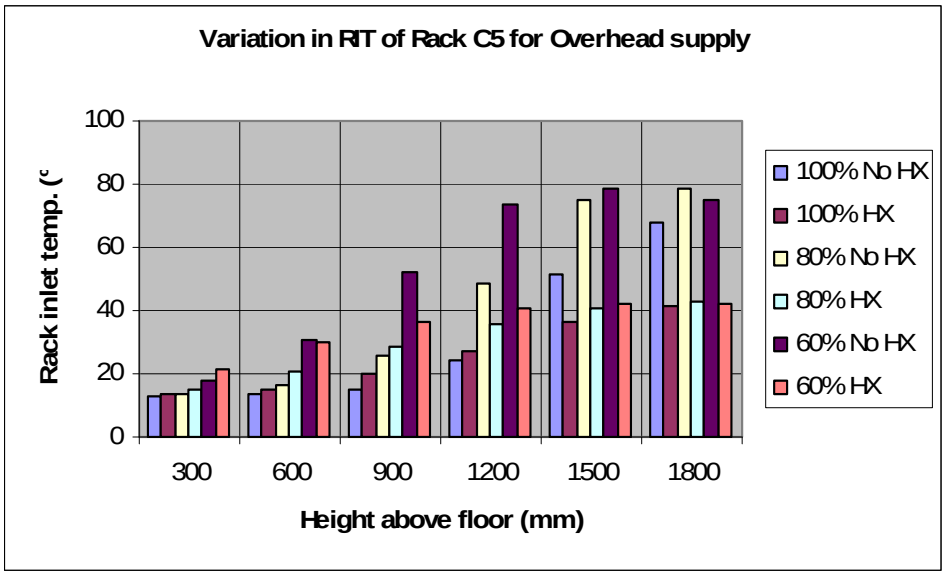

Figure 3.45 Overhead Supply: Comparisons of Rack Inlet Temperatures at Rack C5.

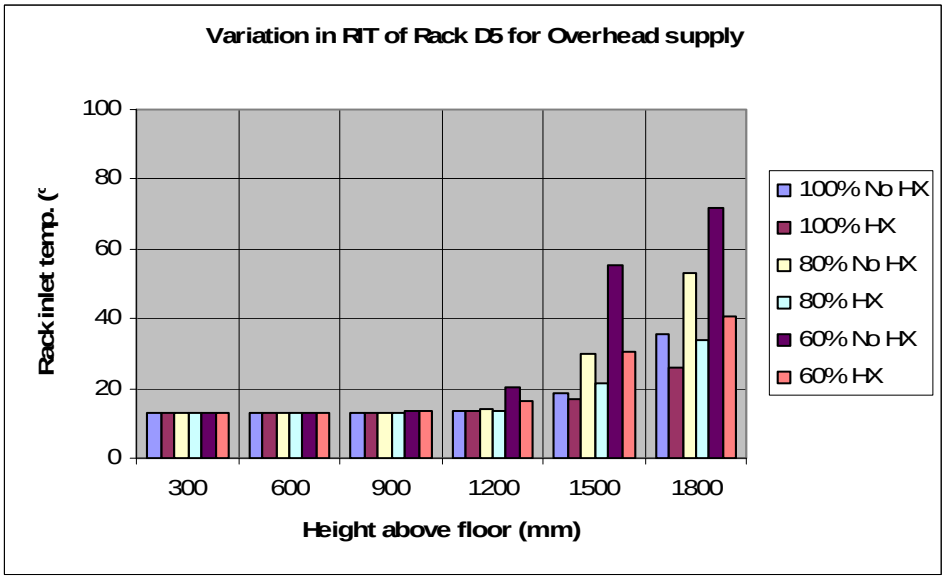

Figure 3.46 Overhead Supply: Comparisons of Rack Inlet Temperatures at Rack D5.

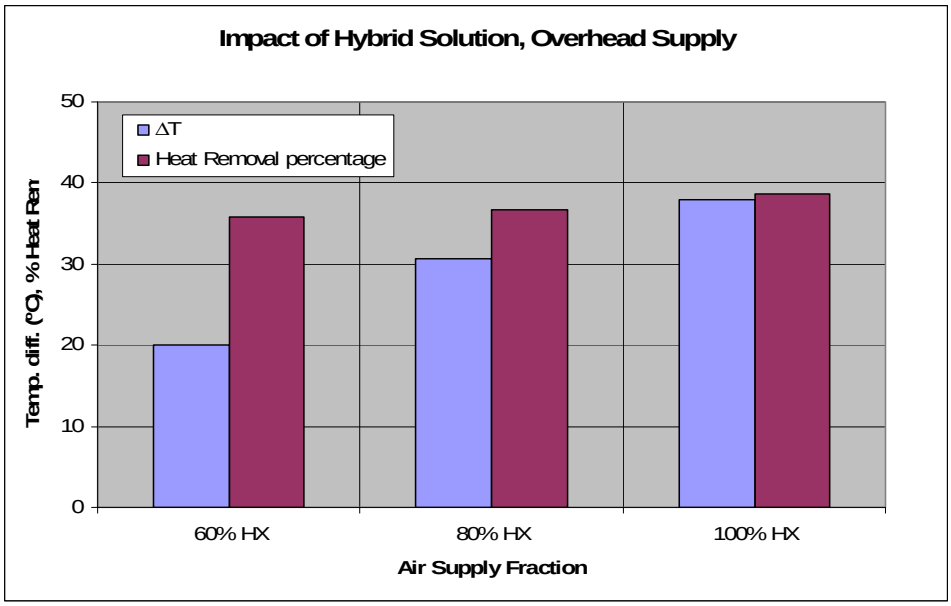

Figure 3.47 Overhead Supply: The Impact of the Rear Door Heat Exchanger.

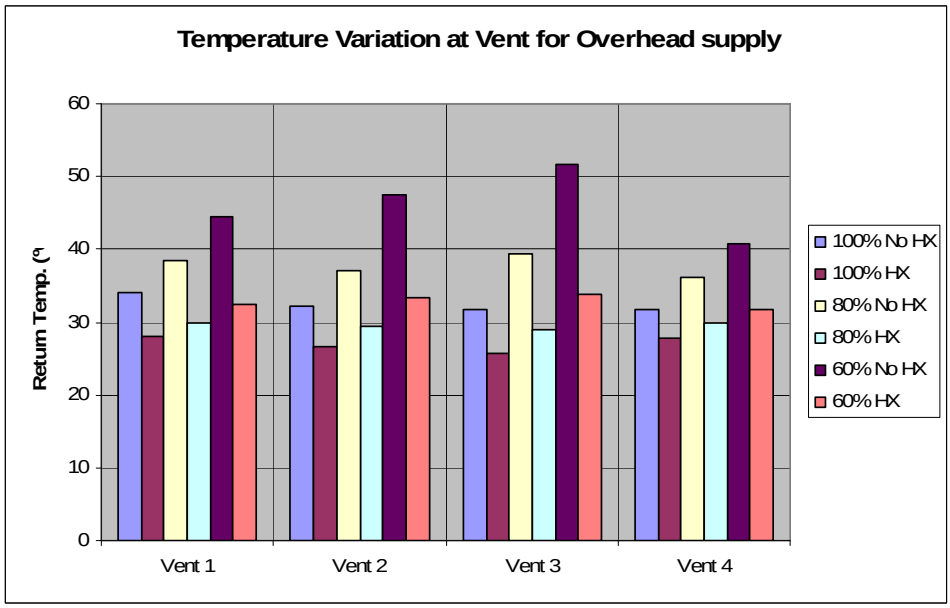

Figure 3.48 Overhead Supply: Variations in Return Temperatures.

3.3.3. The Impact of the Rear Door Heat Exchanger

The impact of hybrid solution is summarized in fig. 3.47 for different air supply fractions. For 60% air supply case, the heat exchanger removes 36% of the total 32KW heat while reducing the rack inlet temperature by 20°C. For the cases of 80% and 100% supply, the heat removal is 38% and 39% respectively.

3.3.4. The Effect on the Return Temperatures

It can be seen from fig. 3.48 that hybrid solution helps in reducing the overall maximum temperature and hence the temperature of air returning to the air handlers. These low return temperatures in turn reduce the load on air handlers and yield better supply temperatures.

3.4 Improved Cooling with Efficient Cabinet Design

The server cabinets are an important part of the data center and can considerably impact the airflow patterns within the data center. The servers when stacked in a cabinet with perforated doors and the cables are added; perform differently than they would in bench tests. The cabinets provide some isolation of cold air from hot exhaust air when placed in hot aisle-cold aisle layout. Also, by directing the cold air through servers, they can minimize the wastage of cold air which would result from otherwise bypassing cold air.

In this study, various cabinet designs as shown in Fig. 3.49 – 3.50 are discussed. Isolating the supplied cold air from hot exhaust air is always a challenge in thermal management of data center facilities. A cabinet design that employs chimney to aid the isolation of hot and cold air is discussed. A computational model of representative data center is created to study the effectiveness of design under various supply air fractions. Three different cases considered are as follows:

1. Cabinet with chimney and solid back door
2. Cabinet with chimney and perforated back door

3. Cabinet without chimney

Figure 3.49 Cabinet without Chimney.

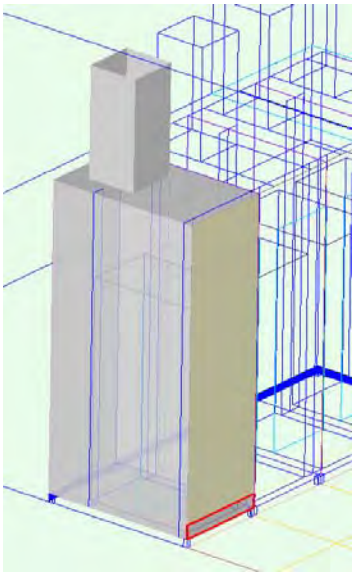

Figure 3.50 Cabinet with Chimney.

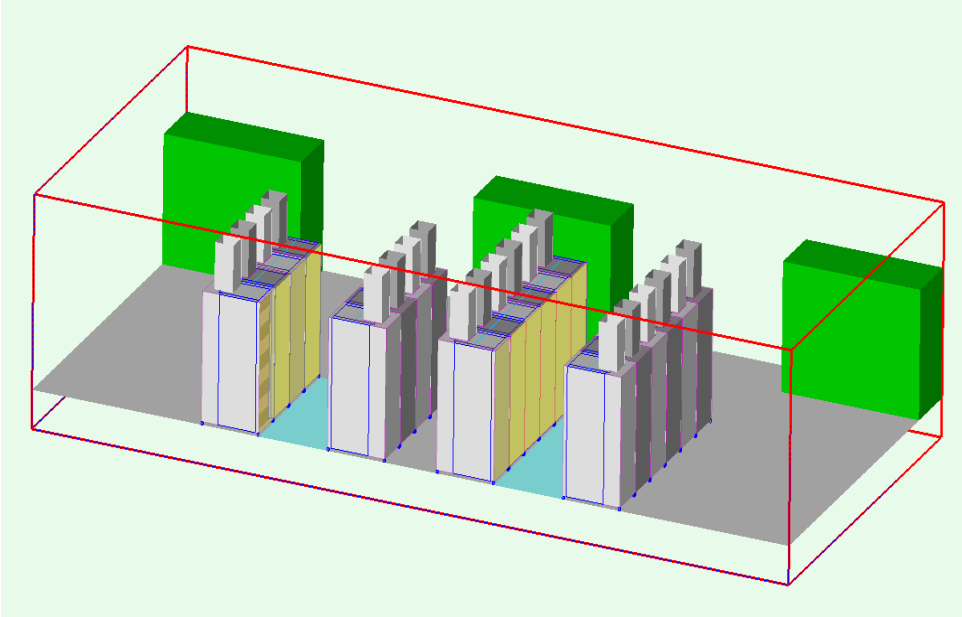

Figure 3.51 The Model of a Representative Data Center.

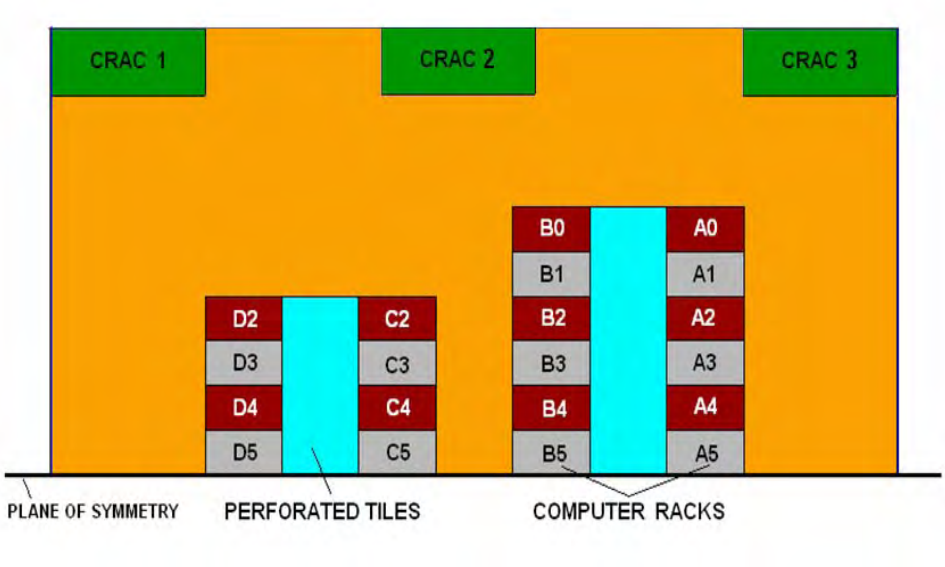

Figure 3.52 The Layout of a Representative Data Center.

3.4.1. Computational Modeling

A representative data center with underfloor configuration as shown in Fig. 3.51 is modeled using commercially available CFD code [8].. The half symmetry model of data center "cell" has 20 racks arranged in cold aisle – hot aisle layout as shown in Fig. 3.52.

From Fig. 3.52, the footprint dimensions of the half-symmetry "cell" are 20ft (6.09 m) by 44 ft (13.42 m), and the room was 10 ft (3.048 m) tall. The cabinets are 600mm wide, 1000mm deep and 45U or 2000mm tall. The servers are partially populated. Each server is considered 3U high and 10 such servers are stacked together. A blanking panel is used to block off the remaining space to avoid the cold air bypass. The air-moving device inside the racks is assumed to force the air straight through the rack, with a constant velocity across the front and back of the racks. Each rack is assumed to be a 11 kW (37,534 Btu/h) rack, with a rack airflow rate of 965 cfm (0.45 m^3/s). This corresponded to an air temperature rise through the rack of 20°C (36°F) considering the specific heat, c_p=1.006 kJ/kg°K and the density of air 1.2 kg/m^3 . The temperature of the chilled air entering the room through the perforated tiles was fixed at 13°C (56°F). The CRAC unit had a 3 ft × 8 ft (0.91 m x 2.44 m) footprint and was 1.8 m (6 ft) high. Each CRAC unit delivers 6435cfm at set point temperature of 15°C. The perforated tiles in cold aisles are 30% open. The chimney has a cross section of 322.5mm X 322.5mm and is 725mm high. The doors have 61.25% open area.

The effect of using different cabinet designs in overhead supply configuration is simulated in this study. Three different cabinet designs namely cabinet with chimney and solid back door, cabinet with chimney and perforated back door, cabinet without chimney are considered. In CFD model, symmetry boundary condition was applied to the wall touching the racks. The elements count was within 1,000,000 to 2,000,000. For each configuration, a mesh sensitivity analysis was carried out to insure the independence of output variables from the grid size. On a PC with Pentium D, 2.8GHz processor and 4 GB RAM,, convergence for temperature and continuity was satisfactorily achieved in about 2000 iterations within 8-10 hours.

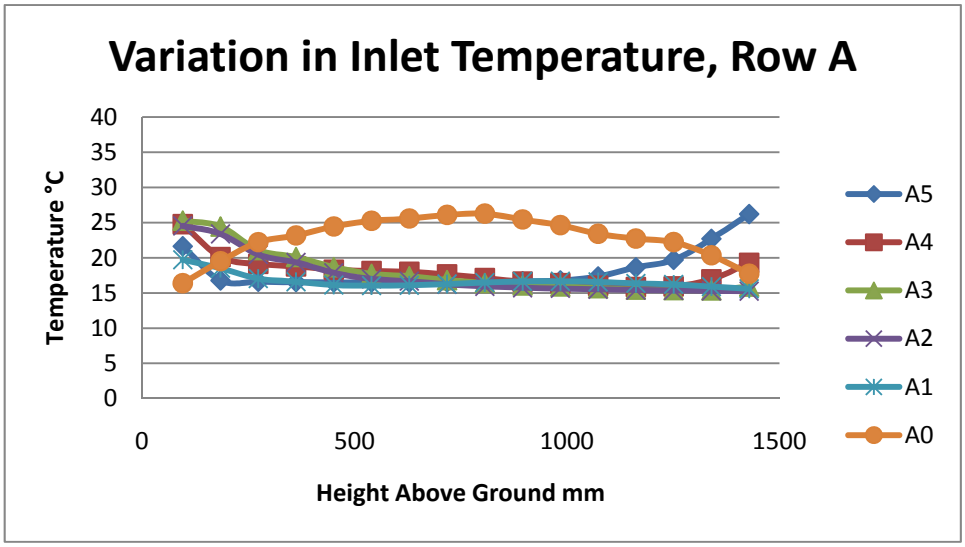

Figure 3.53 The Variations in Inlet Temperatures in Row A for the Cabinets with Chimney and Solid Back Door.

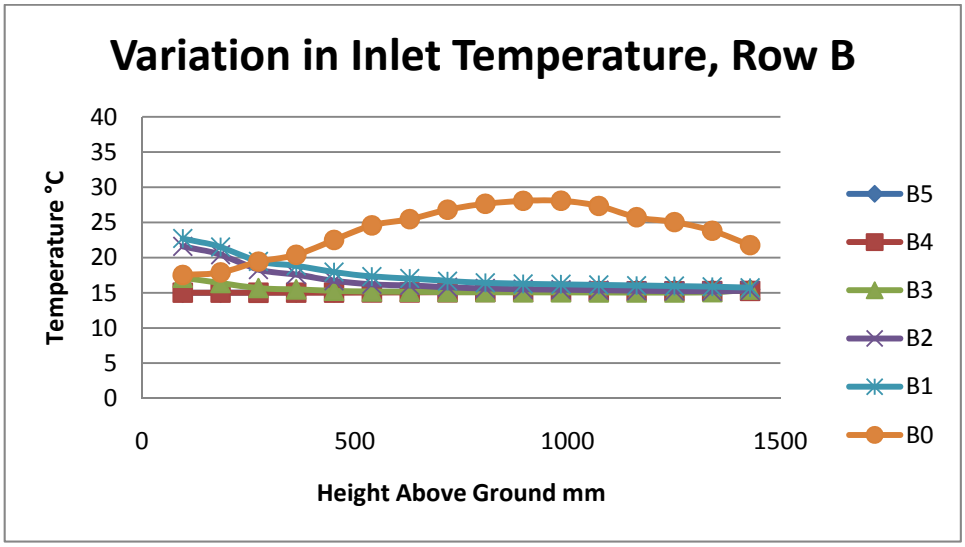

Figure 3.54 The Variations in Inlet Temperatures in Row B for the Cabinets with Chimney and Solid Back Door.

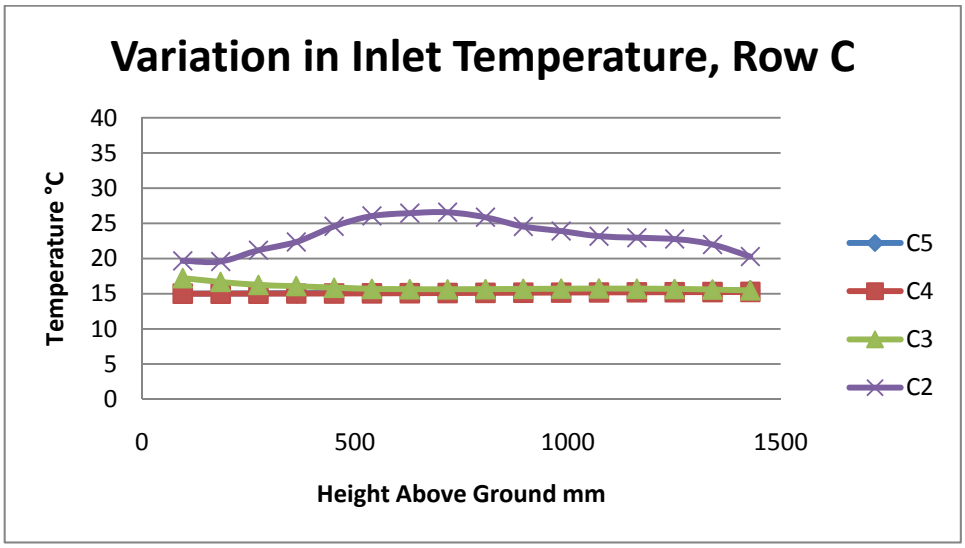

Figure 3.55 The Variations in Inlet Temperatures in Row C for the Cabinets with Chimney and Solid Back Door.

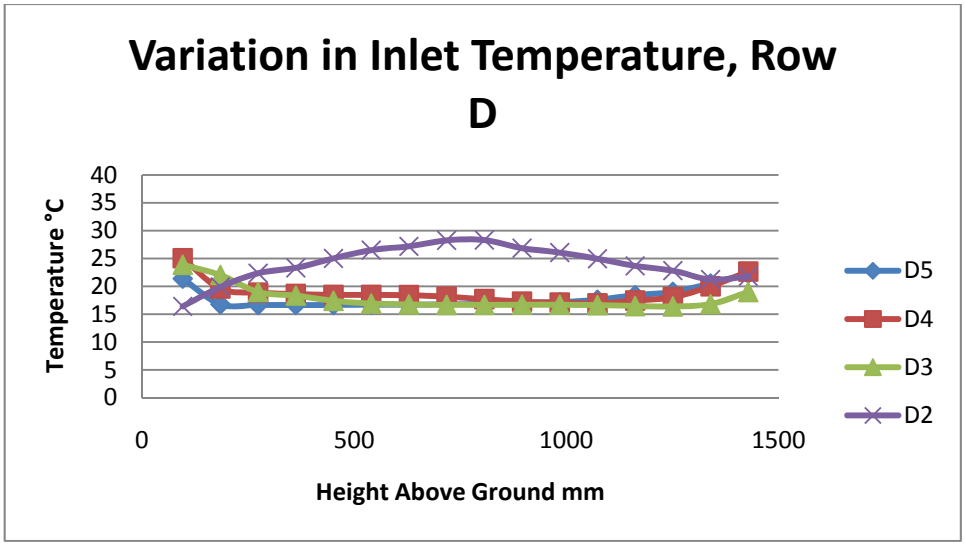

Figure 3.56 The Variations in Inlet Temperatures in Row D for the Cabinets with Chimney and Solid Back Door.

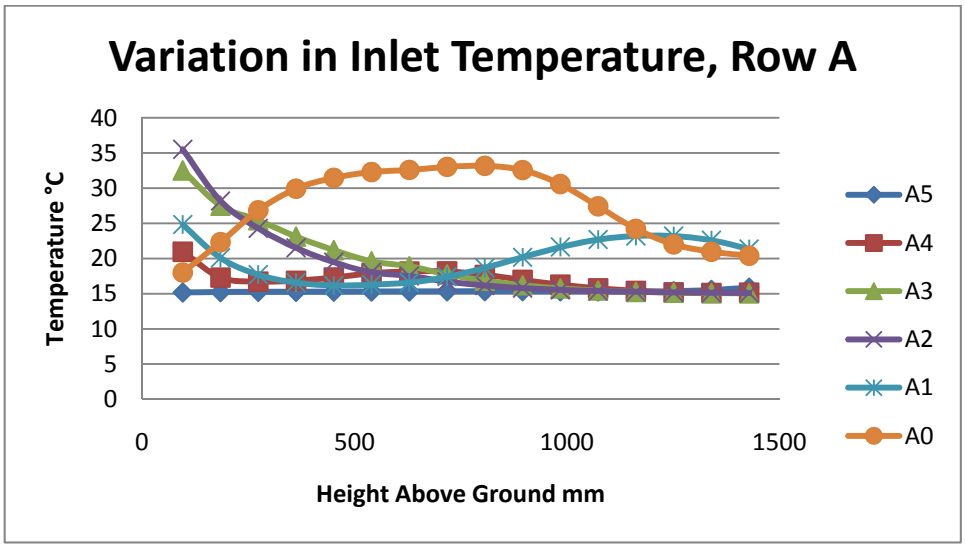

Figure 3.57 The Variations in Inlet Temperatures in Row A for the Cabinets with Chimney and Perforated Back Door.

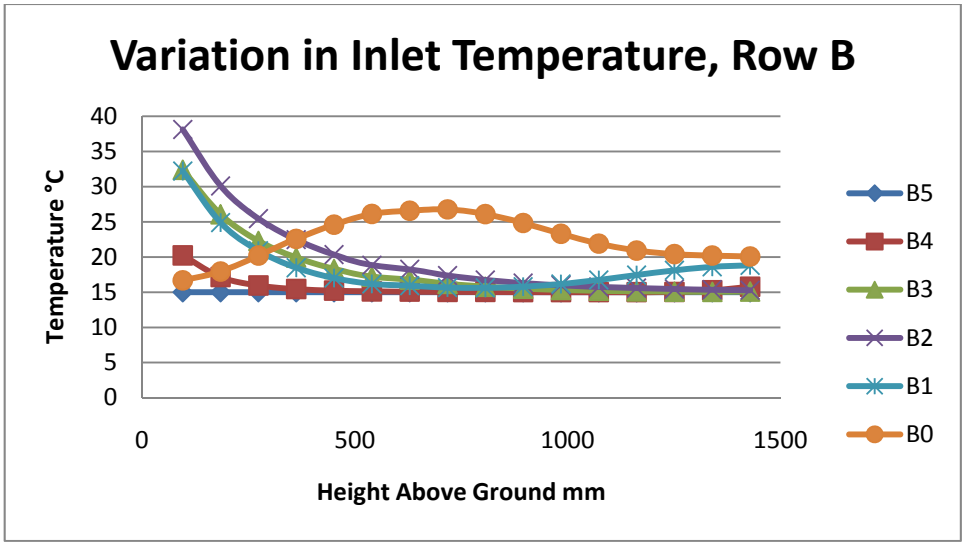

Figure 3.58 The Variations in Inlet Temperatures in Row B for the Cabinets with Chimney and Perforated Back Door.

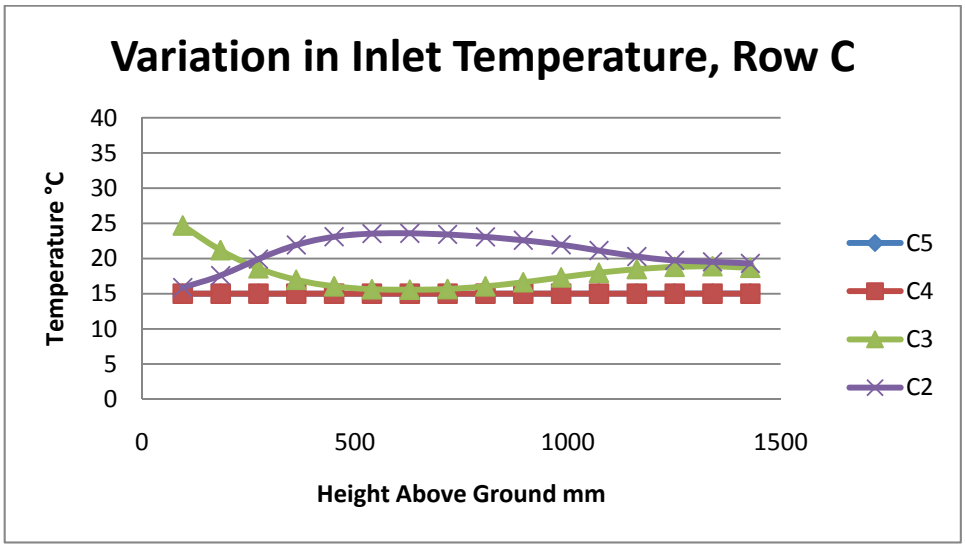

Figure 3.59 The Variations in Inlet Temperatures in Row C for the Cabinets with Chimney and Perforated Back Door.

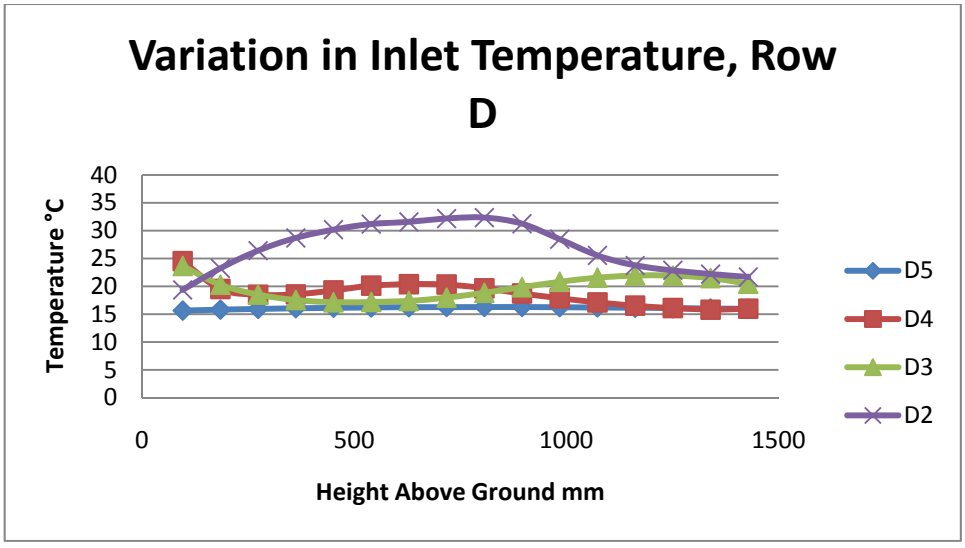

Figure 3.60 The Variations in Inlet Temperatures in Row D for the Cabinets with Chimney and Perforated Back Door.

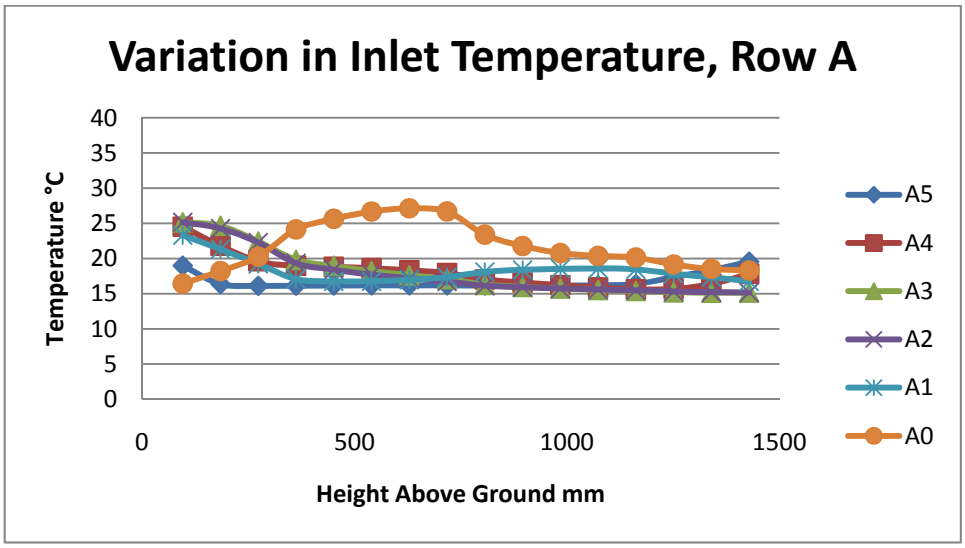

Figure 3.61 The Variations in Inlet Temperatures in Row A for the Cabinets without Chimney.

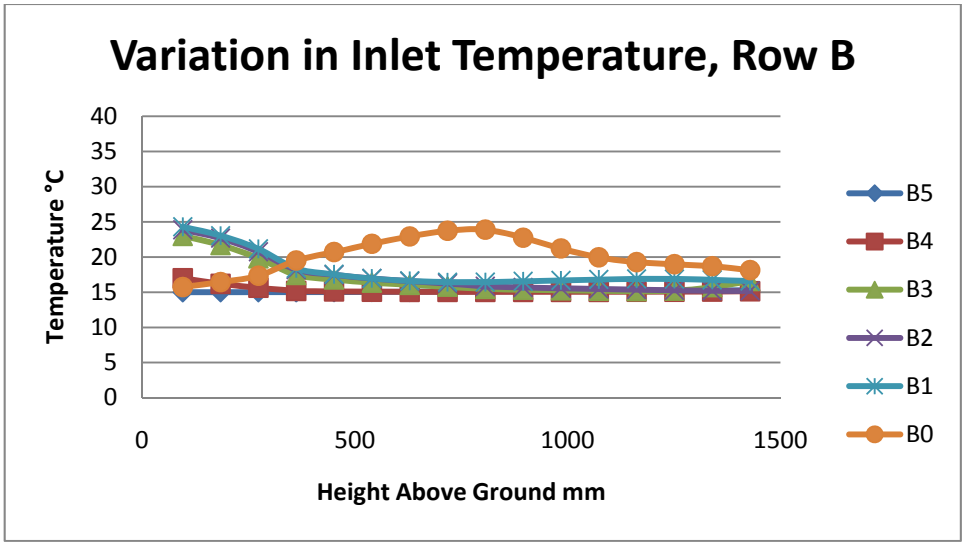

Figure 3.62 The Variations in Inlet Temperatures in Row B for the Cabinets without Chimney.

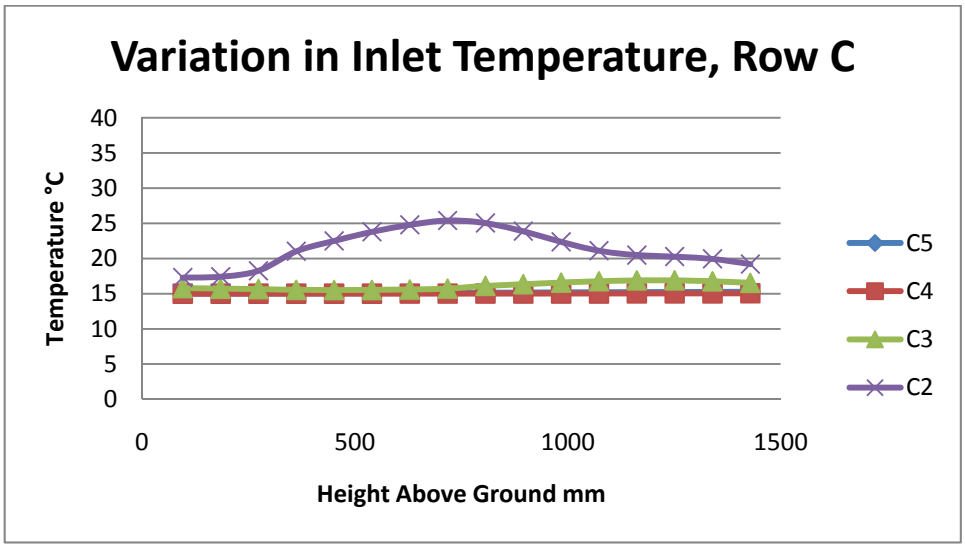

Figure 3.63 The Variations in Inlet Temperatures in Row C for the Cabinets without Chimney.

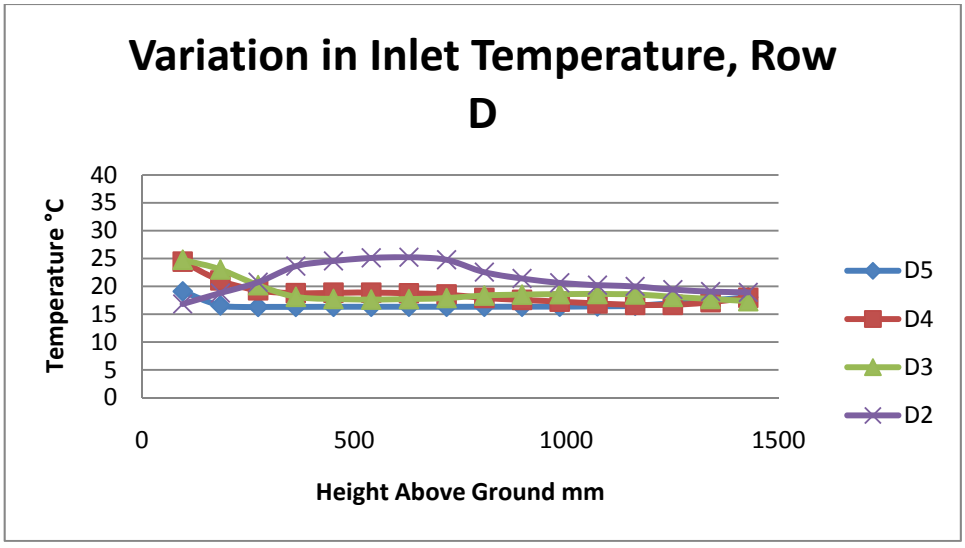

Figure 3.64 The Variations in Inlet Temperatures in Row D for the Cabinets without Chimney.

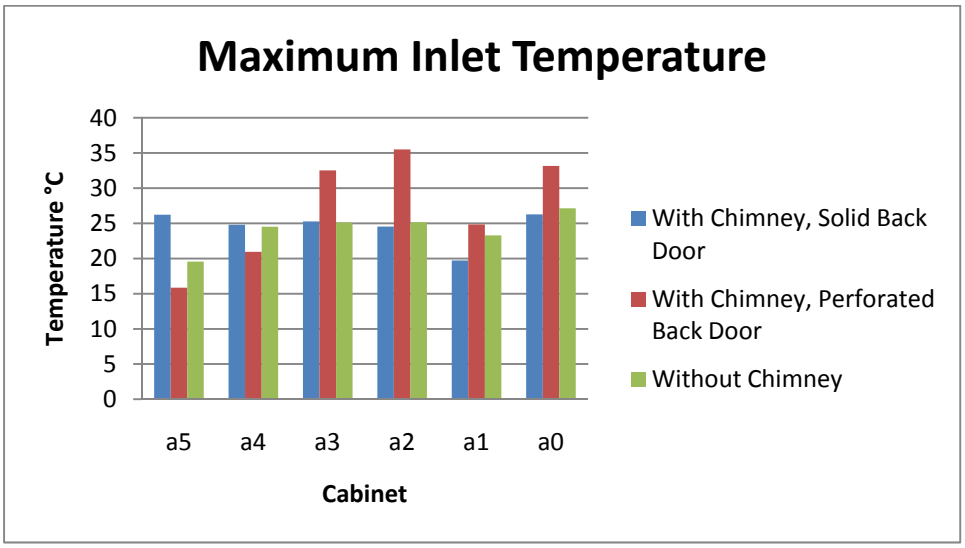

Figure 3.65 The Comparisons of the Maximum Inlet Temperatures in Row A.

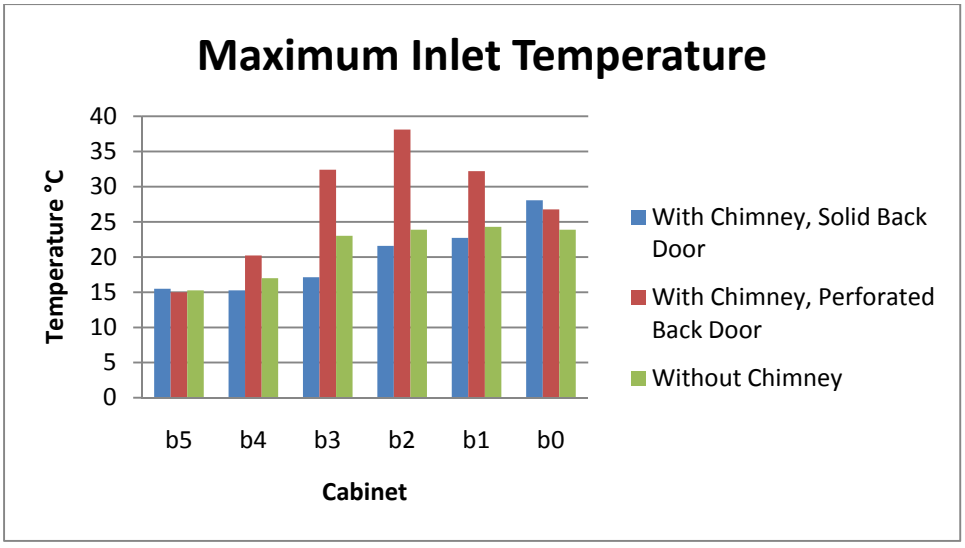

Figure 3.66 The Comparisons of the Maximum Inlet Temperatures in Row B.

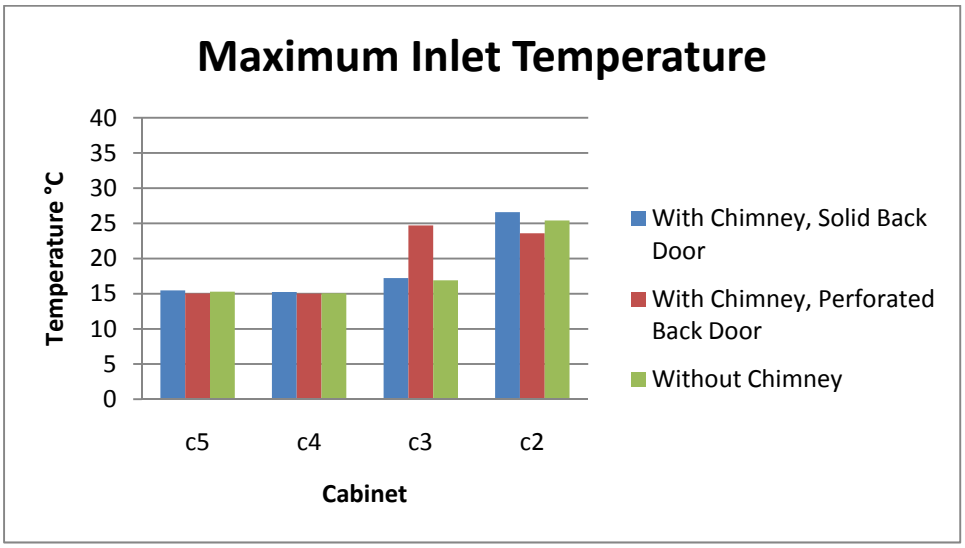

Figure 3.67 The Comparisons of the Maximum Inlet Temperatures in Row C.

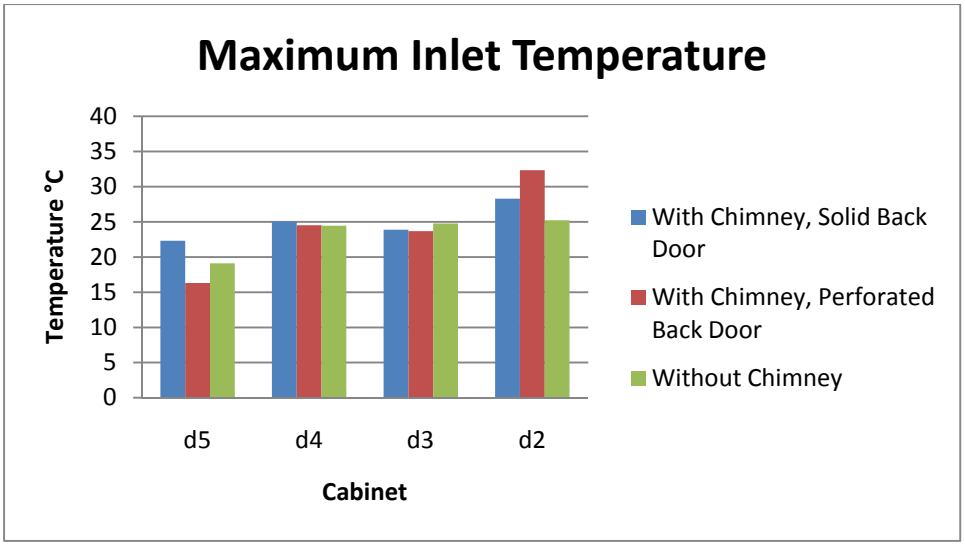

Figure 3.68 The Comparisons of the Maximum Inlet Temperatures in Row D.

Figures 3.53 -3.64 show the inlet temperature variation along the height of cabinets. Cabinets A0, B0, C2, and D2 are referred to as outside cabinets, and cabinets A5, B5, C5, and

D5 are referred to as inside cabinets. Figures 3.53-3.56 show the trends for all the cabinets with chimney and solid back door. Figures 3.57-3.60 show the trends for all the cabinets with chimney and perforated back door. Figure 3.61 – 3.64 indicate the same information for the cabinets without chimney. The key observations are summarized below.

3.4.2. Recirculation and Ambient Mixing of Air

For all cases, large temperature gradients exist at outside cabinets. Severe recirculation pattern is observed at outside cabinets as hot air exiting into hot aisle is drawn into cold aisle from the side as well as from top of the cabinets. For inner cabinets, although hot and cold air mixing is present, it is less than the outside cabinets as the air is only drawn from top.

Figures 3.70 – 3.72 show the thermal profile of the data center taken at plane Z=3900mm which runs through the center of cabinets D2, C2, B2 and A2. The infiltration of hot air into cold aisle can be seen clearly in all the three cases. Figure 3.69 shows an enlarged section of vector plot taken in Y direction for cabinet D2, an outside cabinet with chimney and solid back door. It can be seen that the hot exhaust air mixing with cold air and then passing through the servers.

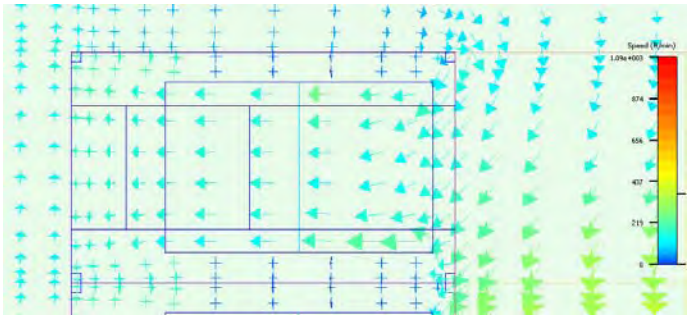

Figure 3.69 The Vector Plot.

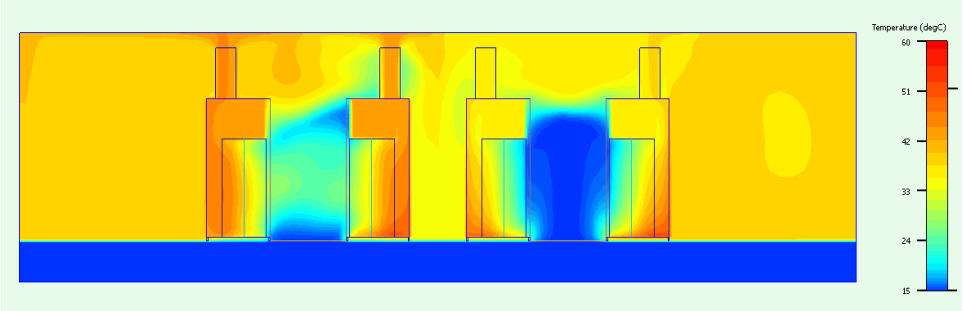

Figure 3.70 The Thermal Contours for the Cabinets with Chimney and Solid back Door.

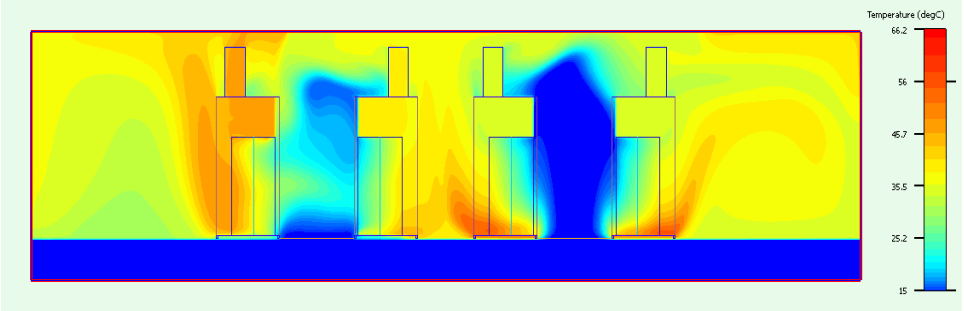

Figure 3.71 The Thermal Contours for the Cabinets with Chimney and Perforated back Door.

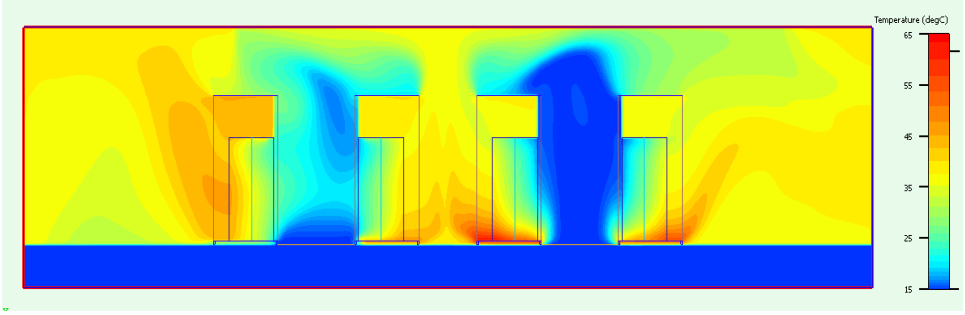

Figure 3.72 The Thermal Contours for the Cabinets without Chimney.

The maximum inlet temperatures recorded for each cabinet in all the three cabinets are shown in fig. 10. It can be seen that for the cabinet with chimney and perforated door, as many as 35% cabinets exceed the ASHRAE recommended limit of 32°C [6]. The other two designs, the cabinets with chimney and solid back door, and the cabinets without chimney experience reasonable inlet temperatures, all of which fall below the limit of 32°C.

3.4.3. Blanking Strips

From the figures 7-9, higher inlet temperatures are noticed at the lower heights. This is attributed to the gap between the raised floor and the cabinet due to the casters. When this gap is closed using the blanking strips, the lower temperatures are observed at lower heights. The use of blanking strips eliminates the bypass of cold air into hot air and infiltration of hot air into cold aisle from beneath the cabinet. The figure below shows the thermal profile taken beneath the cabinet without any blanking strips in place. The hot air infiltration can clearly be seen.

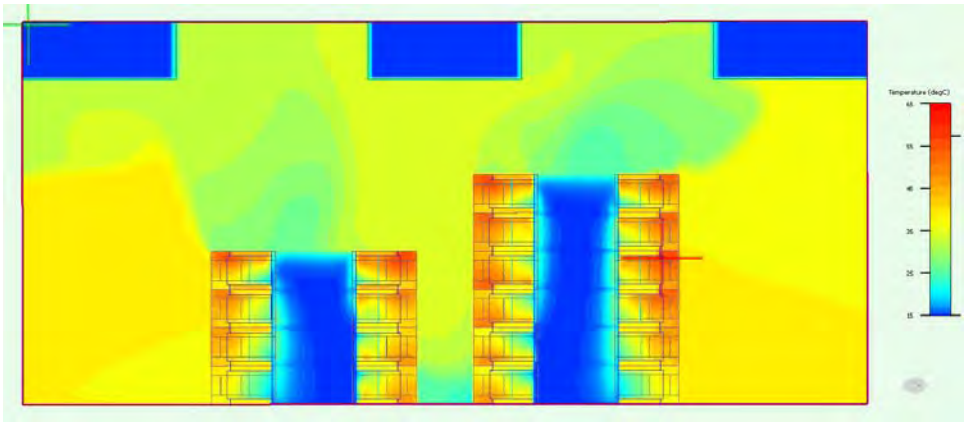

Figure 3.73 The Thermal Profile at the Floor Level for the Cabinets without Blanking Strips.

3.4.4. Cabinet with Chimney

When compared to the cabinet without chimney and the cabinet with chimney and perforated back door, the inlet temperatures remain almost identical except sometimes the cabinet with chimney and solid back door yields slightly lower temperatures. This configuration results in cooler cabinets than those in other two configurations. These lower temperatures are achieved as a result of better containment of cold aisle from hot aisle is achieved in the case of cabinet with chimney and solid back door. Because of better isolation, the mixing and recirculation is minimized.

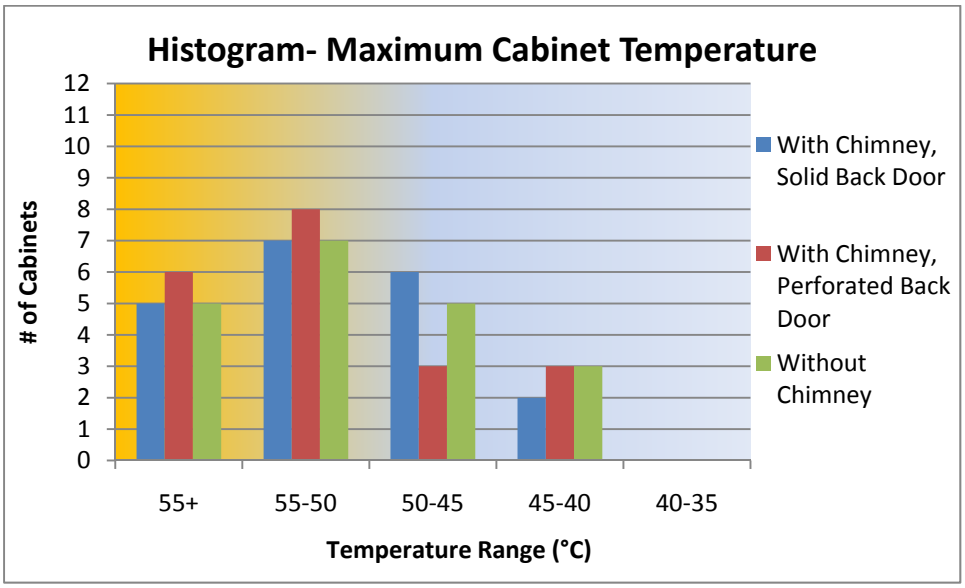

Figure 3.74 The Histogram of the Maximum Inlet Temperatures of the Cabinets.

3.5 Airside Economizers

The use of airside economizers leads to different configuration than what is discussed above. The air handling units in this scenario are placed outside the data center, often on rooftop. The air is then ducted into the data center and also from the data center. The outside air can be utilized 100% for the cooling of IT equipment when the outside temperature is either less than or equal to the supply temperature. This eliminates the use of chiller circuit entirely. However, when the temperature of outside air is greater than the supply temperature but still less than the temperature of return air, then the outside air can be used with chiller circuit. A schematic arrangement of airside economizer is shown in fig. 3.75.

In their proof of concept test, Intel IT has been running 900 production servers at very high rate of utilization [46]. This high density data center used 100% air exchange at 90°F and without humidity restrictions. The filtration was kept at the minimal level. It was estimated that with economizer in use 91% of the time, 67% energy can be saved which is estimated at USD 2.87 million/yr in a 10MW data center. The proof of concept test by Intel also showed no significant rise in server failure rates when air side economizer is used.

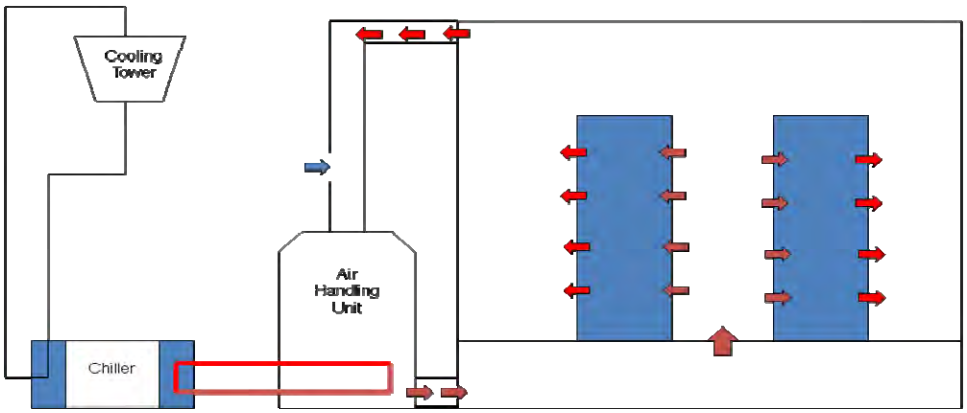

Figure 3.75 Schematic of the Airside Economizer Configuration.

A study by Shehabi et al. [47] compares the energy implications of conventional data centers with newer technologies employing waterside and air side economizers in five different climate zones in the state of California. They report that airside economizer performs consistently better in all climate zones. In fact according to another study by Syska Hennessy Group [48], outside air can be used for almost entire year in San Francisco.

3.5.1. Computational modeling

Four different scenarios are modeled. The baseline scenario is conventional datacenter configuration with CRAC units and underfloor supply. Three different configurations are modeled to represent the airside economizer scenario of supplying the outside air into the datacenter.

3.5.1.1 Case 1

A representative data center with underfloor configuration as shown in Fig. 3.76 is modeled using commercially available CFD code [9]. The half symmetry model of data center "cell" has 12 racks arranged in cold aisle – hot aisle layout as shown in Fig. 5. The footprint dimensions of the half-symmetry "cell" are 19ft (5.7 m) by 20 ft (6.0 m), and the room was 10 ft

(3.0 m) tall. It has the raised floor with a plenum of 2 ft depth. The cabinets are 600mm wide, 1000mm deep and 45U or 2000mm tall. The air-moving device inside the racks is assumed to force the air straight through the rack, with a constant velocity across the front and back of the racks. Each rack is assumed to be a 11 kW (37,534 Btu/h) rack, with a rack airflow rate of 965 cfm (0.45 m^3/s). This corresponded to an air temperature rise through the rack of 20°C (36°F) considering the specific heat of air 1.006 kJ/kg°K and the density 1.2 kg/m^3. The temperature of the chilled air entering the room through the perforated tiles was fixed at 15°C (56°F). The CRAC unit had a 3 ft × 8 ft (0.91 m x 2.4 m) footprint and was 2.4 m (8 ft) high.

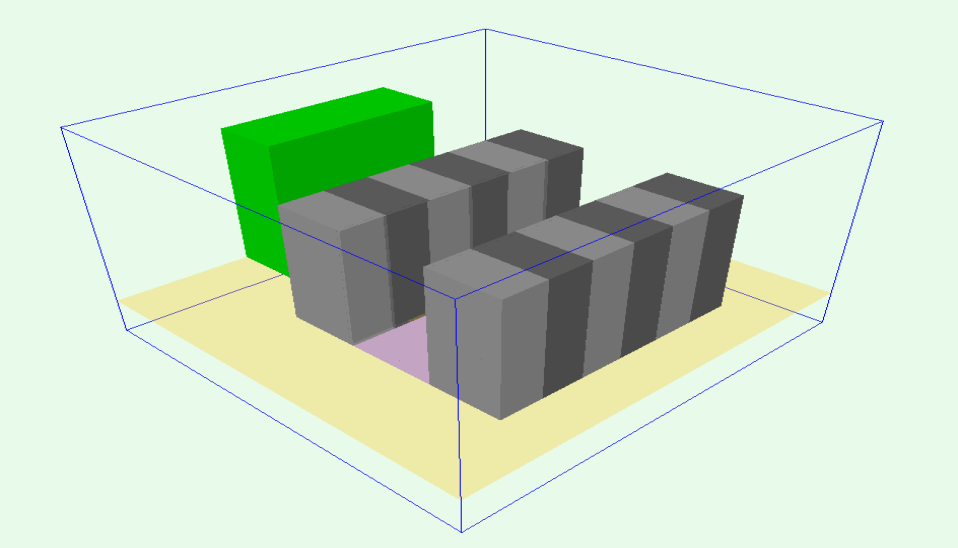

Figure 3.76 The Data Center Model for Case 1.

3.5.1.2 Case 2

Figure 3.77 shows the model used in case 2. This model is similar to case 1 except that the CRAC is replaced by two air handling units. One of the unit delivers the outside air into the data center while the other acts as the outlet for returning hot air which is subsequently dumped into the ambient. Depending upon the outside temperature, various possibilities of chiller usage exist. If the temperature outside is cooler than the supply temperature, the chiller is not used at

all. If outside temperature is more than the supply temperature but less than the temperature of returning air, partial chiller operation is required to obtain set point temperature. However if the

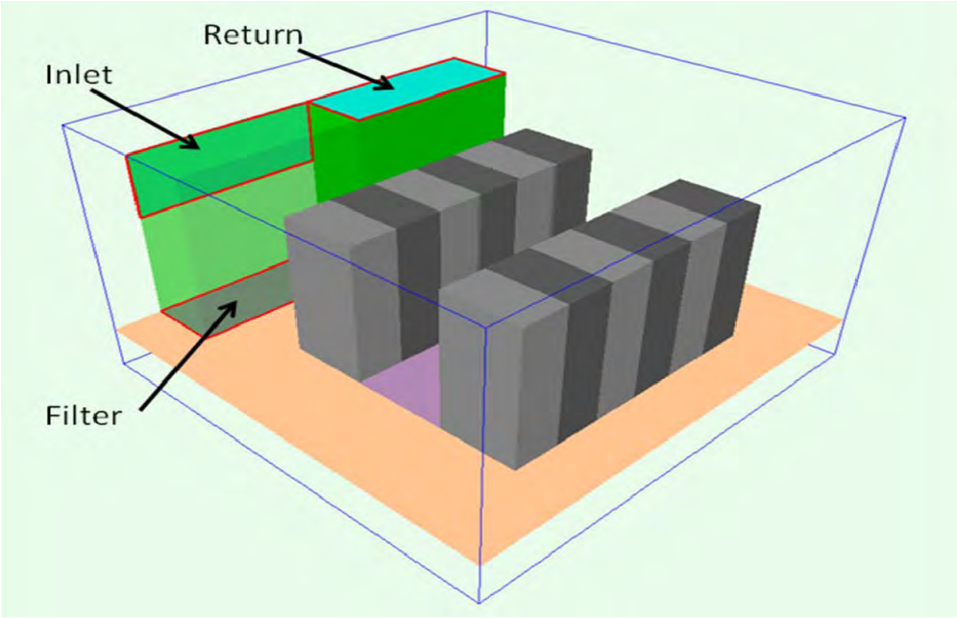

Figure 3.77 The Data Center Model for Case 2.

outside temperature is more than the return temperature, the conventional CRAC unit is operational. Here however, it is assumed that the outside temperature is same as the supply temperature and no chiller or mixing is required.

3.5.1.3 Case 3

In this model, as shown in figure 3.78, a duct is created which has two fans at either end. Each of the fans delivers 5790 cfm of outside air into the duct. Through the opening in the duct, the air is introduced into the underfloor plenum and subsequently is delivered into the room. The model is shown below in figure 3.78.

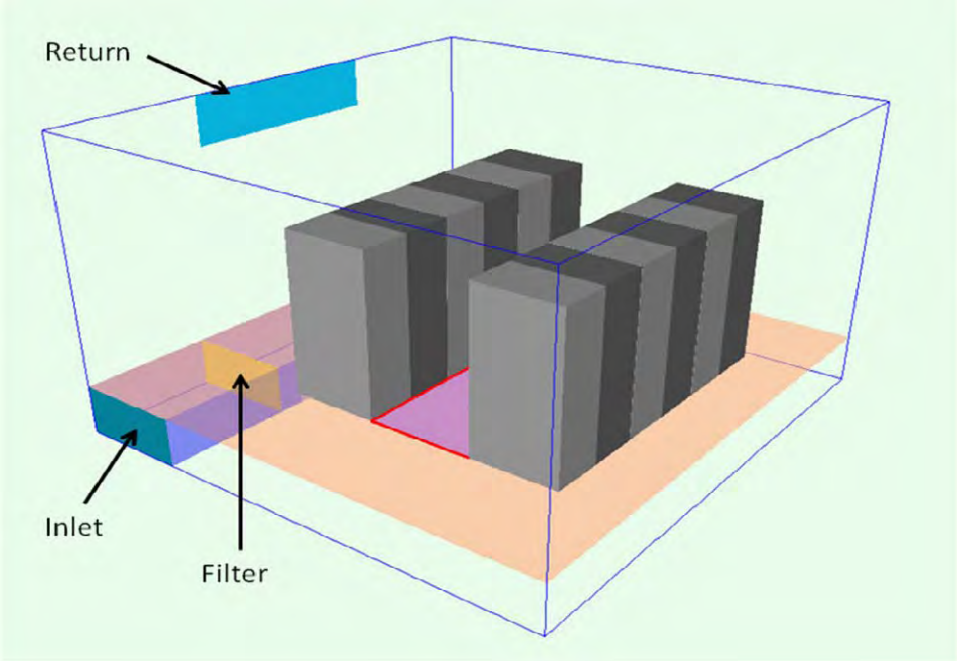

Figure 3.78 The Data Center Model for Case 3.

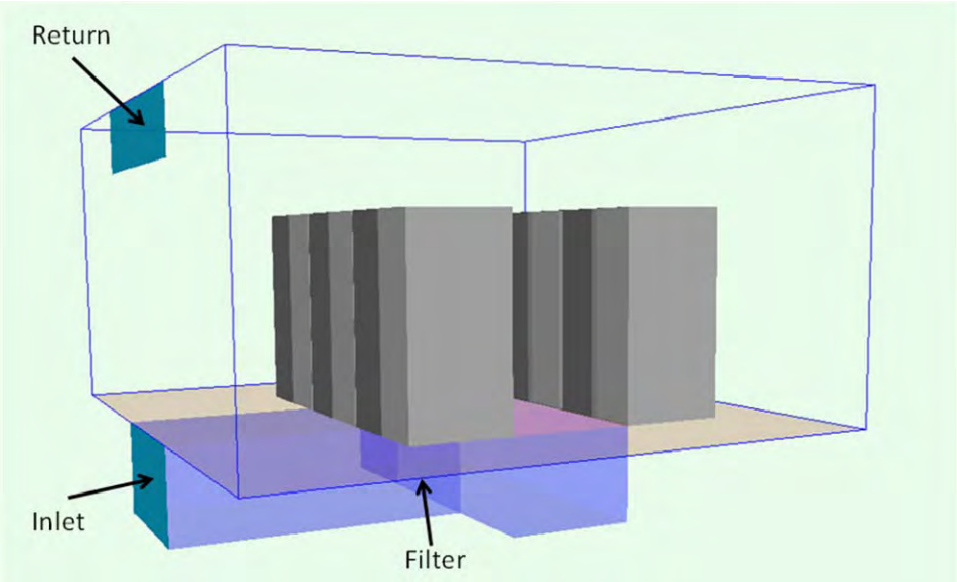

Figure 3.79 The Data Center Model for Case 4.

3.5.1.4 Case 4

In this model, the air is delivered by single duct into the cold aisle. The incoming duct is connected to another duct beneath the cold aisle. The filter is applied at the junction of these two ducts. The total airflow into the ducts and into the room is 11580 cfm. The model is shown in figure 3.79.

3.5.2. The Mesh Sensitivity Analysis

A mesh sensitivity analysis was carried out for each case to insure the grid independence of output variables. The grid cells count selected is within the range where output variables show no variation. Figure 3.80 shows the graph for case 1.

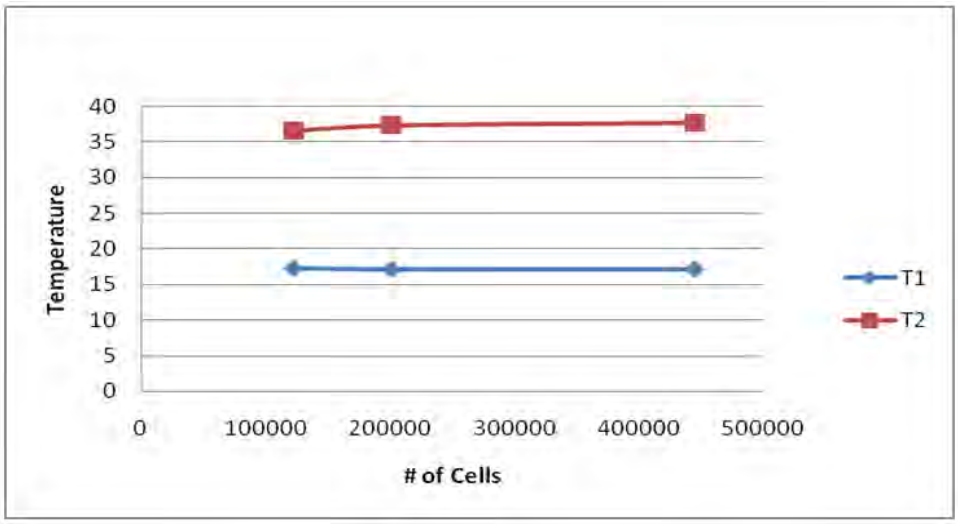

Figure 3.80 Mesh Sensitivity Analysis for Case 1.

3.5.3. The Variation in Rack inlet Temperatures

Aforementioned cases were solved using K-ε turbulence model in Flotherm [117]. The rack inlet temperature was monitored for all the racks along the height at the interval of 300mm. Figures 3.81 through 3.88 indicate the variation in RIT.

For case 1, the rack inlet temperature recorded at the outer racks is higher than the rack inlet temperatures at inner racks. The temperature profiles are symmetric in nature. Racks 1 and 6 show similar trends and so do the inner pairs of racks 2 and 5, and racks 3 and 4. There are at least 10 instances where the critical temperature of 35°C is exceeded.

In case 2, the temperature profiles do not follow the pattern described above for case 1. This irregularity is attributed to the uneven distribution of air as a result of inlet and return locations not being centrally located. 5 instances exceeding 35° are reported in this scenario.

In case 3, the temperature profile pattern hold good as the pair of racks indicate similar temperatures. The rack inlet temperatures recorded in second row are lower than those recorded in the first row. All recorded rack inlet temperatures are at or below 35°C.

Amongst all 4 cases, the minimum rack inlet temperatures are recorded in Case 4. It follows the pattern of similar profiles. Also, as noted in case 3, the rack inlet temperatures recorded in second row are lower than those recorded at first row.

There is significant maldistribution of the cold air in cold aisle. Each tile is supposed to dispense the airflow required for the rack next to it. Some tiles however deliver more air than required whereas other tiles deliver less amount of cold air. This maldistribution results in severe recirculation as a result of which the rack inlet temperatures increase.

3.5.4. The Energy Consumption

The advantage offered by airside economizer is the savings in energy due to reduced or no chiller operation. In conventional data center operation, typical power consumption of a 30 ton CRAC unit is about 7.5kW [*]. Although in case 1, the cooling required is more than 30 ton, for comparison purpose, the consumption is considered to be 7.5kW. The energy consumed by the fans in cases 2-4 is estimated using the equations 1-4. Table 2.1 provides the summary of the estimates.

Power P, consumed by fan:

$$P(hP) = \frac{Q \times TP}{6356 \times \eta_m}$$

$$P(KW) = \frac{P(hP)}{1.3}$$

Total Pressure,

$$TP = SP + VP$$

Velocity Pressure,

$$VP = \left[\frac{V\ (fpm)}{4005}\right]^2$$

where,

P: Power (KW, hP), Q: Flow rate (cfm)

SP: Static pressure (in. of H_2O)

TP: Total pressure (in. of H_2O)

V: Cross-sectional velocity (fpm)

VP: Velocity pressure (in. of H_2O)

η_m: Mechanical efficiency (75%)

Table 2.1 Power Consumption Estimates

Case	Power Consumption (kW)
1	7.5
2	0.9
3	2.38
4	1.97

The energy consumed by fans in cases 2 through 4 is dependent on the fan static pressure. The fan static pressure varies with variation in duct size. Larger the duct size, lesser is the pressure drop which results in lesser power consumption.

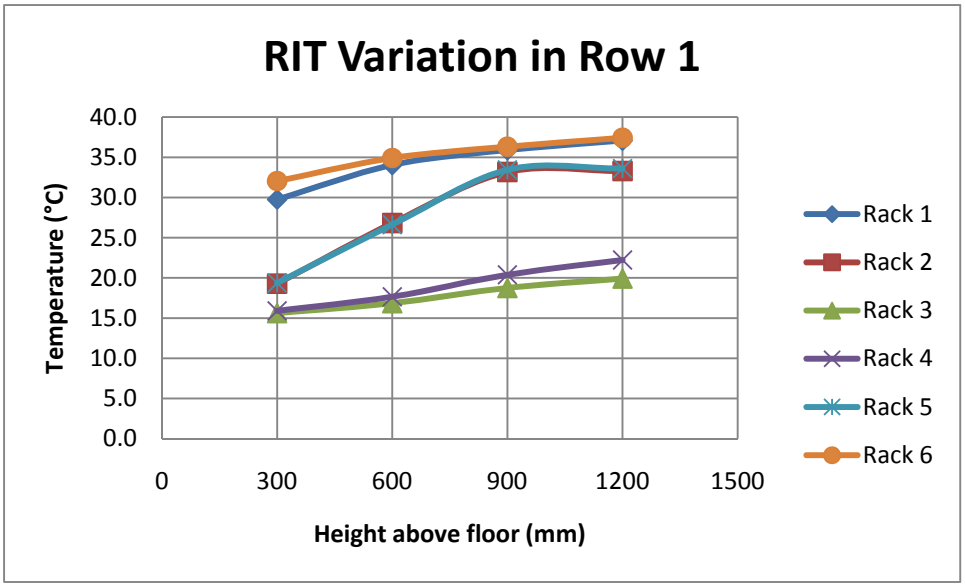

Figure 3.81 The Variations in Inlet Temperatures in Row 1 for the Case1.

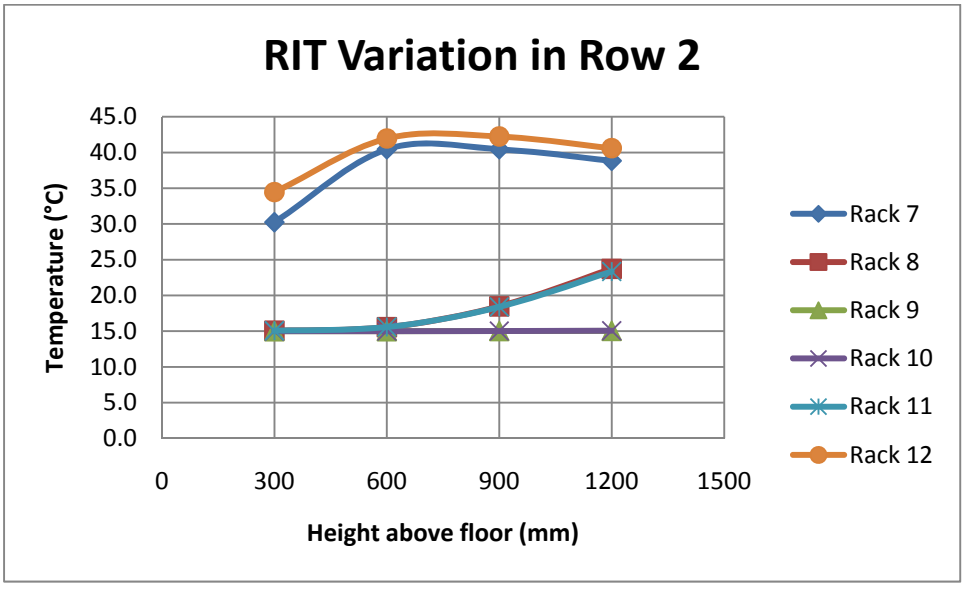

Figure 3.82 The Variations in Inlet Temperatures in Row 2 for the Case1.

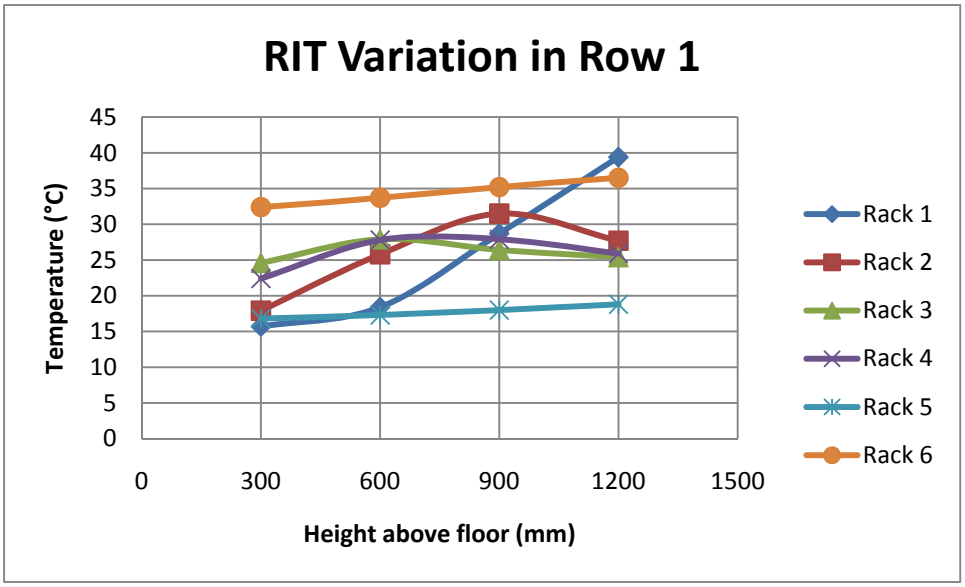

Figure 3.83 The Variations in Inlet Temperatures in Row 1 for the Case 2.

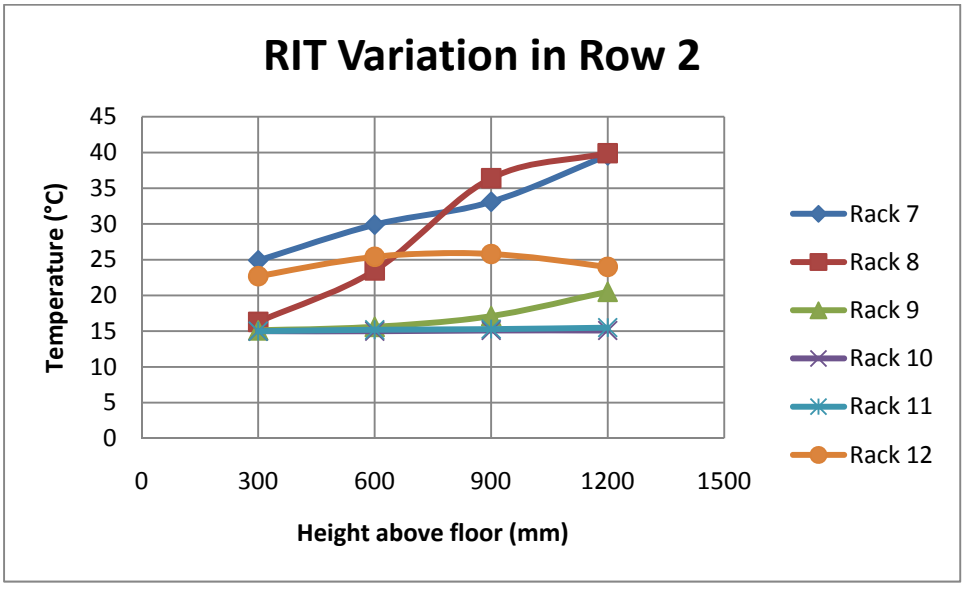

Figure 3.84 The Variations in Inlet Temperatures in Row 2 for the Case 2.

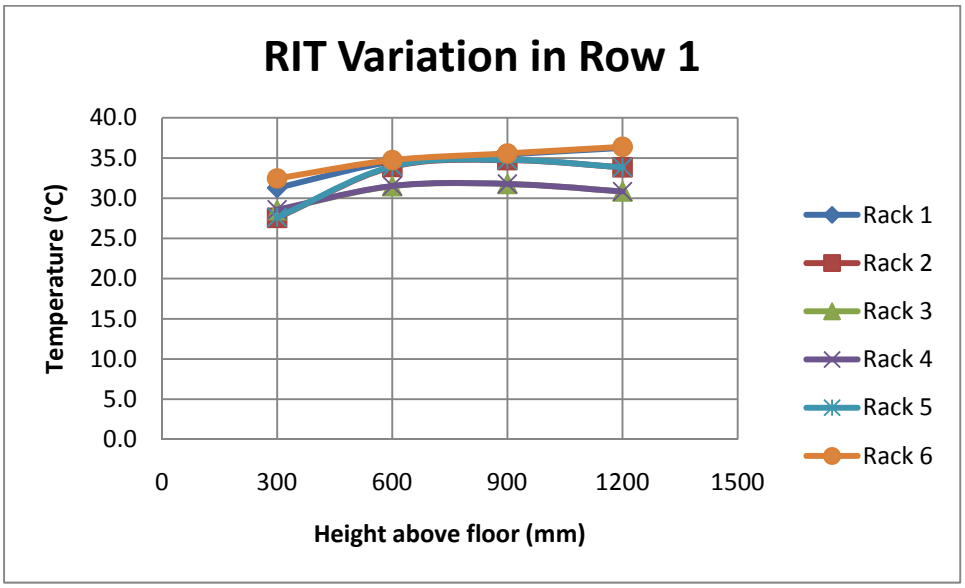

Figure 3.85 The Variations in Inlet Temperatures in Row 1 for the Case 3.

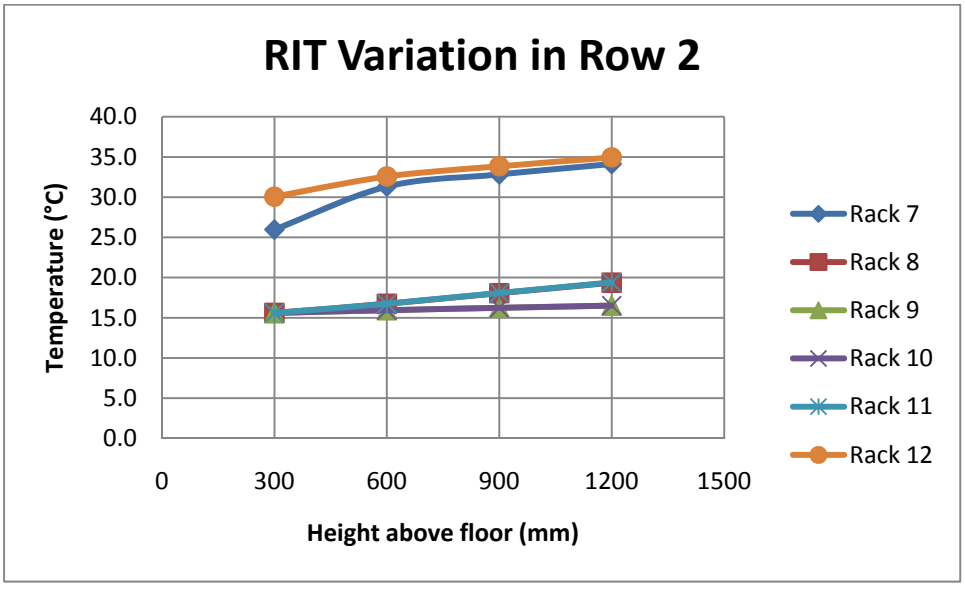

Figure 3.86 The Variations in Inlet Temperatures in Row 2 for the Case 3.

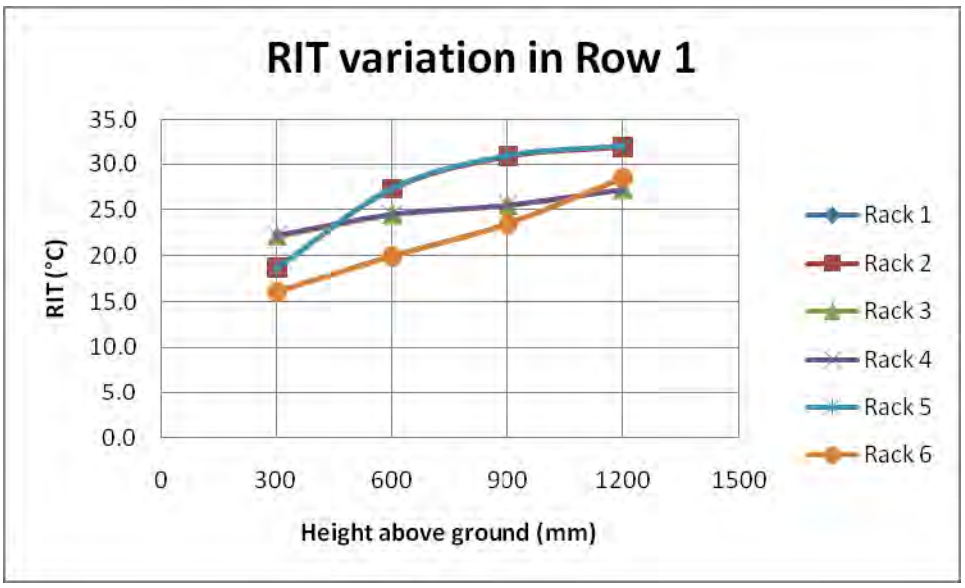

Figure 3.87 The Variations in Inlet Temperatures in Row 1 for the Case 4.

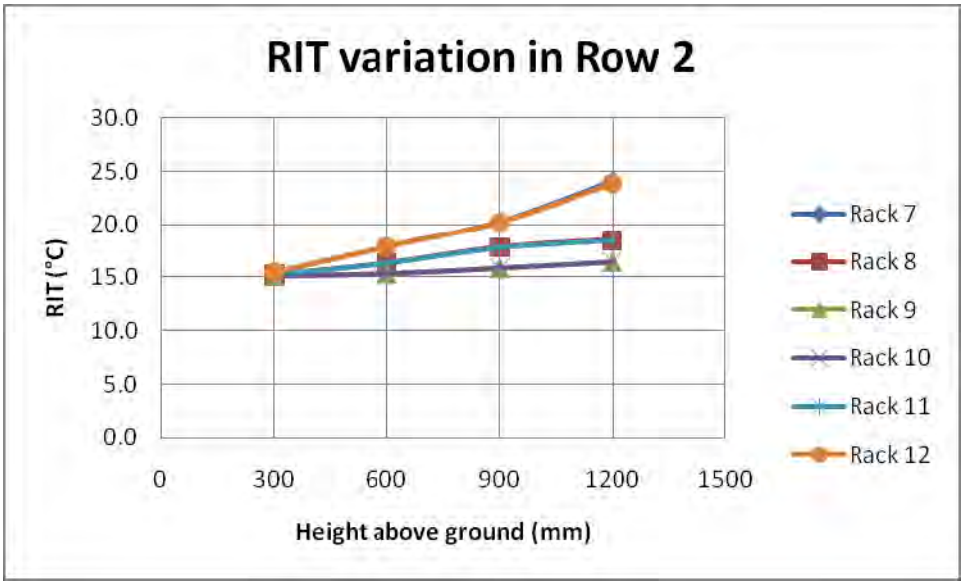

Figure 3.88 The Variations in Inlet Temperatures in Row 2 for the Case 4.

3.6 Hot Aisle Containment

The effectiveness of cabinets with chimney can be seen when 100% containment of hot air is achieved. In an underfloor air supply configuration, the cabinets with chimney and solid back door can be used with chimneys extended into the drop ceiling for a ceiling return. This configuration isolates the cold air completely which will reduce all the inlet temperatures to set point temperature or the supply temperature ideally. As a result, lower global temperatures are recorded. Figure 3.83 shows such a scenario modeled. The thermal profile for this scenario taken at Z=3900mm is shown in figure 3.84.

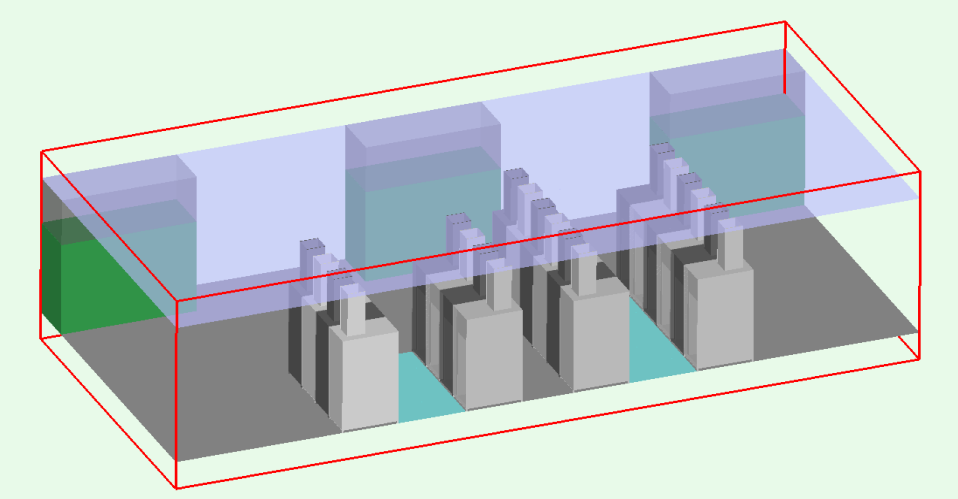

Figure 3.89 The Hot Aisle Containment using Cabinets with Chimneys.

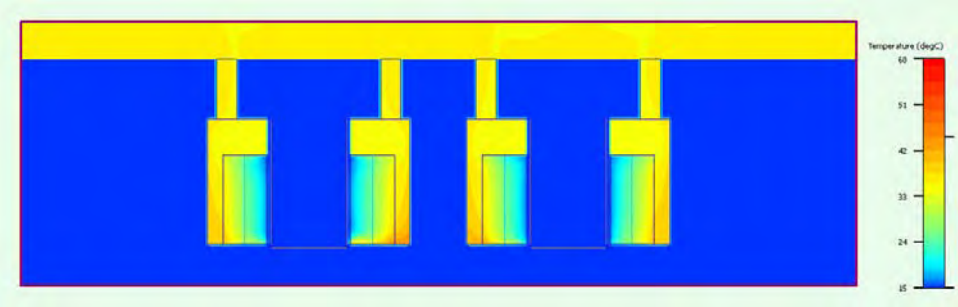

Figure 3.90 Thermal Profile of the Hot Aisle Containment using Cabinets with Chimneys.

CHAPTER 4

ANALYTICAL MODEL

The data centers exist in the variety of plant layouts and the infrastructural arrangements. Numerous studies analyzing various configurations are available in the literature [1-112]. In this chapter, a simple data center plant is considered for the analysis. This plant model consists of the IT load and the cooling infrastructure. The IT load is essentially the servers. The non-IT load has following components

- The cooling infrastructure
- The distribution and transformer losses
- The office lighting

These components and overall energy consumption is discussed in the following sections with respect to the simple plant model under consideration.

4.1 The Data Center Facility Model

Figure 4.1 below shows the heat energy flow in a simple data center facility considered for analysis. It contains the ensemble of varying orders of magnitude. The individual components vary not only in size but also in their energy consumption by orders of magnitude. For example, a processor measures few millimeters in length while the data center room is few meters. A server fan consumes few watts while the CRAH fan consumes few kilowatts.

The path of dissipated heat energy begins in the data center room where the heat from the servers is carried away by the CRAH units. The CRAH units reject this heat to the chiller plant via the chilled water loop. There is heat transfer at the chiller plant between the water loop and the refrigerant loop. This heat is then carried to the cooling tower where it is finally rejected to the ambient. This flow is indicated in the figure 4.1 below.

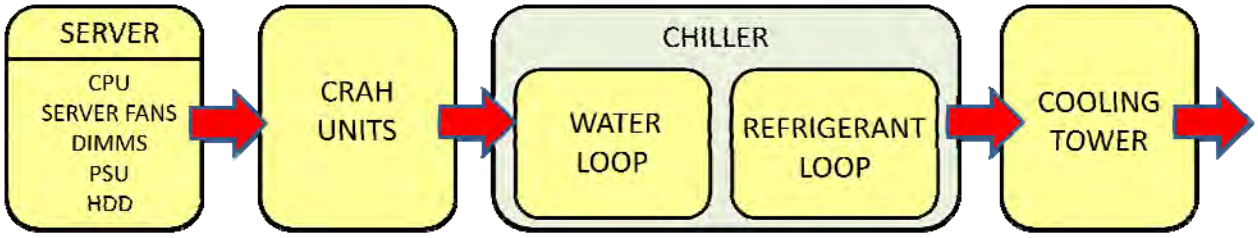

Figure 4.1 The Heat Dissipation in the Data Center Facility.

4.2 The Server

The primary components of server that consume the power are

- The central processing units
- The server fans
- The memory modules
- The power supply unit
- The hard disk drives
- Other including the motherboard planar losses

Figure 4.2 below shows an example of a 2 processor Intel Server [118]. It is worth noting that the thermal solutions are not shown in the figure and neither are the DIMM modules.

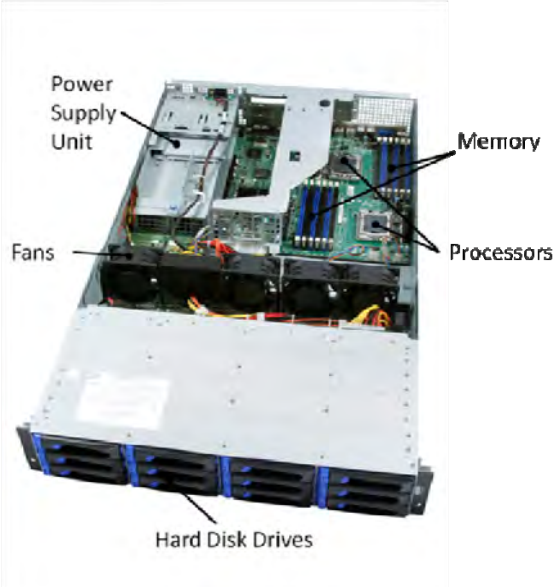

Figure 4.2 Typical Server Components [118].

4.2.1. The Central processing Units

Depending upon number of CPUs and the selection of platform, the server power will change. The power consumption of CPU is temperature dependent. Although the dynamic power of the CPU is relatively unaffected by the temperature, the static power is greatly affected as temperature dictates the leakage current. Post Pentium-II, the leakage current and the static power have become significant components of the CPU power. The new generation of the processors use technologies such as demand based switching and enhanced speed step in order to save the power consumption [119].

4.2.1.1. Thermal profile of the processor

The thermal specifications or the thermal profile of the processor are aimed at achieving reliable operation for longer life while achieving the lower levels of acoustic noise by fan speed control. This thermal profile is often mentioned in terms of the case temperature (T_{case}), which is taken at the center of the intermediate heat spreader. The effective thermal solution is the one which will keep the die temperature below T_{case} all the time and thus achieve the long term reliability.

The modern processors have the logic and monitoring feature integrated into the silicon. It makes the use of a Thermal Control Circuit (TCC) which modulates the clock to ensure that the die temperature will remain below T_{case}. When the die temperature is near the case temperature, the TCC modulates the duty cycle of clock thereby bringing the power to lower levels. Although this results into lower frequencies, the die temperature is also lowered. Thus, the TCC gives an option to design the thermal solution by finding out the maximum power consumed while running an application(s). This power level, which is lower than the maximum power a processor can dissipate, is called the Thermal Design Power (TDP). The thermal solutions are designed to dissipate this TDP and any thermal excursions beyond TDP are then handled by TCC by adjusting the duty cycles of processor clocks.

4.2.1.2. Thermal Resistances

The performance measuring metrics for the thermal solution are the thermal resistances. There are three such resistances namely the case to ambient thermal resistance, the case to sink thermal resistance and the sink to ambient thermal resistance.

The case to ambient thermal resistance is an indication of heat dissipated by the device from the case surface to the local ambient. Although this heat transfer has more than one path, it is assumed that all the heat is dissipated through the integrated heat spreader (IHS). This case to ambient thermal resistance is defined as

$$\theta_{CA} = \frac{T_{case} - T_A}{TDP} \qquad (1)$$

The case to sink thermal resistance is the measure of heat dissipated through the thermal interface material (TIM). It is defined as

$$\theta_{CS} = \frac{T_{case} - T_{sink}}{TDP} \qquad (2)$$

The sink to ambient thermal resistance is the measure of heat dissipated to the local ambient through the heat sink. It is defined as

$$\theta_{SA} = \frac{T_{sink} - T_A}{TDP} \qquad (3)$$

The case to sink thermal resistance is dependent on the thermal conductivity and the thickness of TIM while the sink to ambient thermal resistance varies not only with thermal conductivity and geometry of the heat sink but also with the air velocity through the heat sink.

The thermal behavior of processor indicating the correlation between the TDP and the T_{case} is called as the thermal profile of the processor and is given by

$$T_{case} = (\theta_{CA}) \cdot TDP + T_A \qquad (4)$$

The thermal profile for Intel Xeon Processor 5500 series basic SKU [119] is shown in fig. 4.3 below. The X axis represents the power dissipated by the processor and the Y axis represents the case temperature. The highest endpoint on the thermal profile, indicated by letter "A", corresponds to the thermal design power of the processor. The corresponding case temperature would be the maximum case temperature. The lowest endpoint on the thermal profile represents the power of value $P_{control\_base}$ and corresponding case temperature $T_{control}$.

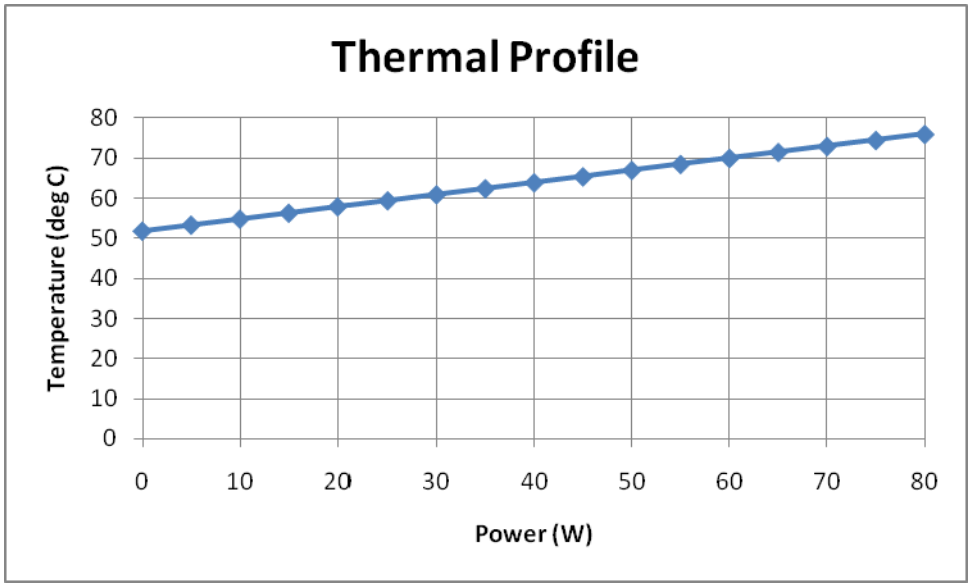

Figure 4.3 Thermal Profile of the Processor.

4.2.1.3. Thermal Monitor Function:

The thermal monitor comprises of the TCC and the DTS (Digital Thermal Sensor). The functions of thermal monitor include reducing the case temperature by activating the TCC and provide the temperature through DTS to achieve fan speed control (FSC).

4.2.2. The Server Fans

The server fans are critical element in the heat transfer process across the server. The heat transfer is dominated by the convection and can be expressed as

$$q = h_{eff}.A_{eff}.(T_{sink} - T_{LA})$$

Since the effective area available for heat transfer is constant, for a given heat load, the convective heat transfer coefficient is inversely proportional to the temperature differential. This temperature differential is however forced to assume smaller values to keep the processor on thermal profile. This means the heat transfer coefficient has to assume larger values. By considering the simple convection process, the convective heat transfer coefficient can be related to the velocity of the air through Nusselt and Reynold's numbers. This dependence is given by

$$h \propto v^{4/5}$$

Thus, in order to have a very large convective heat transfer coefficient, velocity has to be even higher which translates into higher flow rate. Finally, the higher flow rate implies the increased power consumption because according to the fan laws, increase in flow rate is associated to increase to the 3rd power of the power consumed.

4.2.2.1. Fan Speed Control (FSC)

The objective of FSC algorithm is to vary the fan speed in such a way that the case temperature of the processor is kept below the thermal profile while reducing the noise level for entire server system. The FSC plays an important role in achieving the goal of long term reliable operation of the processor. When based on the digital thermal sensor and the local ambient, the FSC algorithm may use local ambient temperature to scale the fan speed and the DTS to control.

A representative fan duty cycle is shown in figure. The control temperature is plotted along the X axis and the fan power is plotted on the Y axis. T1, T2…are the control points defined in the FSC algorithm at which the fan duty cycle will change. P1, P2… are the %duty cycles. These duty cycles are scaled based on the local ambient temperature of the CPU. So when $T_{control}$ exceeds T1, the fan will speed up and provide more airflow to ensure that the

processor adheres to the thermal profile. During this process, the power consumption of the fan will increase from P0 to P1.

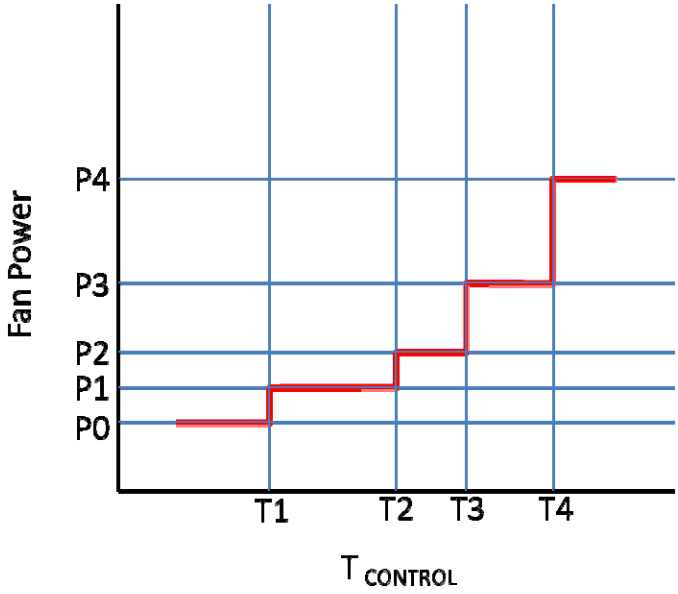

Figure 4.4 Fan Speed Control.

4.2.3. The Memory Modules

The memory modules can consume power from 5W to 21W depending on the technology. This power consumption continues to grow due to following reasons.

- Increased cores in processors enable increased memory use
- Increase in number of data centers using virtualization
- Internet Protocol data centers using memory intensive search applications.

4.2.4. The Power Supply Units

The efficiency of the power supply unit depends on its load. The loads at 50-75% utilization are the most efficient. Below 50% utilization, the efficiency drops drastically. It does not improve dramatically once the loads have crossed 75% utilization.

4.3 The CRAH Unit

The total heat load carried by the CRAH unit can be calculated using following expression.

$$q_{CRAH,Total} = \sum_{i=1}^{n} \varepsilon_{CRAH,i}.C_{min}.(T_{ret,i} - T_{cho})$$

Where, ε_{CRAH} is the effectiveness defined for the heat exchanger, C_{min} is the minimum capacitance rate of the two, $T_{ret,i}$ is the temperature of air returning to the CRAH unit and T_{cho} is the temperature of chilled water entering the CRAH unit.

The effectiveness of the heat exchanger can be calculated from the expression below.

$$\varepsilon_{CRAH} = \frac{1 - e^{-C_r.A}}{C_r}$$

Where,

$$A = 1 - e^{-NTU}$$

and

$$C_r = \frac{C_{min}}{C_{max}}$$

NTU is a number of transfer units for the CRAH heat exchanger coil. It is defined as

$$NTU = \frac{(UA)_{CRAH}}{C_{min}}$$

UA_{CRAH} is the thermal conductance of the CRAH heat exchanger and is typically within 10000-25000 W/°K.

The temperature of air supplied by the individual CRAH unit can then be calculated by using following expression.

$$T_{sup,i} = T_{ret,i} - \left[\frac{q_{CRAH,i}}{\dot{m}.(C_p)_{air}}\right]$$

4.4 The Chiller Unit

The factors affecting chiller efficiency are

- Type and size of the chiller
- Supply temperature of chilled water
- Differential temperature of chilled water
- Water temperature at the condenser entry
- Part load efficiency

A simple analytical model of the chiller operation, the Gordon-Ng model is presented by Jiang et al. [120]. The same model is used here.

$$y = a_1 x_1 + a_2 x_2 + a_3 x_3$$

Where,

$$x_1 = \frac{T_{cho}(1000)}{q_{chiller}}$$

$$x_2 = \frac{(T_{chi} - T_{cho}).1000}{T_{cdi}.q_{chiller}}$$

$$x_3 = \frac{1}{T_{cdi}}\left[\frac{q_{chiller}}{1000}\left(\frac{1}{COP} + 1\right)\right]$$

$$y = \left[\left(\frac{1}{COP} + 1\right)\frac{T_{cho}}{T_{cdi}}\right] - 1$$

The coefficients a1, a2 and a3 are determined through regression analysis.

CHAPTER 5

THE CASE STUDY OF ENERGY EFFICIENT THERMAL MANAGEMENT

Heydari and Mulay [121] presented the study of cold aisle containment and the data center energy efficiency. The data center room used for this case study was 7700 square feet and was populated with 100 racks. Three different types of servers were distributed amongst them. The racks were laid out in 5 rows, each row containing 20 racks. They were arranged in hot aisle-cold aisle arrangement with 3 cold aisles. There were 11 CRAH units distributed along the periphery of the room. The room also housed 5 PDU banks with each bank containing two PDUs. The servers were at OEM specified power and airflow configuration.

The case study had following objectives:

1. Determine if the room is overcooled.
2. Achieve nearly uniform rack inlet temperatures.
3. Improve the energy efficiency by dynamic thermal management.

5.1 The Computational Model

A commercially available CFD software tool [117] was used to create a computational model of the layout. Figure 5.1 shows the computational model and the layout. The k-ε model was used. The two-equation turbulence model (also known as the standard k- ε model) is more complex than the zero-equation model. The standard k- ε model [115] is a semi-empirical model based on model transport equations for the turbulent kinetic energy (k) and its dissipation rate (ε). The model transport equation for k is derived from the exact equation, while the model transport equation for ε is obtained using physical reasoning and bears little resemblance to its mathematically exact counterpart.

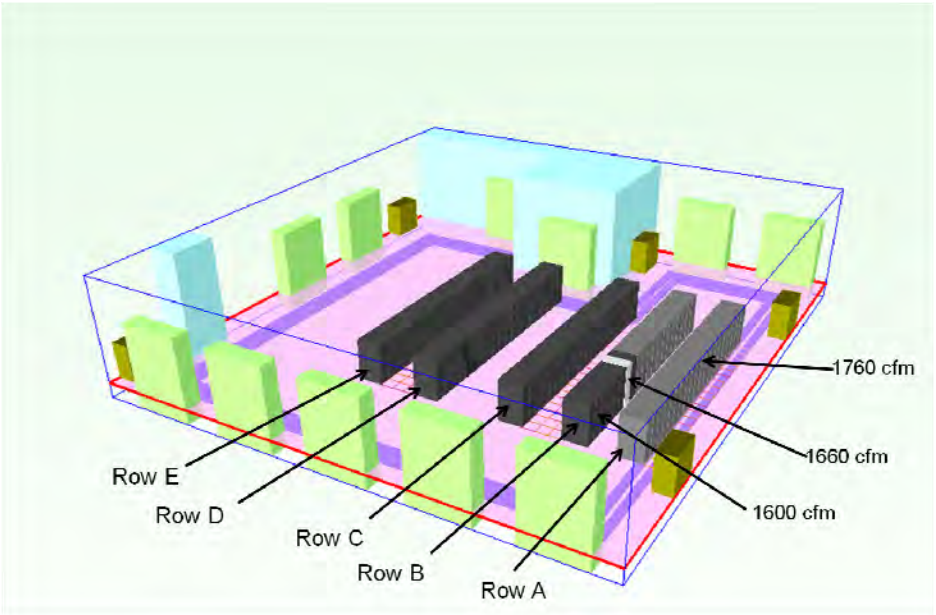

Figure 5.1 Computational Model of the Test Facility.

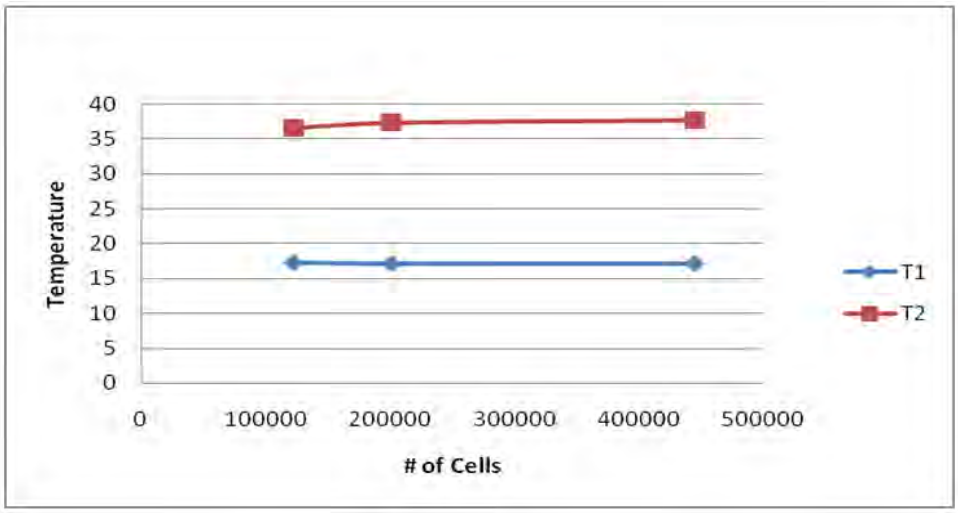

Figure 5.2 Mesh Sensitivity Analysis.

5.2 The Mesh Sensitivity Analysis

For different grid sizes, output variables were monitored to arrive at the correct mesh size and number of grid cells to ensure the independence of output variables from the grid size. The figure 5.2 indicates the variation of two such monitored points with increased grid cells. Based on the graph the grid selected for the analysis contained 3,000,000 cells.

5.3 Rack Cooling Indices

Herrlin [74] introduced the rack cooling indices in his paper "Rack cooling effectiveness in data centers and the telecom central offices: the rack cooling index (RCI) ^{TM}" as a measure of equipment health both at the low and the high end of temperature spectrum. The rack cooling index at the high end (RCI_{HI}) is an indication of the servers having inlet temperatures greater than the maximum allowed inlet temperature. Similarly, the rack cooling index at the low end (RCI_{LO}) is an indication of the servers getting air at a temperature below the minimum allowed temperature.

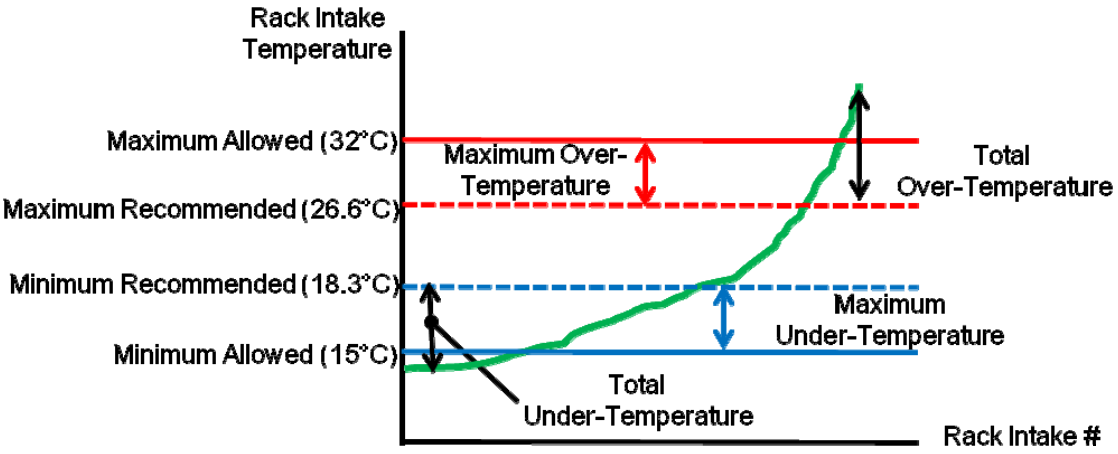

Figure 5.3 The Over and the Under Temperatures [74].

As shown in the figure 5.3, the rack inlet temperatures (either measured or calculated from CFD models) are sorted in increasing order and are plotted. The ASHRAE recommended

temperature range and allowed temperature range is also indicated. The difference between maximum recommended temperature and the maximum allowed temperature is called “the maximum over-temperature”. Similarly, the difference between minimum allowed and minimum recommended temperatures is called “the maximum under-temperature”. The difference between the recorded rack inlet temperature and the maximum recommended temperature is called “the total over-temperature”. Similarly, the difference between the recorded rack inlet temperature and the minimum recommended temperature is called “the total under-temperature”. The rack cooling indices are then defined as,

$$RCI_{HI} = \left[1 - \frac{\text{total over-temperature}}{\text{maximum over-temperature}}\right] \times 100\%$$

$$RCI_{LO} = \left[1 - \frac{\text{total under-temperature}}{\text{maximum under-temperature}}\right] \times 100\%$$

The RCI_{HI} of 100% indicates that no server has intake temperature greater than the maximum allowed intake temperature. The RCI_{LO} of 100% indicates that no server has intake temperature less than the minimum allowed intake temperature.

5.4 Case 1: No Containment

The CFD simulation was carried out for the model shown in fig. 5.1. As stated earlier, there are 11 CRAH units, each delivering 16,500 cfm. The thermal profiles captured at three different levels above the floor. Figures 5.4 through 5.6 indicate the thermal profile taken at 1’, 3.5’ and 6’ above floor respectively. From these thermal profiles, it is evident that the hot exhaust air is being recirculated into the cold aisle where it is mixing with the supplied cold air. This recirculation and ambient mixing has caused the intake temperatures of several racks to elevate much above the supply temperature. This recirculation is severe at the end racks and the effect can be seen in all the three profiles.

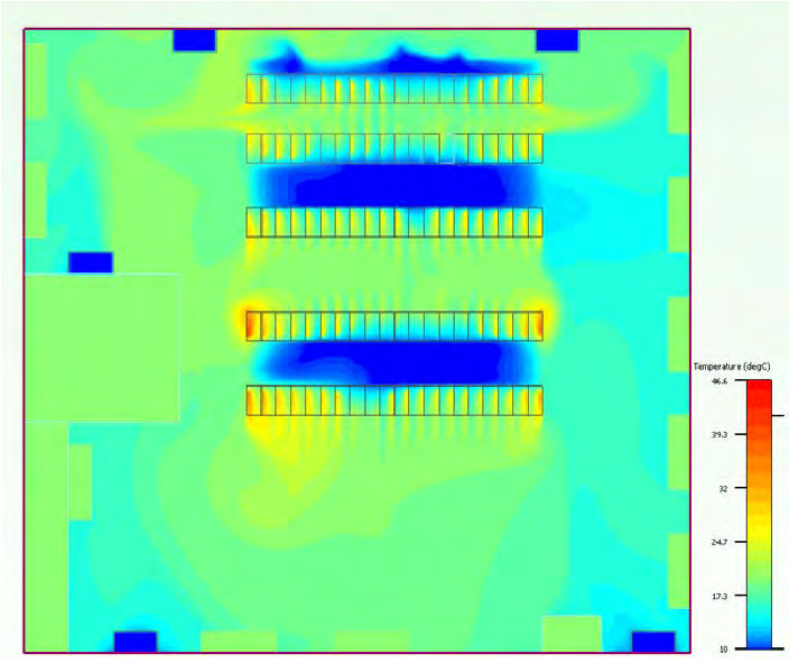

Figure 5.4 Thermal Profile at 1’ Above the Floor Level without Containment.

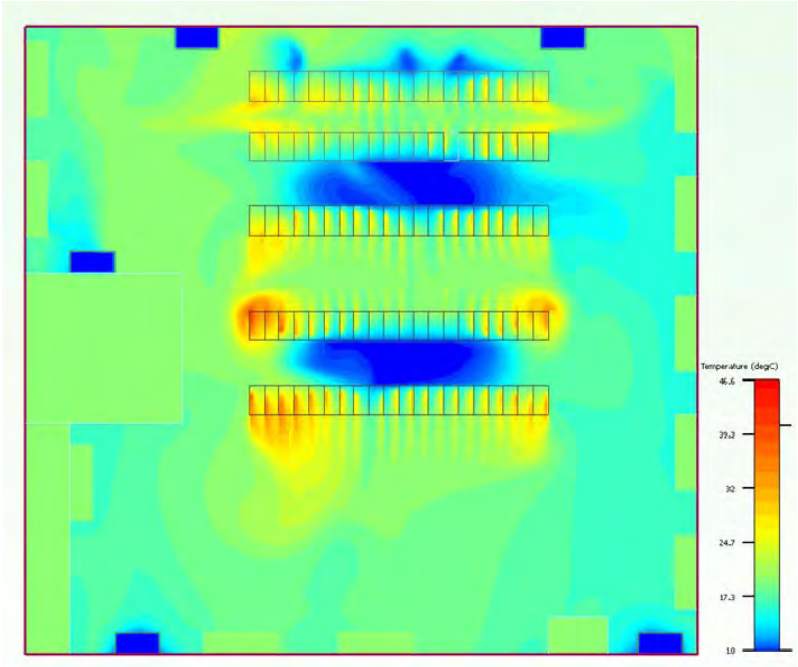

Figure 5.5 Thermal Profile at 3.5’ Above the Floor Level without Containment.

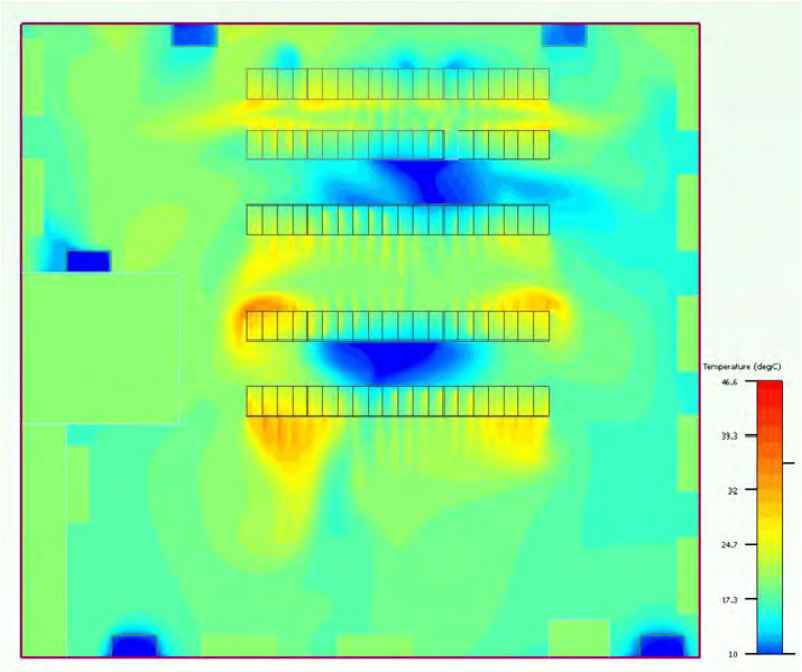

Figure 5.6 Thermal Profile at 6' Above the Floor Level without Containment.

5.5 Case 2: Cold Aisle Containment

In order to eliminate the recirculation of hot air and the rise in inlet temperatures, the cold aisle containment technique is utilized. The cold aisles now have "the roof" of fire rated material hung with fusible links and "the end caps" making them enclosed spaces. Figure 5.7 shows the cold aisle with installed roof and end caps.

The CFD model is now modified to include the containment system. As shown in fig. 5.8, all the three cold aisles are enclosed. Although in reality some leakages from the cold aisle and infiltration into the cold aisle are experienced, the CFD model assumes that the containment is 100% leak proof. The CFD simulations were carried out on the modified model with the cold aisle containment. The thermal profiles obtained at 1', 3.5' and 6' above the floor level. From these profiles, we can see that the cold aisle containment has been able to eliminate the recirculation completely. By stopping the infiltration of hot air into the cold aisle, this arrangement has also resulted in more uniform server inlet temperatures.

Figure 5.7 The Cold Aisle Containment System.

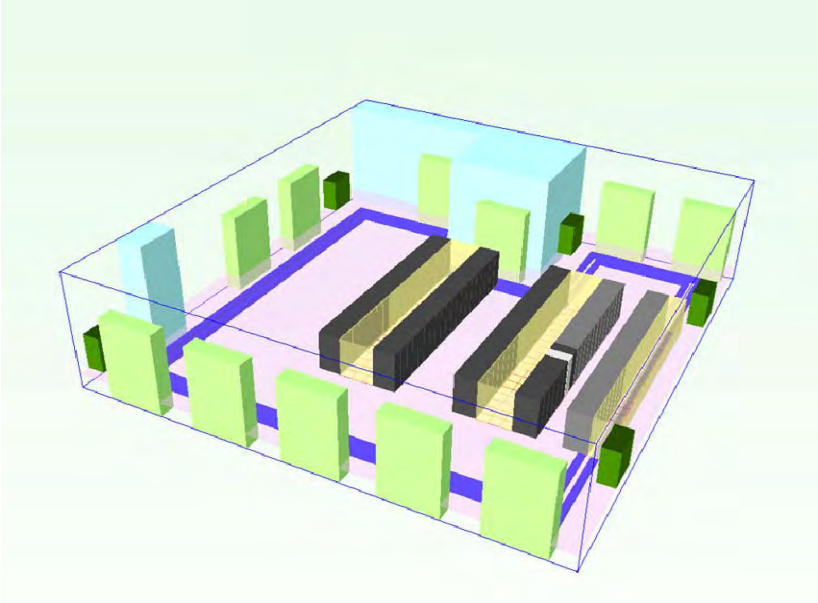

Figure 5.8 Computational Model of the Test Facility with Cold Aisle Containment.

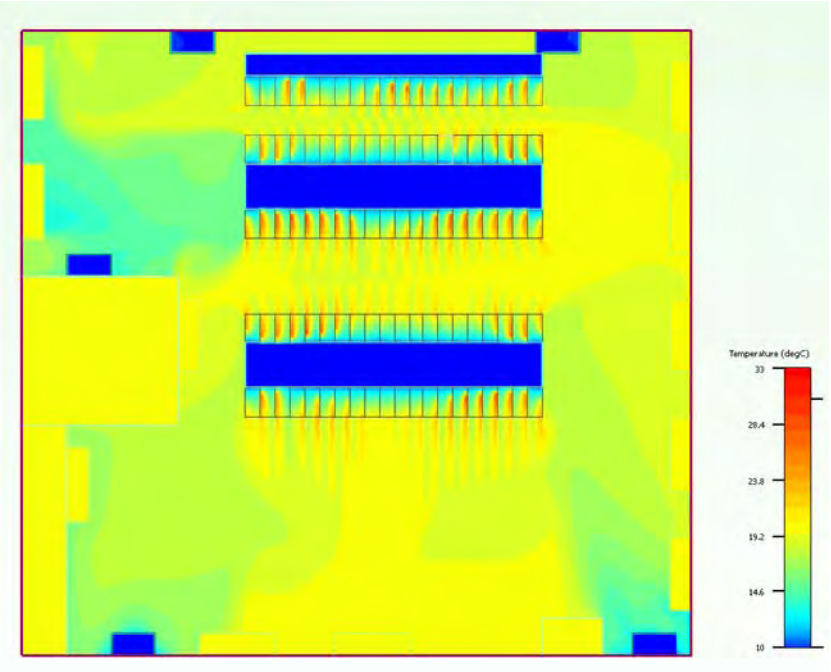

Figure 5.9 Thermal Profile at 1’ Above the Floor Level with Containment.

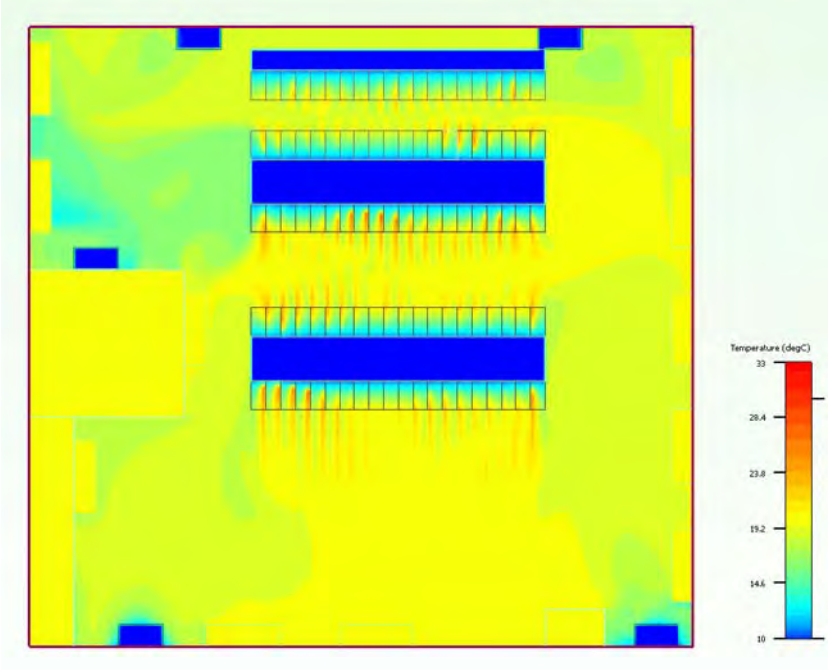

Figure 5.10 Thermal Profile at 3.5’ Above the Floor Level with Containment.

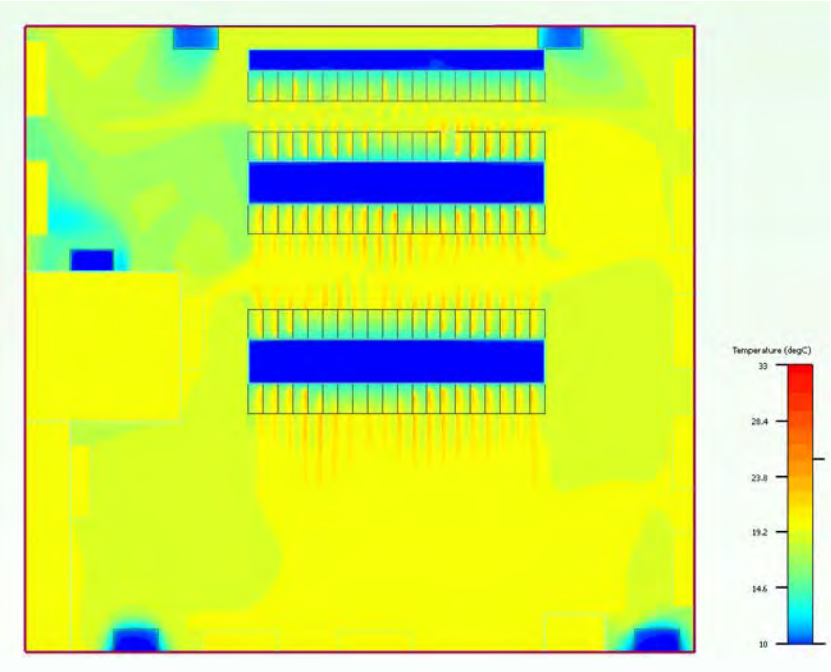

Figure 5.11 Thermal Profile at 6’ Above the Floor Level with Containment.

5.6 Computation of The Rack Cooling Indices

For both the cases, with and without cold aisle containment, rack inlet temperature was monitored for each rack at 6’ above the floor level. Using these monitored temperatures the rack cooling indices, both high and low are calculated. The graph below indicates the rack inlet temperatures sorted in ascending order. The RCIs are provided in table 5.1.

Table 5.1 The Rack Cooling Indices

Case	RCI-HI %	RCI-LO %
No containment	25.13	22.2
Cold Aisle Contained	100	87

From the figure 5.12 and the table 5.1, we can see that in the case of no containment, the rack inlet temperatures recorded exceeded the allowable limits on both the ends. There are temperatures higher than the maximum allowed temperature and there are temperatures below

the minimum allowed temperature. This is reflected in both rack cooling indices being below 100%. Containing the cold aisles eliminates the recirculation and the infiltration of hot air into the cold aisles. This reflects in RCI_{HI} being 100% as there is no temperature above maximum allowed temperature. In both cases however, the RCI_{LO} is very low which is indicative of an overcooled room.

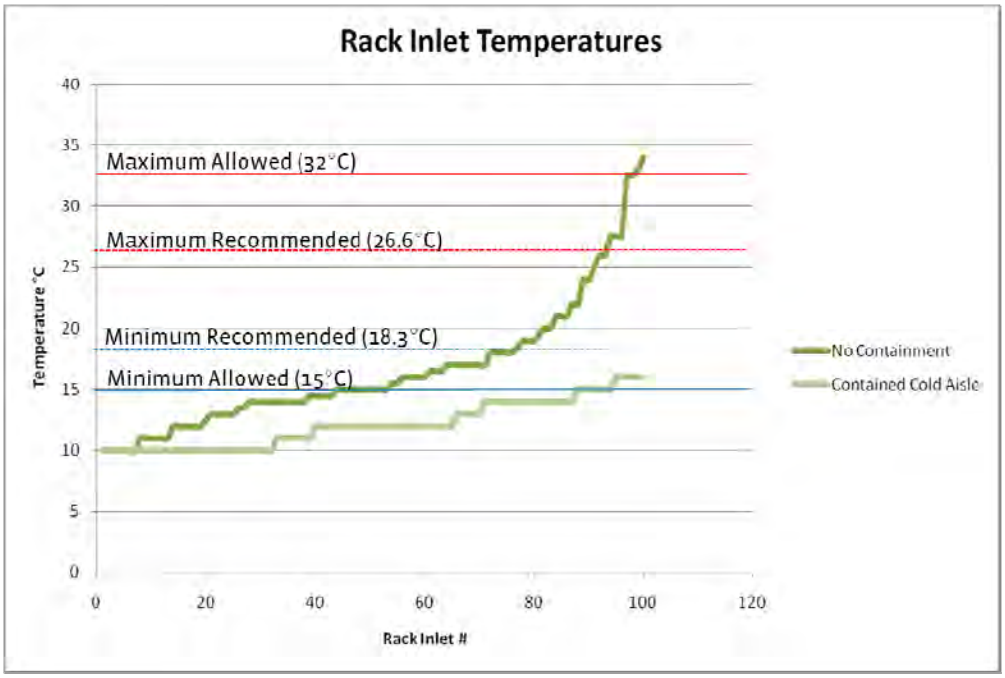

Figure 5.12 The Rack Cooling Indices.

Considering the rack cooling indices mentioned above and the specifications from the OEM regarding the airflow requirement of the servers, the room was clearly over-provisioned. This presented an opportunity to reduce the airflow by turning some of the CRAH units off.

5.7 The CRAH Units' Shutdown

Considering the OEM specifications and the redundancy, it was concluded that 4 CRAH units can be turned off and the data center operation was still reliable. The choice of which CRAH units to be shut down was based on

1. The CRAH zone of influence analysis.

2. The distribution of CRAHs in the electrical grid.
3. The sub-floor pressure distribution.

5.7.1 The CRAH zone of influence analysis

The CFD simulations were carried out with all the CRAHs operational and then shutting down one CRAH unit at a time to study the effect on airflow distribution. The vector plot at the subfloor level shown in fig. 5.13 below indicates the zone of influence for each CRAH unit.

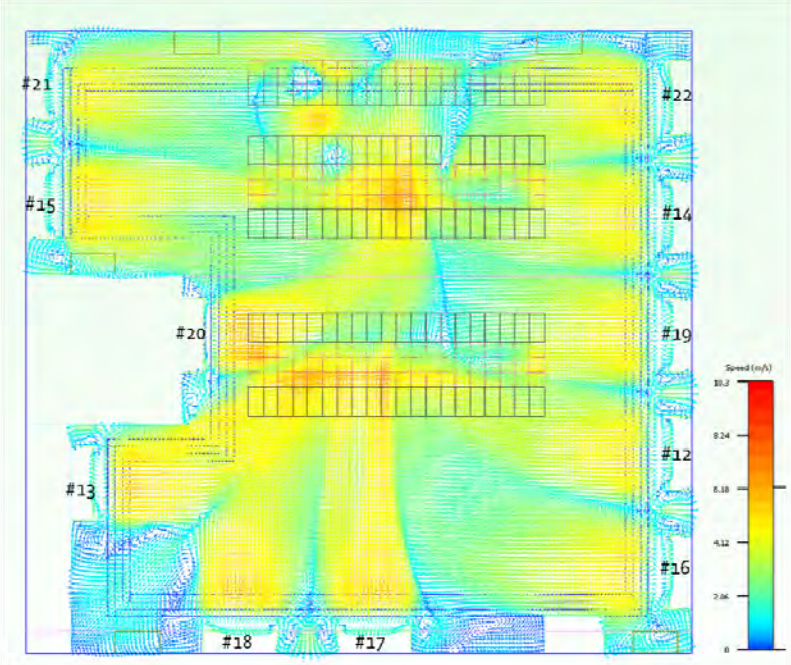

Figure 5.13 The Zones of CRAH Influence.

5.7.2 The distribution of the CRAH units in the electrical grid

These 11 CRAH units are distributed amongst three electrical busses. Their distribution is given in table 5.2 below. This is to ensure the reliable operation of data center in the event of an electrical bus-failure.

From the zone of influence analysis, it was evident that units 21, 17 and 14 were essential from the airflow distribution perspective. There were some racks which were getting

air when these CRAHs were operational. Also, the fact that they are distributed on three different busses is advantageous.

Table 5.2 The Electrical Distribution of the CRAH Units

Bus A	Bus B	Bus C
#21	#15	#18
#13	#17	#16
#19	#12	#14
	#22	#20

Hence these units were excluded from shut-down process and they were to remain operational all the time. Thus, there was a possibility of turning 1 CRAH unit from Bus A and 1 or 2 each from Busses B and C off making the total of turned off units to 4.

5.7.3 The sub-floor pressure distribution

The table 5.3 below shows the DOE matrix for the CRAH shut down scenarios. It takes into consideration the constraints outlined in the preceding sections. The CFD simulations were ran for each scenario by deactivating the respective CRAH units in the model. The airflow distribution and the subfloor pressure were monitored.

The cold aisle containment combined with CRAH units' shutdown caused initial negative pressure in the cold aisles. In some of the scenarios, this lead to the reverse flow in some regions where subfloor pressure was dipped drastically due to CRAH unit in the vicinity being shut down. Based on the sub-floor pressure and the flow distribution, the DOE matrix was reduced from 19 experiments to 3 experiments. These 3 experiments, the scenarios 14, 16 and 17 were tested experimentally at the test site by actually shutting down and covering the respective CRAH units. Each scenario was run for a period of 2 hours and the health of test site was monitored continuously.

Table 5.3 The DOE Matrix

Scenario #	Bus A	Bus B	Bus C	Remarks
1	None	None	None	
2	13	12	16 and 18	
3			18 and 20	
4			16 and 20	
5		15	16 and 18	
6			18 and 20	
7			16 and 20	
8		22	16 and 18	
9			18 and 20	
10			16 and 20	
11	19	12	16 and 18	
12			18 and 20	
13			16 and 20	
14		15	16 and 18	
15			18 and 20	
16			16 and 20	
17		22	16 and 18	
18			18 and 20	
19			16 and 20	

Based on the airflow distribution in the cold aisle, the rack inlet temperatures and the supply and return temperatures of the operational CRAH units, it was decided to pursue scenario 17 as preferred configuration for CRAH shutdown case. Figure 5.14 below indicates the CRAH units that will be shut down.

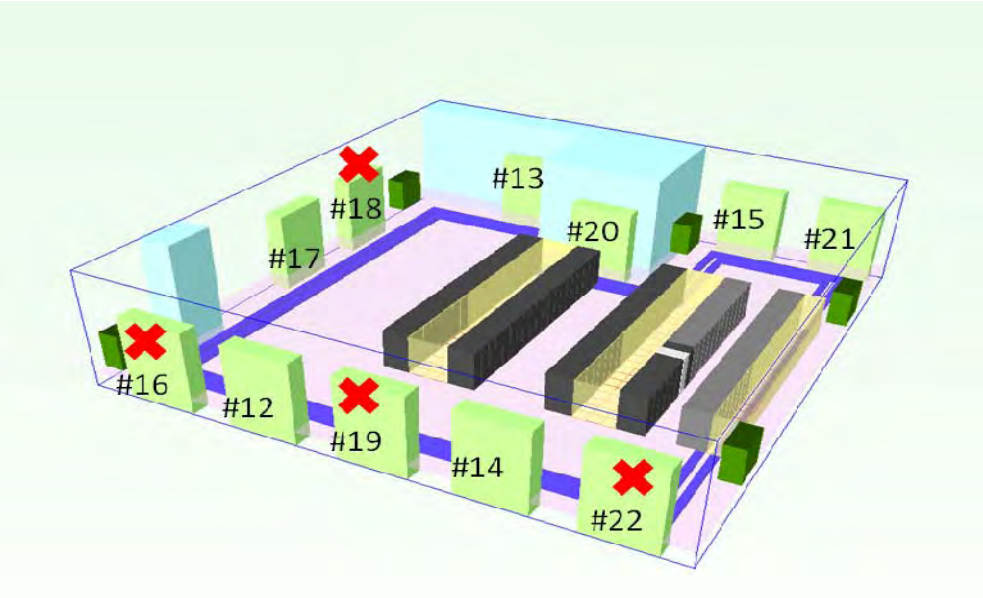

Figure 5.14 The CRAH Units Shut-down Scenario.

5.8 The Experimental Test

The experimental test was run for 2 days. The objectives of the test were

1. To ensure a balanced perforated floor in the cold aisles that will result in a narrower band of inlet temperatures for all the racks.
2. To raise the set point temperature of the CRAH units and still maintain the near uniform temperatures in cold aisles.
3. To raise the rack inlet temperature as high as possible within recommended range without causing an increase in server fans' speed and power (which consequently will increase overall energy consumption).

5.8.1 Test Procedure

The first day of the test was dedicated to the floor balancing and the set point adjustments. On the second day, some adjustments were made in the control strategy and the set points were refined. The major steps taken during the test are as follows:

1. The CRAH units 16, 18, 19 and 22 were turned off and the return air opening was covered to prohibit the cold air in sub-floor plenum from leaking into the room.
2. Initially, all the CRAH units were set to operate at the return air temperature of 72°F. After 4 CRAH units were turned off, the set point for the remaining CRAH units which were operational was raised. The CRAH units 13, 17 and 21 were set to operate at 78°F while the CRAH units 12, 14, 15 and 20 were set to operate at 80°F.
3. After the system was stabilized, the rack inlet temperatures were monitored and based on those, floor was balanced by swapping high resistance perforated tiles with the low resistance perforated tiles or the solid tiles as required.
4. During the floor balancing act, the set points were refined and adjusted so that the rack temperatures were nearly uniform and the control over them was not lost.
5. The control strategy was modified by selecting PID control scheme and changing the sensitivity to 1°F and the integral gain was changed to 5%.

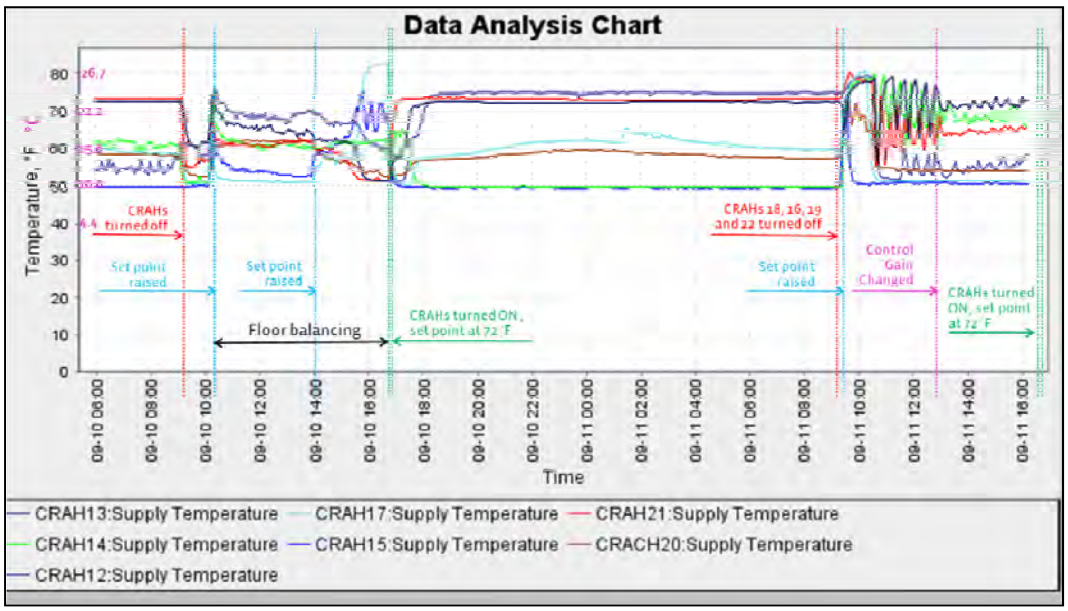

Figure 5.15 The Overview of the Two-day Test.

The chart in figure 5.15 above shows the variation in supply temperatures of the operational CRAH units during this entire test period. The timeline also indicate the major steps described above. The individual steps and their effects are described in following sections in detail.

5.8.2 The shutdown and covering of the CRAH units

After shutting down the CRAH unit, it is important to cover the return air vent on the CRAH unit and seal it off. Some CRAH models do have back draft dampers. These back draft dampers eliminate the possibility of the reverse flow i.e. the air from the subfloor plenum entering into the room through return air vent. In case of the CRAH units without dampers, covers as shown in figure 5.16 below are commercially available [*]. In our case, the covers made of fire-retardant material were used.

Figure 5.16 The Covering of the CRAH Units [122].

5.8.3 The CRAH Set Points

When in normal operating mode, all the CRAH units are set to operate at 72°F. Due to the layout, some of the CRAH units carry more cooling load than the others. This is reflected in

the supply air temperatures. Figures 5.17 and 5.18 below show the supply and the return temperatures of the operational CRAH units during the first day of the test period.

In the figures, the portion on the left of red vertical line (before CRAHs turned off) indicates the normal operating period with all 11 CRAH units operational. It can be seen that the CRAH units 13 and 21 have the return temperatures below the set point temperature of 72°F. This leads to shutting the chilled water valve off and hence those units simply deliver the air at same temperature. The graph of supply temperatures shows that the units 13 and 21 are supplying air at 71-72°F which is return air temperature for those units with some heat gain through the CRAH unit. Once the 4 CRAH units are turned off, the remaining 7 CRAH units which are operational get increased load at slightly higher return temperatures. This can be seen from the upward shift in return temperature curves. As a result, the chilled water valve for all the operational CRAH units is wide open and they start cooling. This immediate effect can be seen in fig. where the supply temperatures for most of the CRAH units drop significantly. From the graph of return temperatures, it can be seen that the units 13, 17 and 21 have relatively lower return temperatures than those of the units 12, 14, 15 and 20. Considering this fact, the set points were raised. The new set point for the units 13, 17 and 21 was 78°F. For the units 12, 14, 15 and 20, it was raised to 80°F. As a result of these new set points, the supply temperatures for all the CRAH units settled at higher levels.

In an effort to reduce the bandwidth of these supply temperatures, the floor balancing was undertaken which is described in following section. When the band of supply temperatures began to converge, in order to bring the rack inlet temperatures to maximum recommended value, set points of units 17 and 15 were further tweaked. The CRAH unit 17 was set to operate at 79°F and the set point of the CRAH unit 15 was raised to 81°F. These increases in set points however lead to the loss of control as the CRAH unit 17 stopped cooling and began circulating the return air due to closed chilled water valve. Even by reducing the set point of the CRAH unit 15 to 80°F did not result in bringing the supply temperatures under control.

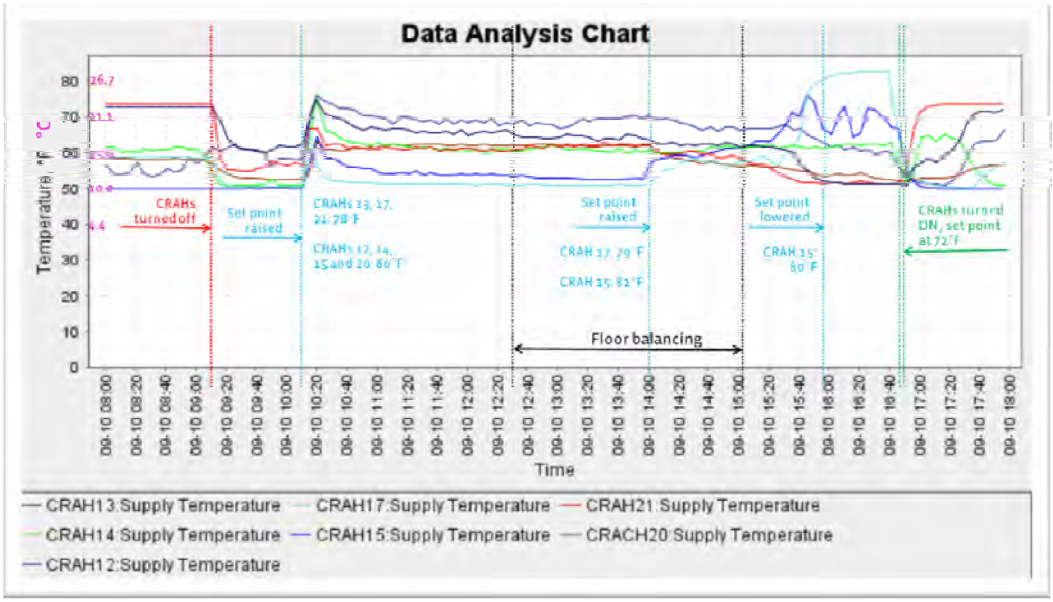

Figure 5.17 The Supply Temperatures of the CRAH Units During First Day of the Test.

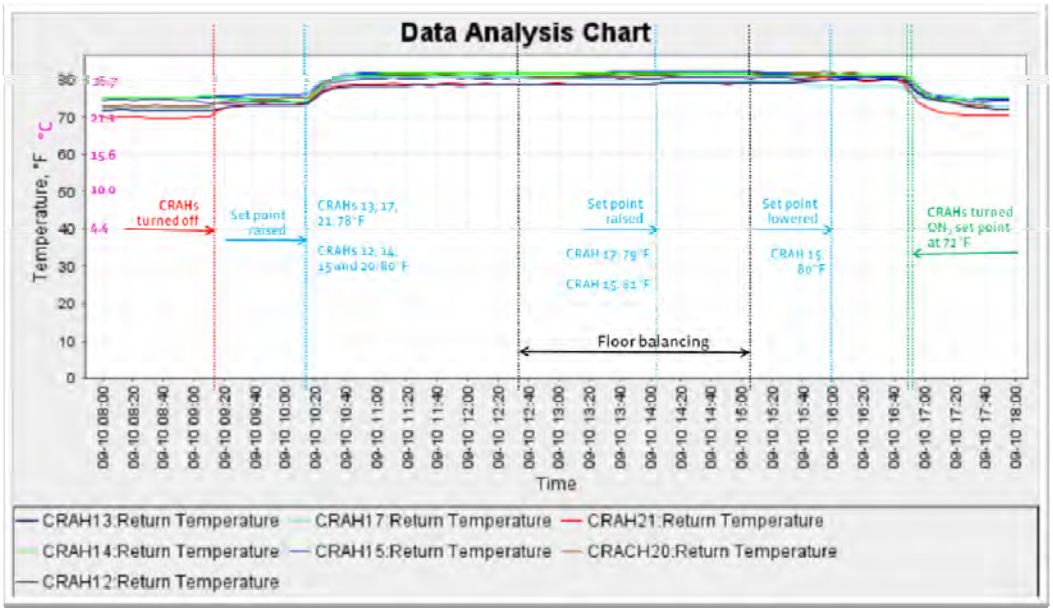

Figure 5.18 The Return Temperatures of the CRAH Units During First Day of the Test.

5.8.4 Floor Balancing

To achieve near uniform rack inlet temperatures, it is very important to have a balanced air-flow distribution rather than a uniform airflow distribution. A balanced air flow distribution is one where the racks exhibiting higher inlet temperatures get more air compared to those with lower inlet temperatures. This is achieved by installing low resistance perforated tiles in the vicinity of warmer racks and the high resistance perforated tiles and/or solid tiles in the vicinity of cooler racks. With proper combination of these, a balanced air-flow distribution can be achieved.

Figures 5.19 through 5.23 below indicate the rack inlet temperatures recorded at the temperature sensing nodes at various racks in each row. The effect of floor balancing can be seen in rows B, C and E more prominently than Rows A and D. It is worth to notice in Row B as the Rack AX exhibits an upward trend in inlet temperature after the set points were raised for the CRAH units 15 and 17 to 81°F and 79°F respectively.

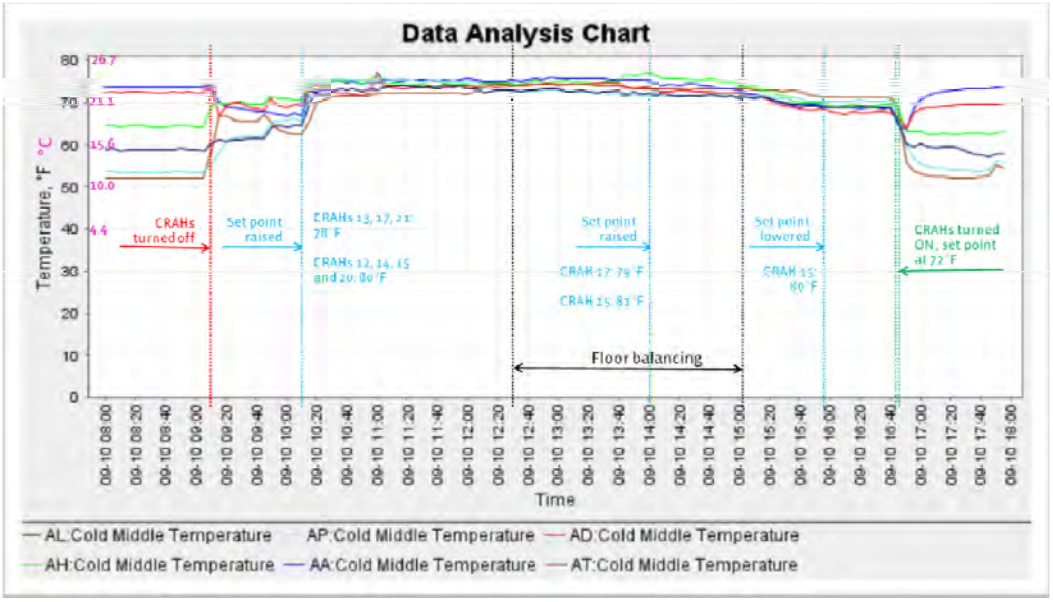

Figure 5.19 The Rack Inlet Temperatures in Row A During First Day of the Test.

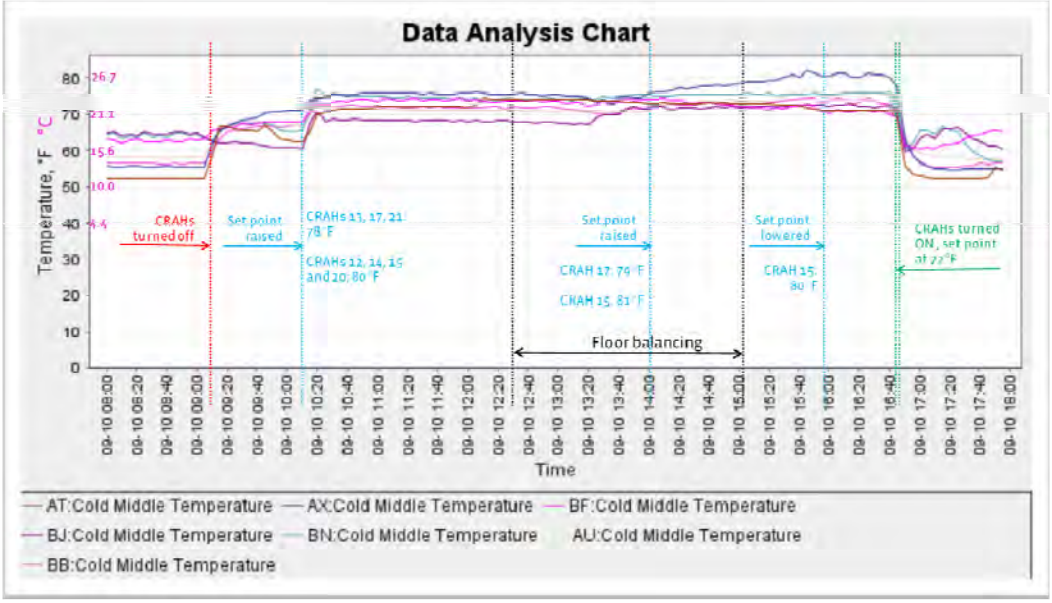

Figure 5.20 The Rack Inlet Temperatures in Row B During First Day of the Test.

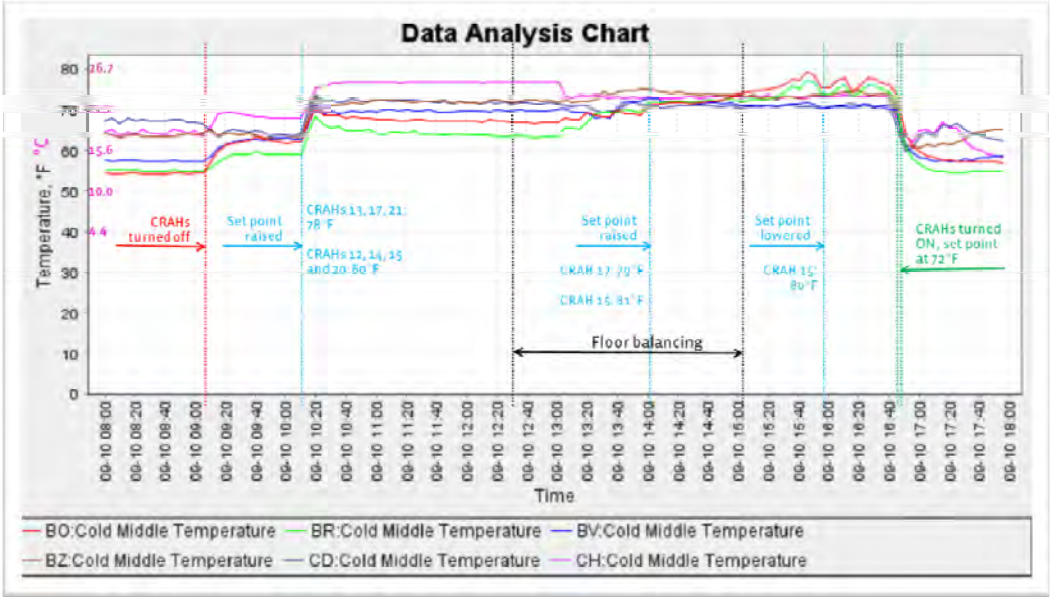

Figure 5.21 The Rack Inlet Temperatures in Row C During First Day of the Test.

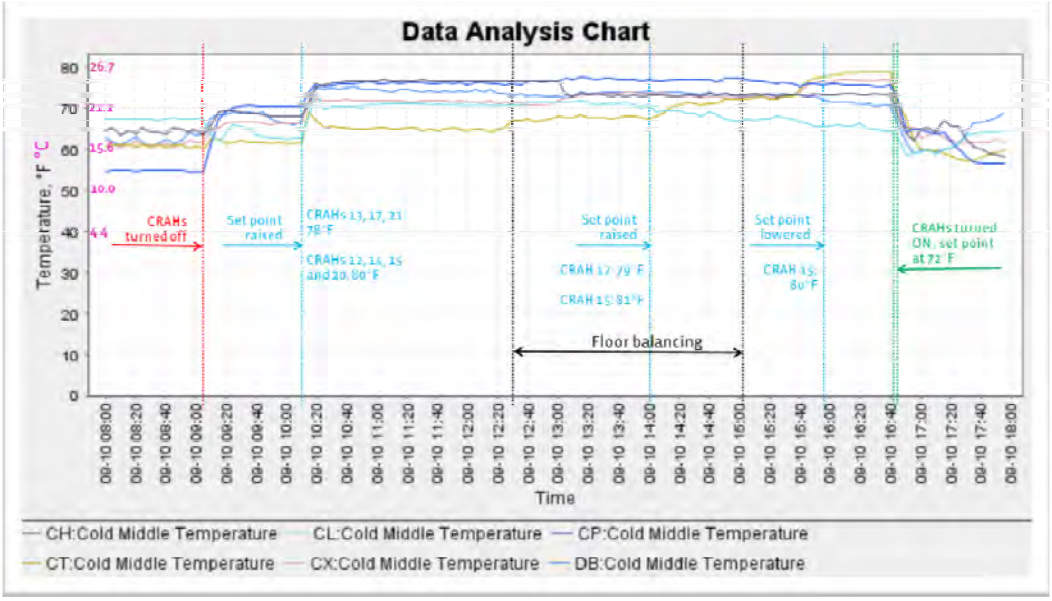

Figure 5.22 The Rack Inlet Temperatures in Row D During First Day of the Test.

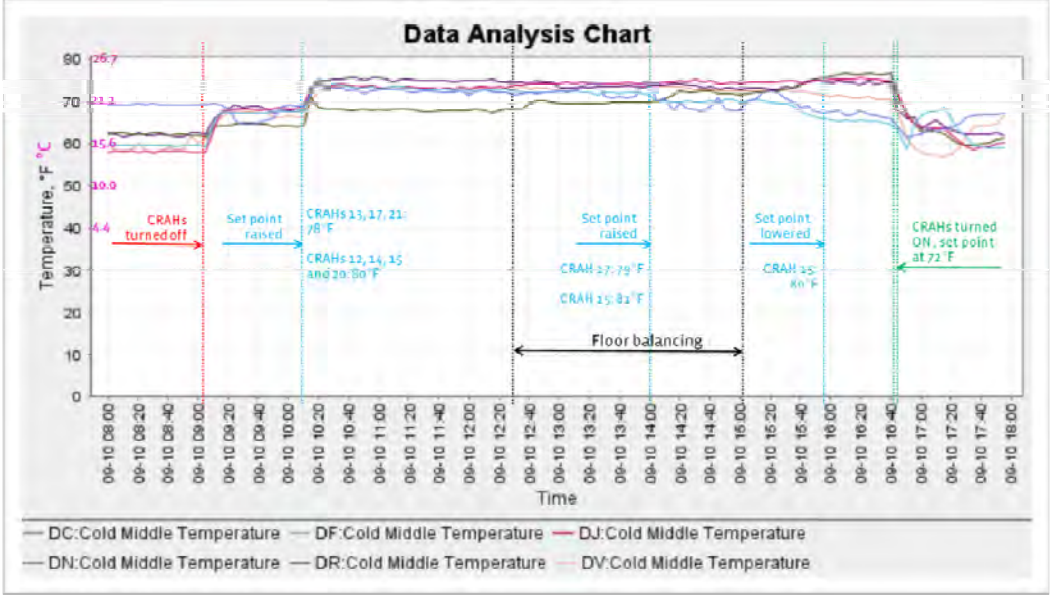

Figure 5.23 The Rack Inlet Temperatures in Row E During First Day of the Test.

From the first day of the test, it was evident that every CRAH unit has a certain limiting value for the set point temperature. Raising the set point beyond that value leads to the closing of chilled water valve and the air being delivered at return temperature which is higher than the desired. The table 5.4 below lists the limiting values of set points for the operational CRAH units.

Table 5.4 The Set Points for Return Temperatures of the CRAH Units

CRAH Unit	Set Point °F
12	78
13	78
14	79
15	79
17	79
20	79
21	78

5.8.5 The Control Strategy

On the second day of the test, the control of the CRAH units was switched to PID control. The integral gain was set to 5% and the sensitivity was changed from 2°F to 1°F. The effect of these changes can be seen in figures 5.24 and 5.25. Figure 5.24 indicates the supply temperatures of the operational CRAH units during second day of the test. It is evident that the CRAH units 12, 15, 17 and 20 start carrying the load and cooling immediately. This is due to the return temperatures of these units are out of the dead band due to change in the sensitivity. The remaining three units 13, 14 and 21 have the return temperatures near the deadband thresholds which cause them to oscillate. But once the integral gain is changed, these oscillations die down and the supply temperatures become relatively steady. The effect of these changes is reflected in the rack inlet temperatures also. Figures 5.26 through 5.30 show the variation of rack inlet temperatures for the racks in Rows A through E respectively.

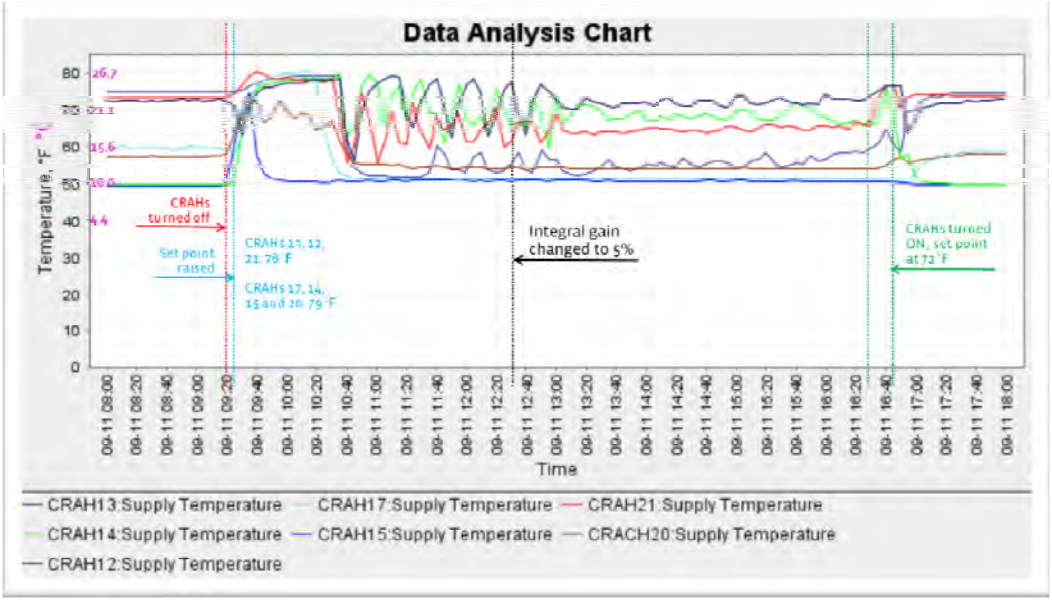

Figure 5.24 The Supply Temperatures of the CRAH Units During Second Day of the Test.

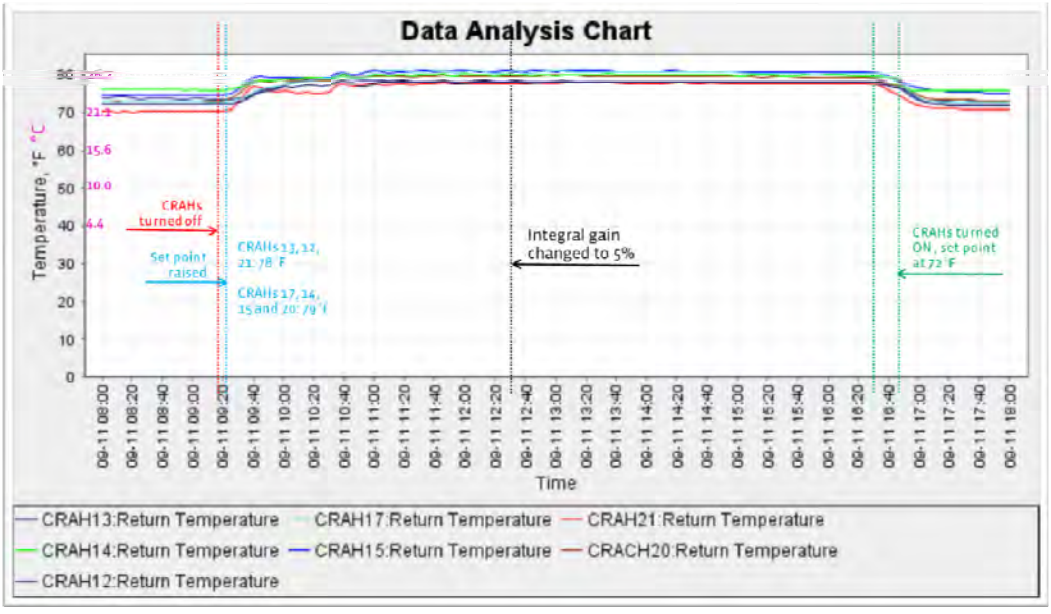

Figure 5.25 The Return Temperatures of the CRAH Units During Second Day of the Test.

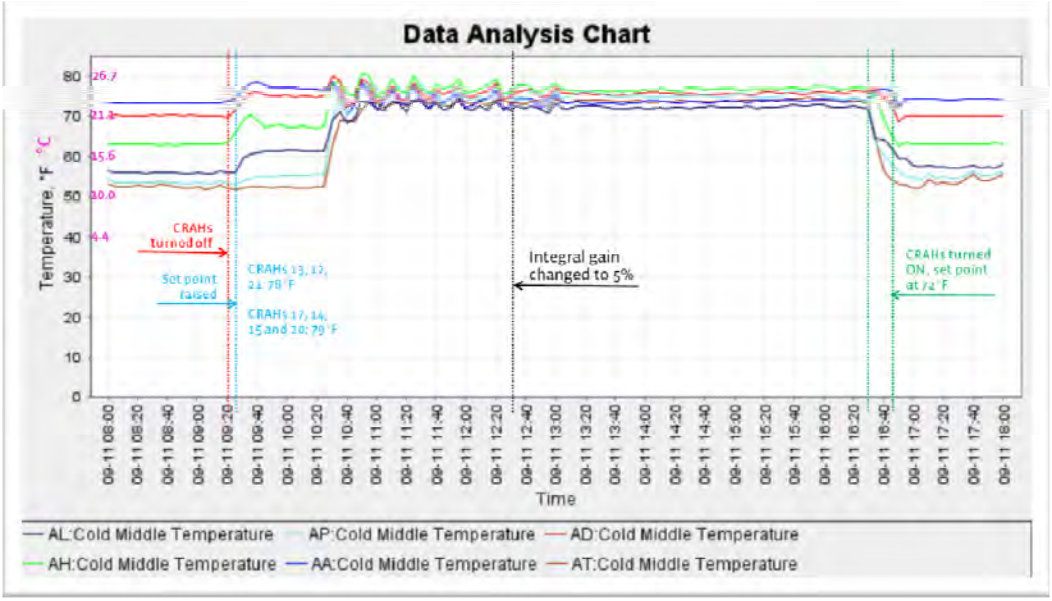

Figure 5.26 The Rack Inlet Temperatures in Row A During Second Day of the Test.

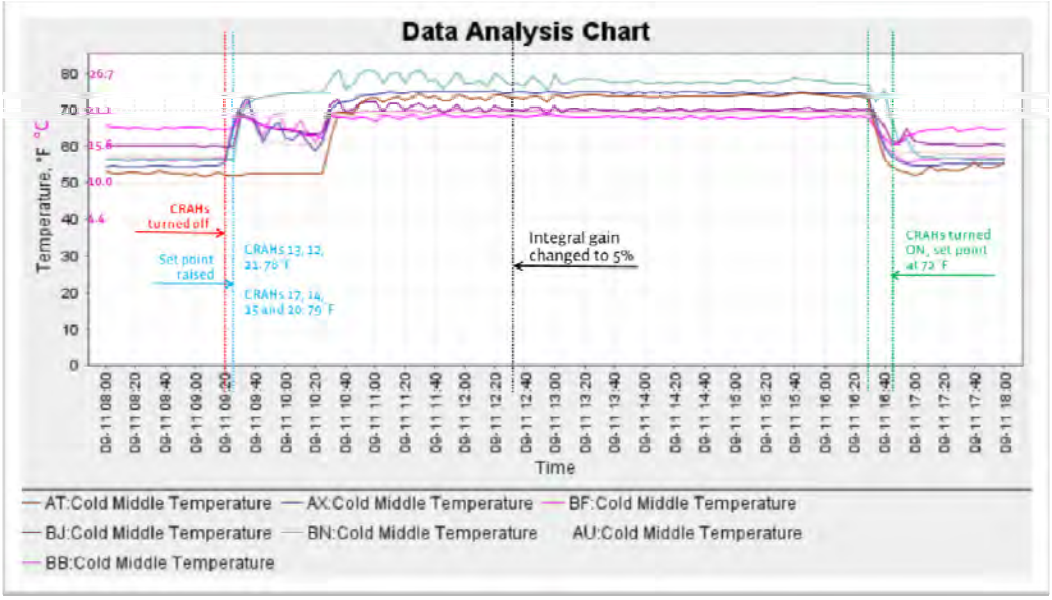

Figure 5.27 The Rack Inlet Temperatures in Row B During Second Day of the Test.

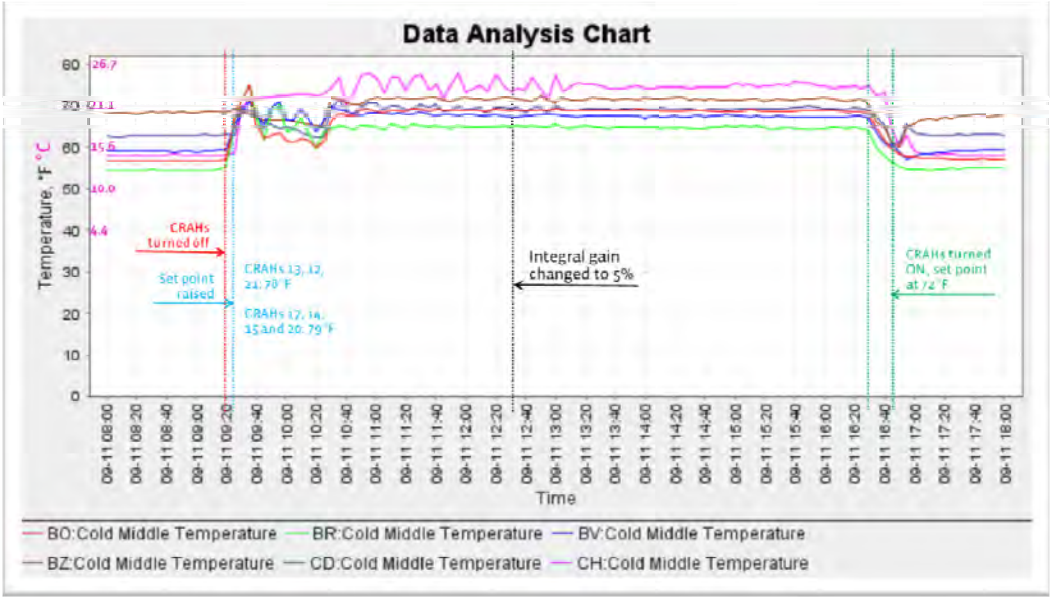

Figure 5.28 The Rack Inlet Temperatures in Row C During Second Day of the Test.

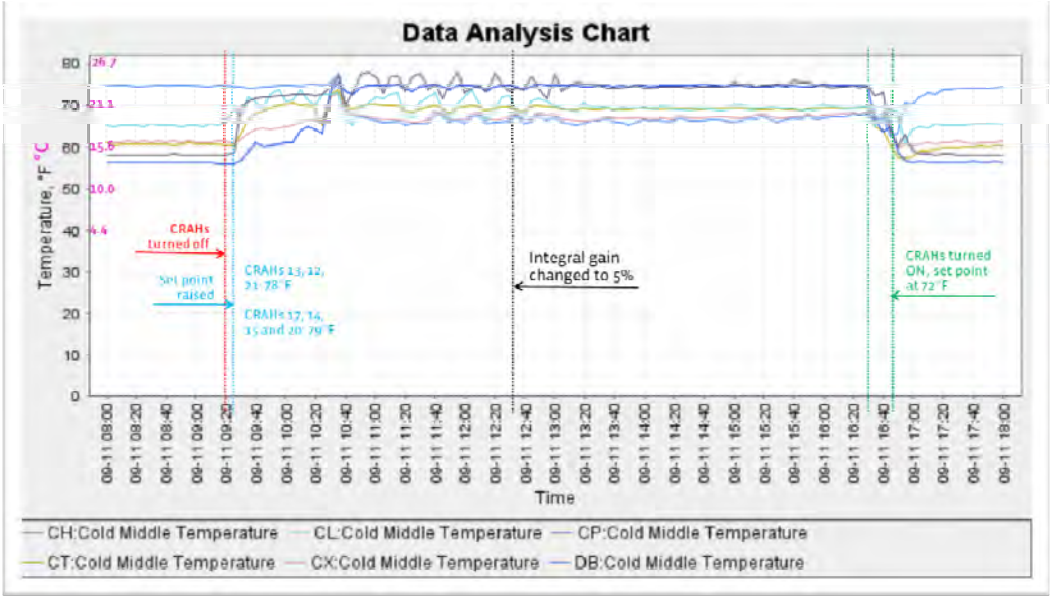

Figure 5.29 The Rack Inlet Temperatures in Row D During Second Day of the Test.

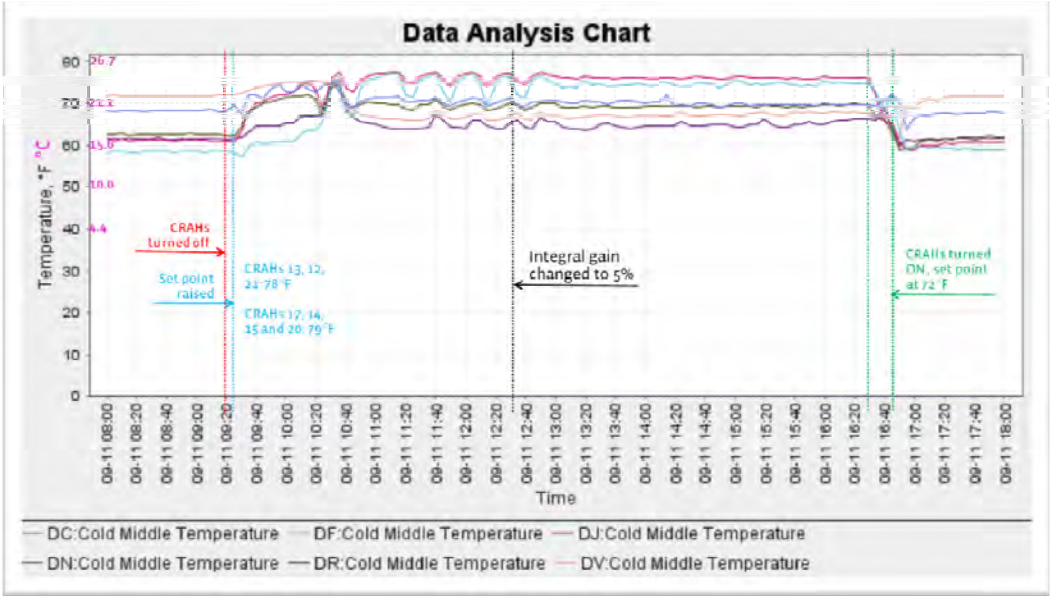

Figure 5.30 The Rack Inlet Temperatures in Row E During Second Day of the Test.

Table 5.5 provides the summary of the potential savings realized after the test. The annual potential savings for the projected supply temperature of 68°F are summarized in table 5.6.

5.9 The Fan Speed Reduction

Based on the application load on the server, available air-flow and the desired supply temperature, an exercise was carried out in collaboration with the server OEM to optimize the fan speed control. An improved fan speed control algorithm was released and was immediately deployed on a server to verify the results. Significant speed reduction was observed which translated into huge potential savings. Figure 5.31 shows the graph of fan speeds for a server before and after the improved algorithm was applied. The potential Savings are tabulated in table 5.7.

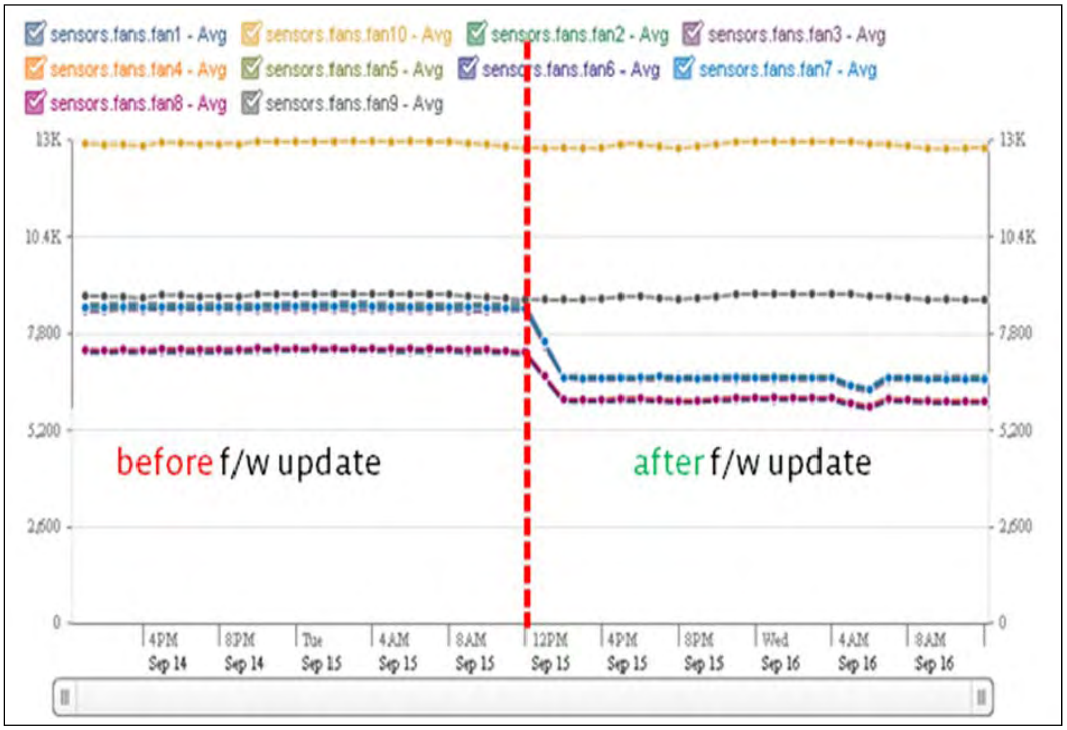

Figure 5.31 The Fan Speed Reduction.

Table 5.5 The Potential Savings After Test

CRAH Unit	Supply Temperature (°F)		Airflow (CFM)		Potential Energy Savings (KW)		Potential Annual Savings (MWH)		
	Before	After	Before	After	CRAH Fans	Compressor	CRAH Fans	Compressor	TOTAL
12	75	54	16500	16500	0	-6.6	0	-57.7	-57.7
13	73	74	16500	16500	0	0.4	0	3.8	3.8
14	50	70	16500	16500	0	6.6	0	57.8	57.8
15	50	51	16500	16500	0	0.4	0	3.6	3.6
16	50	OFF	16500	0	7.6	0.0	66.6	0.0	66.6
17	60	51	16500	16500	0	-2.8	0	-24.9	-24.9
18	50	OFF	16500	0	7.6	0.1	66.6	1.2	67.8
19	74	OFF	16500	0	7.6	0.0	66.6	-0.3	66.3
20	57	54	16500	16500	0	-1.0	0	-8.4	-8.4
21	73	65	16500	16500	0	-2.8	0	-24.7	-24.7
22	53	OFF	16500	0	7.6	0.2	66.6	1.4	68.0
Total Potential Annual Savings (MWH)									218.1
Total Potential Annual Savings ($@$0.1044/KWH)									$22,764

Table 5.6 The Potential Savings Projections After Increasing The Supply Temperature

CRAH Unit	Supply Temperature (°F)		Airflow (CFM)		Potential Energy Savings (KW)		Potential Annual Savings (MWH)		
	Before	After	Before	After	CRAH Fans	Compressor	CRAH Fans	Compressor	TOTAL
12	75	68	16500	16500	0	-2.2	0	-19.4	-19.4
13	73	68	16500	16500	0	-1.5	0	-12.8	-12.8
14	50	68	16500	16500	0	5.9	0	51.7	51.7
15	50	68	16500	16500	0	6.0	0	52.2	52.2
16	50	OFF	16500	0	7.6	0.0	66.6	0.0	66.6
17	60	68	16500	16500	0	2.6	0	22.4	22.4
18	50	OFF	16500	0	7.6	0.1	66.6	1.2	67.8
19	74	OFF	16500	0	7.6	0.0	66.6	-0.2	66.3
20	57	68	16500	16500	0	3.5	0	30.4	30.4
21	73	68	16500	16500	0	-1.7	0	-15.1	-15.1
22	53	OFF	16500	0	7.6	0.2	66.6	1.4	68.0
Total Potential Annual Savings (MWH)									378
Total Potential Annual Savings ($@$0.1044/KWH)									$39,464

Table 5.7 The Potential Savings Projections After Improved FSC Algorithm

Location	Server Power (KW)	Airflow (CFM)	Equivalent CRAHs	CRAH Fan Power (KW)	Chiller Load Reduction (KW) due to		Total Power (KW)	MWH/YR	$/YR (@ $0.1044/KWH)
					Servers	CRAHs			
1	46.3	72,572	4.4	30.4	15.8	10.37	102.9	901.6	$ 94,128
2	20.8	32,554	1.97	7.6	7.09	2.6	38	333.5	$ 34,819
3	0.68	1,061	0.06	0	0.23	0	0.91	7.9	$ 831
4	45.4	71,081	4.31	30.4	15.5	10.37	101.6	890.4	$ 92, 960
Total Potential Annual Savings								2133.4	$ 222,739

CHAPTER 6

GUIDELINES FOR ENERGY EFFICIENT THERMAL MANAGEMENT

The Power Usage Effectiveness (PUE) of the data center is defined as the ratio of total power supplied to the power consumed by IT equipment in a datacenter. The total power supplied to the data center is consumed by critical loads such as IT equipment, UPS and PDUs and the non critical loads such as the cooling resources and the office lighting and other loads. Thus if we neglect the other components, PUE can be expressed as

$$PUE = \frac{IT\ POWER + COOLING\ POWER}{IT\ POWER}$$

Thus, to improve the power usage effectiveness of the data center, one has to reduce the cooling power without increasing the IT power. Based on the computational studies performed and the results of the subsequent validation tests, the guidelines are presented below to achieve improvement in the power usage effectiveness of the data center.

6.1 Evaluation of the Energy Consumption

The first and foremost step is to evaluate the power consumed by each and every component of the data center facility. By performing the energy audit of the facility, one will have the power distribution between IT and non-IT loads. Installation of meters and branch circuit monitoring units enable to itemize the power consumption. The use of intelligent power management infrastructure allows monitoring the health of IT equipment.

The major reason to have a high PUE is the over-provisioning of the cooling resources. Proper metrics should be used to determine the state of the cooling provided to the facility. For

example, the rack cooling indices could be used to find out if the room is being overcooled or not. One has to keep in mind the redundancy of the system while determining the correct amount of cooling. It is also essential to consider the mechanical and electrical distribution of the equipment, their maintenance while deciding on how to downsize the cooling resources. The CFD simulations can offer great insight by means of the “what if” scenarios.

The performance of the cooling system also affects the IT power consumption. The server fans can consume a significant portion of the electrical power attributed to a server. The server fan speed is controlled and the server fans are designed to spin at higher speeds if the cooling is insufficient. So it is important to know the characteristics of all the components and their dependence on each other.

6.2 Containment Systems

The results indicate that the containment systems can eliminate the recirculation of hot air into the cold aisle as well as the bypass of cold air to the CRAH units. The key to achieve better results is to make sure that the hot and cold streams are properly isolated.

The hot aisle containment may be an easy and effective alternative if the data center design permits to install one. By isolating the hot exhaust from the servers and directing it into the plenum, remaining entire data center can be turned into cold aisle. This installation may allow one to not use the cold aisle-hot aisle layout and still get the better results.

The effectiveness of cold aisle containment depends closely on how leak-proof the installed system is. The contained cold aisle eliminates the recirculation resulting in more uniform rack inlet temperatures. However, if the floor is not properly balanced, it may lead to negative pressures in the contained cold aisles resulting in increased fan speeds.

Irrespective of hot aisle containment or the cold aisle containment, it is imperative that the mixing of supplied cold air stream with the exhausted hot air stream should be minimized. There are many opportunities or the proverbial “low hanging fruits” which will result in better

isolation at minimal efforts. The blanking panels should be used to seal off any vacant slots in the rack. Use of blanking strips at the bottom of rack will ensure that the hot air does not seep through into the cold aisle. The cable cutouts should be closed by means of grommets or other sealing solutions to prevent the leakage of cold air from underfloor plenum into the room.

The containment systems make it easier to predict the airflow behavior more accurately. A better isolation of the two streams, hot and cold, in turn make it possible to utilize the CRAH/CRAC units at higher % of their capacities. With CRAH units operating at higher capacities, it is possible to cool more IT load with relatively less cooling power. It finally results in the improvement of the power usage effectiveness of the data center.

6.3 The Set Points and the Control Strategy

The part load efficiencies of various components of the cooling systems should be considered while deciding the set point temperatures. The CRAH units in a room show complex interdependency on other units. Any small change in the operation of one unit can result in significant change in the operation of other. It is observed that the CRAH units in the vicinity of each other are always “fighting” with each other for the load. Depending on the temperature and humidity set points, one unit may humidify the air while other is dehumidifying the air. This fighting of the CRAHs will result in an inefficient operation leading to the significant wastage of energy.

Most of the data centers employing raised floor (underfloor) configuration, have the CRAC/CRAH units that are set to operate based on the temperature of the returning air. This arrangement causes the temperature of the supply air to fluctuate. This leads to air being supplied by different CRAC/CRAH units into the underfloor plenum at different temperatures. Although there is mixing of these different air streams in the underfloor plenum, it does not result in uniform temperature. So there exist air streams with different temperatures. This leads to entry of supply air into cold aisle with non uniform temperature. In other words, the air coming

out one tile may be at different temperature than the air coming out of another tile in the same cold aisle.

This nonuniform temperature distribution is compounded by the recirculation of hot air into the cold aisle. This causes large variation in the temperature of air entering into the servers at different heights in a rack. This in turn causes server fans to spin at different speeds, many times at higher speeds resulting in more energy consumption. The CRAH temperatures should be controlled to supply the air at the highest possible temperature as recommended. But caution should be exercised to not let the server fans run at elevated speeds due to higher temperatures.

The use of supply air temperature as set point to control the CRAH units combined with installation of variable frequency drives (VFD) can eliminate the above drawbacks. The VFDs can control the motor speed depending on the temperature of air being supplied. So it is possible to achieve relatively uniform temperature for the air in the underfloor plenum. This will help server fans to run at relatively lower speeds and consume less power.

6.4 Fan Speed Reduction

It is worth to work with the OEM/ODMs and optimize the fan speed control algorithm. In order to do that, one has to be familiar with the loading that server will experience. It is possible that the load will change with time and may or may not follow any specific trend. A reduced fan speed for server running at high load may actually lead to fans running at high speeds resulting in more power consumption. However, if loading pattern is known, then controlling the CRAH units and the server fan speeds can offer significant savings in energy.

The flowchart in fig. 6.1 summarizes the steps to achieve the energy efficiency in a data center.

6.5 Future Work

The following topics present the opportunities of further research and have the potential of impacting the data center practices.

6.5.1. Air Cooling vs. Liquid Cooling

It is necessary to address the concern that the air cooling in data centers is really nearing its limit and the time has come to accept the liquid cooling as an alternative. The advantages and disadvantages of each cooling technique can be discussed and validated by the experimental data. A TCO analysis can give some insight while comparing these two techniques.

6.5.2. Cabinet designs

The optimization of cabinet design remains a challenging task. A more detailed study of cabinets with chimney and solid door can describe the effect of back pressure on the server fans and the subsequent power consumption and the thermal performance of the servers.

6.5.3. Energy Efficiency Studies

The chiller plant and cooling tower analysis was out of the scope of this work. That analysis can be undertaken to get the complete picture of energy efficient operation of entire plant.

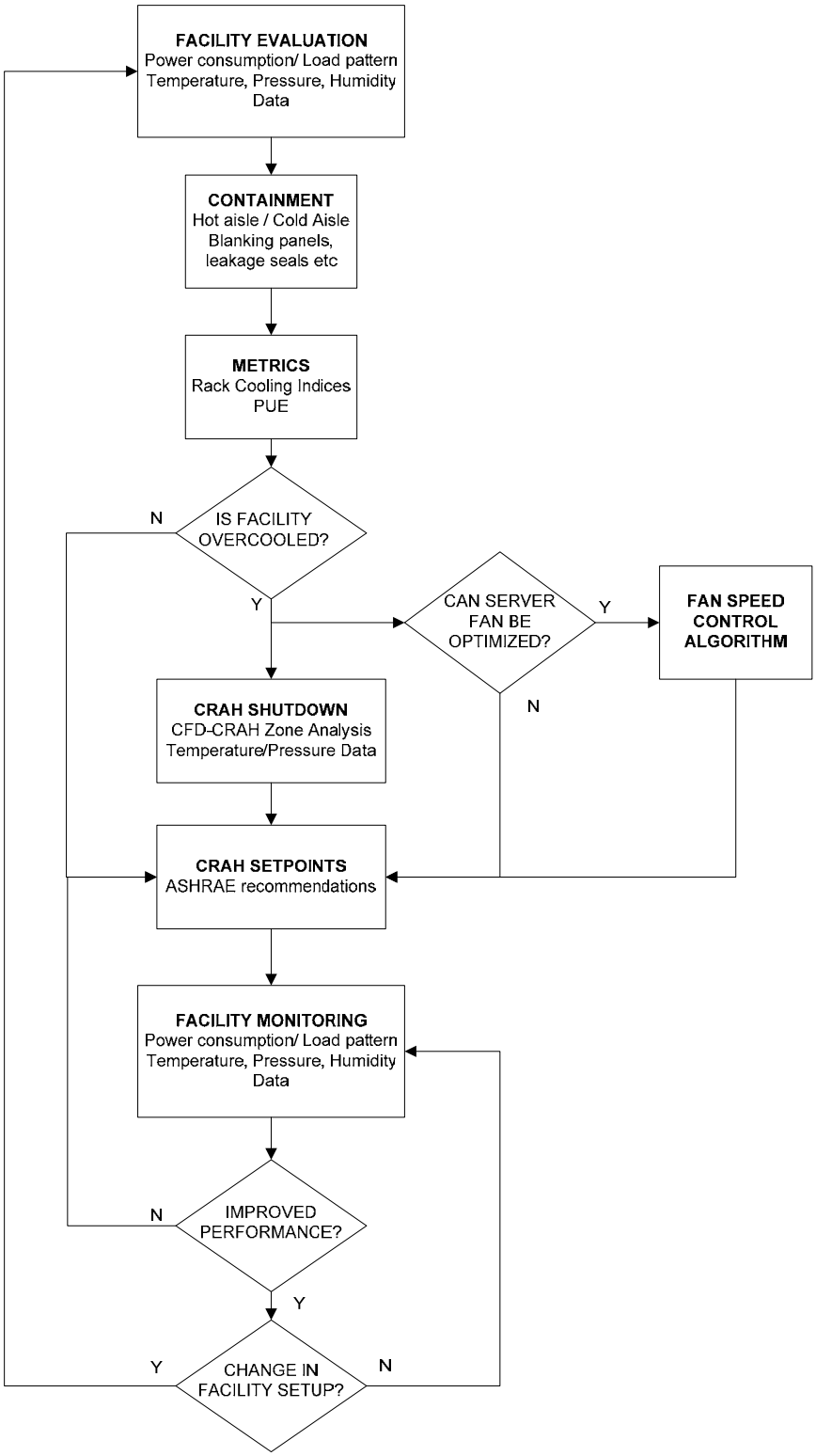

Figure 6.1 The Guidelines for Energy Efficiency.

REFERENCES

[1]. ASHRAE, “Thermal Guidelines for Data Processing Environments”, Atlanta: American Society of Heating, Refrigerating and Air-Conditioning Engineers, Inc., 2004.

[2]. ASHRAE, “Datacom Equipment Power Trends and Cooling Applications”, Atlanta: American Society of Heating, Refrigerating and Air-Conditioning Engineers, Inc., 2005.

[3]. Schmidt, R., “Thermal profile of a high-density data center—Methodology to thermally characterize a data center”, ASHRAE Transactions 110(2):635–42, 2004.

[4]. Schmidt, R., Iyengar M., Beaty D., and Shrivastava S., “Thermal profile of a high-density data center—Hot spot heat fluxes of 512 W/ft^2”, ASHRAE Transactions, 111(2):765–77, 2005.

[5]. Schmidt, R., Iyengar M., and Mayhugh. S., “Thermal Profile of World’s Third Fastest Supercomputer—IBM’s ASCI Purple Cluster”, ASHRAE Transactions 112(2), 2006.

[6]. Schmidt, R. and Iyengar M., “Comparison between Underfloor Supply and Overhead Supply Ventilation Designs for Data Center High-Density Clusters,” ASHRAE Transactions, Volume 113, Part 1.

[7]. Koomey J.G., “Estimating Total Power Consumption By Servers In The US and The World”, A report by the Lawrence Berkeley National Laboratory, February 2007.

[8]. Mitchell-Jackson J., “Energy Needs In An Internet Economy: A Closer Look at Data Centers”, Masters Thesis, UC-Berkeley, 2001.

[9]. Tschudi W., Xu T., Sartor D. and Stein J., “High Performance Data Centers: A research Roadmap”, A report by the Lawrence Berkeley National Laboratory.

[10]. Iyengar M., and Schmidt, R, “Analytical Modeling of Energy Consumption and Thermal Performance of Data Center Cooling Systems – From Chip to Environment”, InterPACK 2007, Vancouver B.C., Canada, 2007.

[11]. Schmidt, R., and H. Shaukatullah. 2003. Computer and telecommunications equipment room cooling: A review of literature. IEEE Transactions on Components and Packaging Technologies 26(1):89-98.

[12]. Schmidt, R., and Iyengar M. 2007. Best Practices for Data Center Thermal and Energy Management: Review of Literature. ASHRAE Transactions.

[13]. Nakao, M., H. Hayama, and M. Nishioka. 1991. Which cooling air supply system is better for a high heat density room: Underfloor or overhead. Proceedings of International Telecommunications Energy Conference (INTELEC), Vol. 12-4, pp. 393-400.

[14]. Noh, H., K. Song, and S.K. Chun. 1998. The cooling characteristic on the air supply and return flow system in the telecommunication cabinet room. Proceedings of

International Telecommunications Energy Conference (INTELEC), Vol. 33-2, pp. 777-84.

[15]. Shrivastava S., Schmidt R., Sammakia B. and Iyengar M., “Comparative analysis of different data center airflow management configurations”, Proceedings of the ASME/Pacific Rim Technical Conference and Exhibition on Integration and Packaging of MEMS, NEMS, and Electronic Systems: Advances in Electronic Packaging 2005, v PART A, Proceedings of the ASME/Pacific Rim Technical Conference and Exhibition on Integration and Packaging of MEMS, NEMS, and Electronic Systems: Advances in Electronic Packaging 2005, 2005, p 329-336.

[16]. Schmidt, R., and Iyengar M., “Comparison between Underfloor Supply and Overhead Supply Ventilation Designs for Data Center High-Density Clusters,” ASHRAE Transactions, Volume 113, Part 1.

[17]. Sorell, V., S. Escalante, and J. Yang. 2005. Comparison of overhead and underfloor air delivery systems in a data center environment using CFD modeling. ASHRAE Transactions 111(2):756-64.

[18]. Herrlin, M., and C. Belady. 2006. Gravity assisted air mixing in data centers and how it affects the rack cooling effectiveness. Proceedings of the Inter Society Conference on Thermal Phenomena (ITherm), San Diego, CA, May 30-June 2.

[19]. Mulay V., Karajgikar S., Iyengar M., Agonafer D. and Schmidt R.,“ Computational study of hybrid cooling solution for thermal management of data centers, ” 2007 ASME/JSME Thermal Engineering and Summer Heat Transfer Conferences & InterPACK ’07, July 8-12, 2007.

[20]. Mulay V., Karajgikar S., Agonafer D., Iyengar M. and Schmidt R., “Parametric Study of Hybrid Cooling Solution for Thermal Management of Data Centers”, International Mechanical Engineering Congress and Exposition, November11-15, 2007.

[21]. Mulay V., Agonafer D. and Schmidt R., “Liquid Cooling in Data Centers”, International Mechanical Engineering Congress and Exposition, October 31-November 6, 2008.

[22]. Furihata, Y., H. Hayama, M. Enai, and T. Mori. 2003. Efficient cooling system for IT equipment in a data center. Proceedings of International Telecommunications Energy Conference (INTELEC), Yokohama, Japan, October 19-23, pp. 152-159.

[23]. Hayama, H., M. Enai, T. Mori, and M. Kishita. 2003. Planning of air conditioning and circulation systems for data center. Proceedings of International Telecommunications Energy Conference (INTELEC), Yokohama, Japan, pp. 152-59.

[24]. Hayama, H., M. Enai, T. Mori, and M. Kishita. 2004. Planning of air conditioning and circulation systems for data center. IEICE Transactions on Communications 87(12):3443-50.

[25]. Beaty, D., and T. Davidson. 2003. New guideline for data center cooling. ASHRAE Journal 45(12):28-34.

[26]. Beaty, D., and T. Davidson. 2005. Data centers--Datacom airflow patterns. ASHRAE Journal 47(4):50-54.

[27]. Beaty, D., and R. Schmidt. 2004. Back to the future: Liquid cooling data center considerations. ASHRAE Journal 46(12):42-46.

[28]. Mulay V., Agonafer D., Irwin G. and Patell D.," Effective thermal management of data centers using efficient cabinet designs, " 2007 ASME/JSME Thermal Engineering and Summer Heat Transfer Conferences & InterPACK '07, July 8-12, 2007.

[29]. Kang S., Schmidt R., Kelkar K., Radmehr A. And Patankar S., "A Methodology for the design of perforated tiles in raised floor data centers using computational flow analysis", IEEE Transactions on Components and Packaging Technologies, v 24, n 2, p 177-183, June, 2001.

[30]. Karki, K., S. Patankar, and A. Radmehr. 2003. Techniques for controlling airflow distribution in raised floor data centers. Proceedings of the ASME InterPACK '03 Conference, July 6-11, Maui, HI.

[31]. Patankar, S.V., and K.C. Karki. 2004. Distribution of cooling airflow in a raised flow data center. ASHRAE Transactions 110 (2):629-34.

[32]. VanGilder, J., and R. Schmidt. 2005. Airflow uniformity through perforated tiles in a raised floor data center. Proceedings of the ASME InterPACK '05 Conference, San Francisco, CA, paper IPACK2005-73375.

[33]. Bhopte S., Agonafer D., Schmidt R. and Sammakia B., "Optimization of Data Center Room Layout to Minimize Rack Inlet Temperature", ASME Journal of Electronic Packaging, December 2006

[34]. Schmidt, R. 2001. Effect of data center characteristics on data processing equipment inlet temperatures. Proceedings of the ASME InterPACK '01 Conference, July 8-13, Kauai, HI.

[35]. Shrivastava, S., M. Iyengar, B. Sammakia, R. Schmidt, and J. VanGilder. 2006. Experimental-numerical comparison for a high-density data center: Hot spot heat fluxes in excess of 500 W/[ft.sup.2]. Proceedings of the InterSociety Conference on Thermal Phenomena (ITherm), San Diego, CA, pp. 402-411.

[36]. Shrivastava, S., B. Sammakia, M. Iyengar, and R. Schmidt. 2005b. Significance levels of factors for different airflow management configurations of data centers. Proceedings of ASME Winter Annual Meeting (IMECE), paper IMECE2005-81607.

[37]. Sorell, V., Y. Abrogable, K. Khankari, V. Gandhi, and A. Watve. 2006. An analysis of the effects of ceiling height on air distribution in data centers. ASHRAE Transactions 112(1):623-31.

[38]. Schmidt, R., "Thermal profile of a high-density data center - Methodology to thermally characterize a data center", 2004 Annual Meeting - Technical and Symposium Papers, American Society of Heating, Refrigerating and Air-Conditioning Engineers, 2004, p 604-611

[39]. Radmehr A., Schmidt R., Karki K. and Patankar S., “Distributed leakage flow in raised-floor data centers”, Proceedings of the ASME/Pacific Rim Technical Conference and Exhibition on Integration and Packaging of MEMS, NEMS, and Electronic Systems: Advances in Electronic Packaging 2005, v PART A, Proceedings of the ASME/Pacific Rim Technical Conference and Exhibition on Integration and Packaging of MEMS, NEMS, and Electronic Systems: Advances in Electronic Packaging 2005, 2005, p 401-408.

[40]. Schmidt, R. and Iyengar M., “Effect of Data Center Layout on Rack Inlet Air Temperatures”, Proceedings of the ASME/Pacific Rim Technical Conference and Exhibition on Integration and Packaging of MEMS, NEMS, and Electronic Systems: Advances in Electronic Packaging 2005, v PART A, Proceedings of the ASME/Pacific Rim Technical Conference and Exhibition on Integration and Packaging of MEMS, NEMS, and Electronic Systems: Advances in Electronic Packaging 2005, 2005, p 517-526.

[41]. Bhopte S., Sammakia B., Iyengar M., and Schmidt R., "Guidelines on Managing Under Floor Blockages for Improved Data Center Performance" Proceedings of the ASME International Mechanical Engineering Congress (IMECE), Chicago, November (2006).

[42]. Schmidt, R., K. Karki, and S. Patankar. 2004. Raised floor data center: Perforated tile flow rates for various tile layouts. Proceedings of the Inter Society Conference on Thermal Phenomena (ITherm), pp. 571-75.

[43]. Koplin, E.C. 2003. Data center cooling. ASHRAE Journal 45(3):46-53.

[44]. Schmidt, R., and M. Iyengar. 2005. Effect of data center layout on rack inlet air temperatures. Proceedings of the ASME InterPACK '05 Conference, San Francisco, CA, July 17-22.

[45]. PG & E. 2006. High Performance Data Centers--A Design Guidelines Sourcebook. Pacific Gas and Electric Company Report, developed by Rumsey Engineers, Oakland, CA, and Lawrence Berkeley National Laboratory, Berkeley, CA.

[46]. Intel Information Technology, “Reducing Data Center Cost with an Air Economizer”, Intel website, August 2008.

[47]. Shehabi A., Ganguly S., Traber K., Price H., Horvath A., Nazaroff W. and Gadgil A., “Energy Implications of Economizer Use in California Data Centers”, Lawrence Berkley National Laboratory, 2008.

[48]. Syska Hennessy

[49]. HP Technology Brief, “HP Modular Cooling System: technology overview and applications brief,” available at http://www.hp.com/go/mcs, 2006.

[50]. Patel, C., C. Bash, and C. Belady. 2001. Computational fluid dynamics modeling of high compute density data centers to assure system inlet air specifications. Proceedings of the Pacific Rim/ASME International Electronics Packaging Technical Conference and Exhibition (Inter-Pack), Kauai, HI, paper IPACK2001-15622.

[51]. Leonard, P.L., and A.L. Phillips. 2005. Thermal bus opportunity--A quantum leap in data center cooling potential. ASHRAE Transactions 111(2):732-45.

[52]. Patel, C., C. Bash, R. Sharma, M. Beitelmal, and R. Friedrich. 2003. Smart cooling of data centers. Proceedings of the ASME InterPACK '03 Conference, July 6-13, Maui, HI.

[53]. Bash C., Patel C. and Sharma R., "Dynamic Thermal Management of Air Cooled Data Centers", Proceedings of the Inter-Society Conference on Thermal and Thermomechanical Phenomena in Electronic Systems (ITherm), San Diego, California, June (2006).

[54]. Patel, C., R. Sharma, C. Bash, and A. Beitelmal. 2002. Thermal considerations in cooling large scale high compute density data centers. Proceedings of the ITherm Conference, San Diego, CA.

[55]. White, R., and T. Abels. 2004. Energy resource management in the virtual data center. IEEE Symposium Electronics and the Environment, Scottsdale, AZ, pp. 112-16.

[56]. Anton, R., H. Jonsson, and B. Palm. 2002. Modeling of air conditioning systems for cooling of data centers. Proceedings of the Inter Society Conference on Thermal Phenomena (ITherm), San Diego, CA, pp. 552-58.

[57]. ASHRAE. 2005b. Design Considerations for Datacom Equipment Centers. Atlanta: American Society of Heating, Refrigerating and Air-Conditioning Engineers, Inc.

[58]. Baer, D. 2004. Managing data center heat density. HPAC Engineering, February, pp. 44-47.

[59]. Bash, C., C. Patel, and R. Sharma. 2006. Dynamic thermal management of air cooled data centers. Proceedings of ITherm, San Diego, CA, May 30-June 2.

[60]. Boucher, T., D. Auslander, C. Bash, C. Federspiel, and C. Patel. 2004. Viability of dynamic cooling control in a data center environment. Proceedings of the ITherm Conference, Las Vegas, NV, June 1-4, pp. 593-600.

[61]. Beaty, D. 2005. Cooling data centers with raised-floor plenums. Heating/Piping/Air Conditioning Engineering (HPAC) 77 (9):58-65.

[62]. Beaty, D., N. Chauhan, and D. Dyer. 2005a. High density cooling of data centers and telecom facilities--Part 1. ASHRAE Transactions 111(1):921-31.

[63]. Beaty, D., N. Chauhan, and D. Dyer. 2005b. High density cooling of data centers and telecom facilities--Part 2. ASHRAE Transactions 111(1):932-44.

[64]. Bedekar, V., S. Karajgikar, D. Agonafer, M. Iyengar, and R. Schmidt. 2006. Effect of CRAC location on fixed rack layout. Proceedings of the ITherm Conference, San Diego, CA, May 30-June 2.

[65]. Belady, C., and D. Beaty. 2005. Data centers--Roadmap for datacom cooling. ASHRAE Journal 47(12):52-55.

[66]. Belady, C., and C. Malone. 2006. Data center power projections to 2014. Proceedings of ITherm, San Diego, CA.

[67]. Bhopte, S., R. Schmidt, D. Agonafer, and B. Sammakia. 2005. Optimization of data center room layout to minimize rack inlet air temperature. Proceedings of the ASME InterPACK '05 Conference, July 17-22, San Francisco, CA.

[68]. Bhopte, S., B. Sammakia, R. Schmidt, M. Iyengar, and D. Agonafer. 2006. Effect of under floor blockages on data center performance. Proceedings of the Inter Society Conference on Thermal Phenomena (ITherm), San Diego, CA, May 30-June 2.

[69]. Furihata, Y., H. Hayama, M. Enai, T. Mori, and M. Kishita. 2004a. Improving the efficiency of cooling systems in data centers considering equipment characteristics. Proceedings of International Telecommunications Energy Conference (INTELEC), Chicago, pp. 32-37.

[70]. Furihata, Y., H. Hayama, M. Enai, and T. Mori. 2004b. The effect air intake format of equipment gives to air conditioning systems in a data center. IEICE Transactions on Communication 87(12):3568-75.

[71]. Guggari, S., D. Agonafer, C. Belady, and L. Stahl. 2003. A hybrid methodology for the optimization of data center room layout. Proceedings of the Pacific Rim/ASME International Electronics Packaging Technical Conference and Exhibition (InterPack), Maui, HI, paper IPACK2003-35273.

[72]. Hamann, H., J. Lacey, M. O'Boyle, R. Schmidt, and M. Iyengar. 2005. Rapid 3-dimensional thermal characterization of large scale computing facilities. International Microelectronics & Packaging Society (IMAPS) Symposium, Advanced Thermal Workshop, October.

[73]. Herold, K., and R. Rademacher. 2002. Integrated power and cooling systems for data centers. Proceedings of the ITherm Conference, pp. 808-11.

[74]. Herrlin, M.K. 2005. Rack cooling effectiveness in data centers and telecom central offices: The rack cooling index (RCI). ASHRAE Transactions 111(2):725-31.

[75]. Heydari, A., and P. Sabounchi. 2004. Refrigeration assisted spot cooling of a high heat density data center. Proceedings of the ITherm Conference, pp. 601-06.

[76]. Iyengar, M., R. Schmidt, A. Sharma, G. McVicker, S. Shrivastava, S. Sri-Jayantha, Y. Anemiya, H. Dang, T. Chainer, and B. Sammakia. 2005. Thermal characterization of non-raised floor air cooled data centers using numerical modeling. Proceedings of the ASME Inter-PACK '05 Conference, San Francisco, CA, July 1-22.

[77]. Kang, S., R. Schmidt, K. Kelkar, A. Radmehr, and S. Patankar. 2001. A methodology for the design of perforated tiles in raised floor data centers using computational flow analysis. IEEE Transactions on Components and Packaging Technologies 24(2):177-83.

[78]. Karki, K., and S. Patankar. 2006. Air flow distribution through perforated tiles in raised floor data centers. Transactions of Buildings and Environment 41(6):734-44.

[79]. Karlsson, J.F., and B. Moshfegh. 2003. Investigation of indoor climate and power usage in a data center. Transactions of Energy and Buildings 37(10):1075-83.

[80]. Kurkjian, C., and J. Glass. 2004. Air-conditioning design for data centers accommodating current loads and planning for the future. ASHRAE Transactions 111(2):715-24.

[81]. NEMA. 2001. Metal Cable Tray Installation Guidelines, NEMA VE 2-2001, Report by National Electrical Manufacturers Association, Rosslyn, VA.

[82]. Norota, M., H. Hayama, M. Enai, and M. Kishita. 2003. Research on efficiency of air conditioning system for data center. Proceedings of International Telecommunications Energy Conference (INTELEC), Yokohama, Japan, pp. 147-51.

[83]. Patterson, M., R. Steinbrecher, and S. Montgomery. 2005. Data centers: Comparing data center and computer thermal design. ASHRAE Journal 47(4):38-42.

[84]. Radmehr, A., R. Schmidt, K. Karki, and S. Patankar. 2005. Distributed leakage flow in raised floor data centers. Proceedings of the ASME InterPACK '05 Conference, San Francisco, CA, paper IPACK2005-73273.

[85]. Rambo, J., and Y. Joshi. 2003a. Multi-scale modeling of high power density data centers. Proceedings of the ASME InterPACK '03 Conference, July 6-11, Maui, HI.

[86]. Rambo, J., and Y. Joshi. 2003b. Physical models in data center air flow simulations. Proceedings of the ASME International Mechanical Engineering Exposition and Congress (IMECE), paper IMECE2003-41381.

[87]. Rambo, J., and Y. Joshi. 2005. Reduced order modeling of steady turbulent flows using the POD. Proceedings of the ASME Summer Heat Transfer Conference, San Francisco, CA, paper HT2005-72143.

[88]. Schmidt, R., and E. Cruz. 2002a. Raised floor computer data center: Effect on rack inlet temperatures of chilled air exiting both the hot and cold aisles. Proceedings of the ITherm Conference, pp. 580-94.

[89]. Schmidt, R., and E. Cruz. 2002b. American Society of Mecahnical Engineers, EEP, Vol. 2, Electronic and photonic packaging, Electrical system and photonics design and nanotechnology, pp. 297-309.

[90]. Schmidt, R., and E. Cruz. 2003a. Cluster of high powered racks within a raised floor computer data center: Effect of perforated tile flow distribution on rack inlet temperatures. Proceedings of the ASME International Mechanical cal Engineering Exposition and Congress (IMECE). paper IMECE2003-42240.

[91]. Schmidt, R., and E. Cruz. 2003b. Raised floor computer data center: Effect of rack inlet temperatures when rack flow rates are reduced. Proceedings of the ASME InterPACK '03 Conference, July 6-13, paper IPACK2003-35241.

[92]. Schmidt, R., and E. Cruz. 2003c. Raised floor computer data center: Effect on rack inlet temperatures when adjacent racks are removed. Proceedings of the ASME InterPACK '03 Conference, July 6-13, Maui, HI.

[93]. Schmidt, R. 2004. Thermal profile of a high density data center--Methodology to thermally characterize a data center. ASHRAE Transactions 110(2):635-42.

[94]. Schmidt, R., M. Iyengar, and R. Chu. 2005a. Data Centers--Meeting data center temperature requirements. ASHRAE Journal 47(4):44-48.

[95]. Schmidt, R., R. Chu, M. Ellsworth, M. Iyengar, D. Porter, V. Kamath, and B. Lehman. 2005b. Maintaining datacom rack inlet air temperatures with water cooled heat exchanger. Proceedings of the ASME InterPACK '05 Conference, July 17-22, San Francisco, CA, paper IPACK2005-73468.

[96]. Schmidt, R., M. Iyengar, D. Beaty, and S. Shrivastava. 2005c. Thermal profile of a high density data center--Hot spot heat fluxes of 512 W/[ft.sup.2]. ASHRAE Transactions 111(2):765-77.

[97]. Schmidt, R., E. Cruz, and M. Iyengar. 2005d. Challenges of data center thermal management. IBM Journal of Research and Development 49(4/5):709-724.

[98]. Schmidt, R., M. Iyengar, and S. Mayhugh. 2006. Thermal profile of world's third fastest supercomputer. ASHRAE Transactions 112(2):209-19.

[99]. Schmidt, R., and M. Iyengar. 2007. Comparison between underfloor supply and overhead supply data center ventilation designs for high-density clusters. ASHRAE Transactions 113(1).

[100]. Shah, A., V. Carey, C. Bash, and C. Patel. 2005a. Exergy based optimization strategies for multi-component data center thermal management: Part I, Analysis. Proceedings of the ASME InterPACK '05 Conference, July 17-22, San Francisco, CA.

[101]. Shah, A., V. Carey, C. Bash, and C. Patel. 2005b. Exergy based optimization strategies for multi-component data center thermal management: Part II, Application and validation. Proceedings of the ASME InterPACK '05 Conference, July 17-22, San Francisco, CA.

[102]. Sharma, R., C. Bash, and C. Patel. 2002. Dimensionless parameters for evaluation of thermal design and performance of large scale data centers. Proceedings of the AIAA/ASME Joint Thermophysics and Heat Transfer Conferene, St. Louis, June.

[103]. Sharma, R., C. Bash, C. Patel, and M. Beitelmal. 2004. Experimental investigation of design and performance of data centers. Proceedings of the Inter Society Conference on Thermal Phenomena (ITherm), pp. 579-85.

[104]. Shrivastava, S., B. Sammakia, R. Schmidt, and M. Iyengar. 2005a. Comparative analysis of different data center airflow management configurations. Proceedings of the ASME InterPACK '05 Conference, San Francisco, CA, paper IPACK2005-73234.

[105]. Shrivastava, S., and J. VanGilder. 2006. A statistical prediction of cold aisle end airflow boundary conditions. Proceedings of the InterSociety Conference on Thermal Phenomena (ITherm), San Diego, CA, p. 9.

[106]. Sorell, V., S. Escalante, and J. Yang. 2005. Comparison of overhead and underfloor air delivery systems in a data center environment using CFD modeling. ASHRAE Transactions 111(2):756-64.

[107]. Spinazzola, R.S. 2003. High delta-T cooling server rack increases energy efficiency, reliability for data centers. Energy Engineering: Journal of the Association of Energy Engineering 100(2):6-21.

[108]. SSI. Server System Initiative Web site, http://ssiforum.org/default.aspx.

[109]. TIA. 2005. ANSI/TIA-942, Telecommunications Infrastructure Standard for Data Centers. Telecommunications Industry Association, Arlington, VA. April.

[110]. TIA. 2003. ANSI/TIA-569-B, Commercial Building Standard for Telecommunications Pathways and Spaces. Telecommunications Industry Association, Arlington, VA.

[111]. VanGilder, J., and T. Lee. 2003. A hybrid flow network-CFD method for achieving any desired flow partitioning through floor tiles of a raised floor data centers. Proceedings of the Pacific Rim/ASME International Electronics Packaging Technical Conference and Exhibition (InterPack), Maui, HI, paper IPACK2003-35171.

[112]. Wang, D. 2004. A passive solution to a difficult data center environmental problem. Proceedings of the ITherm Conference, pp. 586-92.

[113]. Personal Communication from Dr. Schmidt.

[114]. ICEPAK, Fluent Inc.

[115]. Launder B. and Spalding D., “Lectures in Mathematical Models of Turbulence”, Academic Press, London, England, 1972.

[116]. ICEPAK Users Manual, Fluent Inc.

[117]. MentorGraphics, Flotherm User’s Guide, 2007

[118]. http://serverconfigurator.intel.com/compare.aspx?CategoryID=3

[119]. Intel, “Intel Xeon Processor 5500 series Thermal/Mechanical Design Guide”, 2009.

[120]. Jiang W. and Reddy T. A., “Reevaluation of the Gordon-Ng Performance Models for Water-Cooled Chillers”, ASHRAE v109, part 2.

[121]. Heydari A. and Mulay V., “Cold Aisle Containment and the Energy Efficiency of the Data Center”, IMAPS Thermal Workshop, 2009.

[122]. PolarDam CRAC covers, www.polargy.com

BIOGRAPHICAL INFORMATION

Veerendra Mulay received his Bachelor of Engineering degree in mechanical engineering at Pune University, Pune, India in 1996. After obtaining his degree, Veerendra worked as a trainee engineer in Irrigation and Process Division of KSB Pumps Ltd., Pune. After finishing his training program, he joined Behar India Pvt. Ltd. As a product design engineer. During his employment with Behr India from 1997 through 2000, Veerendra worked on many projects in the field of the automobile air-conditioning and the engine cooling. In fall 2000, Veerendra began his graduate studies at the University of Texas at Arlington in Arlington, TX. While working as a graduate research assistant, he completed the graduate certificate program in electronic packaging and received his Master of Science in Mechanical Engineering from the University of Texas at Arlington in May 2003. Shortly after receiving his M.S., Veerendra decided to continue the research in the field of electronics cooling and he entered into the doctoral program. During his doctoral studies, Veerendra worked as graduate teaching assistant and graduate research assistant. He accepted the internship offered to him by Facebook Inc. and worked at their facilities in California during Summer and Fall 2009. Veerendra received his Doctor of Philosophy degree in Mechanical Engineering from the University of Texas at Arlington in December 2009.